

SCATTERING OF ELECTROMAGNETIC WAVES
FROM PERFECT ELECTROMAGNETIC
CONDUCTOR (PEMC) STRUCTURES



Shakeel Ahmed

Department of Electronics

Quaid-i-Azam University

Islamabad, Pakistan

2009



**SCATTERING OF ELECTROMAGNETIC WAVES
FROM PERFECT ELECTROMAGNETIC
CONDUCTOR (PEMC) STRUCTURES**

by

Shakeel Ahmed

In Partial Fulfillment of the Requirements

for the Degree of

Doctor of Philosophy

Department of Electronics

Quaid-i-Azam University

Islamabad, Pakistan

2009



CERTIFICATE

It is to certify that Mr. Shakeel Ahmed carried out the work contained in this dissertation under my supervision.



Dr. Qaisar Abbas Naqvi

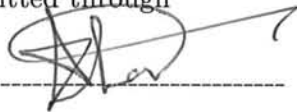
Associate Professor

Department of Electronics

Quaid-i-Azam University

Islamabad, Pakistan

Submitted through



Prof. Dr. Azhar Abbas Rizvi

Chairman

Department of Electronics

Quaid-i-Azam University

Islamabad, Pakistan



Acknowledgments

I humbly thank Almighty Allah, the Most Gracious and the Most Merciful, Who blessed me much more than I wished. I offer my praises to Hazrat Muhammad (Peace Be Upon Him), whose life is a glorious model for the whole humanity.

First of all, I would like to express my sincere gratitude to my advisor Dr. Qaisar A. Naqvi for his knowledge, insight, enthusiasm, and continuous encouragement and support through out this research, he is always there when I need help. Without his support and encouragement completion of this dissertation would not have been possible. I would also thank National Center of Physics, Dr. Q. A. Naqvi and Electronics Department for arranging the visits of Prof. Kohei Hongo, Toho University, Japan. The visits were very beneficial for me and a source of inspiration as well. I am grateful to higher education commission (HEC) of Pakistan for providing opportunity of Ph.D by starting indigenoues Ph.D program.

I would like to thank Professor Dr. Akhlesh Lakhtakia for his extremely valuable suggestions and guidance in the improvement of this work. I would like to mention Fabrizio Frrezza, University of Rome, Italy, for his sincere struggle for arranging my six month visit to Italy. Although I could't manage that visit due to non-availability of funds from HEC but I am thankful to him for the inspiration and encouragement I got from him.

I have a lot to thank my friends who have been around me in the difficult moments during this work. I found Abdul Ghaffar to be the most supportive collaborator, who has a great passion for accurate modeling of important but challenging problems. He is wonderfully persistent in seeking the physical meaning behind the mathematics. I thank my friends Muhammad Naveed, Amjad Imran, Ahsan Ilahi, Fazli Manan, Akhtar Hussain, Husunul Maab, Saeed Ahmed, Abdul Aziz, Anjum Shehzad, Farhat



Majeed, Khalid Nasir, Muhammad Ayub, Shahid Iqbal, Muhammad Faryad and Mudassar Naeem for giving me company which make my study time, a happy moments of my life. Ahsan Illahi just quietly was a great lab mate and co-conspirator in electromagnetic ideas.

Moreover, I would like to thank my brothers, sisters and every member of my family for their lifelong encouragement and support in my studies and for everything they have done for me over the years. Especially I am grateful to my elder brothers Zahoor Ahmed and Manzoor Ahmed for their support and help throughout my educational career. Also I would like to express my deepest gratitude to my wife who I think understands me the most. She has been supporting me greatly by her love and encouragement during this difficult period. Without the support of all my family members, I would have never been able to reach such a highest pedestal of my education. I would say that, without their support and prayers, I wont have been able to carry forward my studies even. I am also grateful to Faheem Ahmed, Sagheer Ahmed, Muhammad Rfaq, Sajid Ali, Rfaqat Ali, A. Wahab, Nobahar and to all those who prayed for my success and bright future.

Finally, I would like to dedicate this work to my parents, Mrs. Fazal Jan and Mr. Muhammad Miskeen. I am indebted to them for every thing they have done for me since my childhood. In particular I would like to extend my heartiest felicitation to my mother who has been a continuous source of inspiration and encouragement for me throughout my studies.

Shakeel Ahmed

To

My Parents

Abstract

Scattering of electromagnetic waves from two dimensional cylindrical structures composed of perfect electromagnetic conductor (PEMC) material has been studied. Response of these two dimensional structures in terms of co-polarized and cross-polarized scattered fields, scattering widths, and radiation power gain has been observed. Scattering behavior of parallel PEMC circular cylinders, rectangular PEMC strip, and strip grating in free space have been considered when they are illuminated by an electromagnetic plane wave. Characteristics of a coated PEMC cylinder are found in comparison to an uncoated one taking dispersion and dissipation of the coating layer into account. Effects of many electromagnetic plane waves on a coated PEMC cylinder has also been analyzed. The effects of the PEMC core has been noted on the directivity of the geometry containing a line source nearby a coated PEMC cylinder. Also contribution to the the scattered field in free space due to a PEMC circular cylinder buried inside the dielectric half space is found. Throughout discussion, the numerical results are compared with the published literature under some special conditions and are found in good agreement.

Contents

<i>Acknowledgements</i>	<i>iii</i>
<i>Dedication</i>	<i>v</i>
<i>Abstract</i>	<i>vi</i>
<i>List of publications</i>	<i>ix</i>
Chapter 1: Introduction	1
1.1. Perfect electromagnetic conductor (PEMC)	6
1.2. Realization of planar PEMC boundary	8
1.3. PEMC boundary	8
1.4. Reflection from a planar PEMC boundary	10
1.5. Realization of a cylindrical PEMC boundary	12
Chapter 2: Electromagnetic scattering from parallel PEMC cylinders	20
2.1. Single PEMC cylinder	20
2.1.1. Numerical results and discussion	22
2.2. Parallel PEMC cylinders	26
2.2.1. Solution of the unknown scattering coefficients	28
2.2.2. Numerical results and discussion	36
2.3. Two dimensional rectangular PEMC strip and strip grating	43
2.3.1. Numerical results and discussion	44
Chapter 3: Electromagnetic scattering from a coated PEMC circular cylinder	51
3.1. Scattering of single plane wave from a coated PEMC cylinder	51
3.1.1. Numerical results and discussion	55
3.2. Scattering of two or more plane waves from a coated PEMC cylinder ...	68
3.2.1. Numerical results and discussion	70

Chapter 4: Directive EM scattering from a coated PEMC cylinder	79
4.1. DNG coated PEMC cylinder	79
4.1.1. Line source outside the coating layer	79
4.1.2. Numerical results and discussion	82
4.1.3. Line source inside the coating layer	84
4.1.4. Numerical results and discussion	86
Chapter 5: Analysis of field due to a buried PEMC cylinder	91
5.1. Buried PEMC cylinder	91
5.1.1. Initial reflected and transmitted fields	92
5.1.2. Scattered fields inside dielectric half space (Region I)	93
5.1.3. Scattered field in free space (Region 0)	98
5.1.4. Numerical results and discussion	99
Chapter 6: Conclusions	105
References	108

List of publications

Publications which are included in this thesis

- [1] Ahmed, S., and Naqvi, Q. A., "Electromagnetic scattering from a perfect electromagnetic conductor cylinder buried in a dielectric half space," Progress In Electromagnetics Research, PIER 78, 25-38, 2008.

- [2] Ahmed, S., and Naqvi, Q. A., "Electromagnetic scattering form parallel perfect electromagnetic conductor cylinders of circular cross-sections using iterative procedure," J. of Electromagn. Waves and Appl., Vol. 22, 987-1003, 2008.

- [3] Ahmed, S., and Naqvi, Q. A., "Electromagnetic scattering from a two dimensional perfect electromagnetic conductor (PEMC) strip and PEMC strip grating simulated by circular cylinders," Opt. Commun., 281, 4211-4218, 2008.

- [4] Ahmed, S., and Naqvi, Q. A., "Electromagnetic scattering from a perfect electromagnetic conductor cylinder coated with a metamaterial having negative permittivity and/or permeability," Opt. Commun., 281, 5664-5670, 2008.

- [5] Ahmed, S., and Naqvi, Q. A., "Electromagnetic scattering of two or more incident plane waves by a perfect electromagnetic conductor cylinder coated with a metamaterial," Progress In Electromagnetics Research B, Vol. 10, 75-90, 2008.

- [6] Ahmed, S., and Naqvi, Q. A., " Directive EM radiation of a line source in the presence of a coated PEMC circular cylinder," Progress in electromagnetic research, PIER 92, pp. 91-102, 2009.

Publications which are not part of this thesis

- [7] Ahmed, S., and Naqvi, Q. A., "Directive em radiation of a line source in the presence of a coated nihility cylinder," J. of Electromagn. Waves and Appl., Vol. 23, 761-771, 2009.
- [8] Ahmed, S., and Naqvi, Q. A., "Scattering of electromagnetic waves by a coated nihility cylinder," Journal of infrared, millimeter and terahertz waves., 30, 1044-1052, DOI 10.1007/ s10762-009-9531-5, 2009.
- [9] Majeed, F., Ahmed, S., and Naqvi, Q. A., "Analysis of electromagnetic field due to a buried coated PEC cylinder," (Accepted for publication) Journal of infrared, millimeter and terahertz waves., 2009.
- [10] Shehzad, A., Ahmed, S., and Naqvi, Q. A., "Analysis of electromagnetic field due to a buried coated PEMC cylinder," (Submitted for publication), 2009.

CHAPTER I

Introduction

Scattering is a physical process where some forms of radiation, such as light, sound or moving particles are forced to deviate from a straight path by one or more localized non-uniformities in the medium through which they pass. In conventional application, this also includes deviation of reflected radiation from the angle given by the law of reflection. The types of non-uniformities which can cause scattering are known as scatterers or scattering centers. The effects of such features on the path of almost any type of propagating wave or moving particle can be described in the framework of scattering theory.

Scattering theory has played a major role in the 20th century mathematical physics. Starting from Rayleigh's explanation of why the sky is blue, to Rutherford's discovery of atomic nucleus, through the modern medical applications of computerized tomography, scattering phenomena has attracted, puzzled and challenged scientists, engineers and mathematicians for more than hundred years. Broadly speaking the scattering theory is concerned with the effect of an inhomogeneous medium on an incident wave. In particular, the total field is viewed as the sum of an incident field and a scattered field from a knowledge of incident field and the differential equations governing the wave motion. Our interest here is to study the scattering behavior of electromagnetic waves by cylinders of circular cross section.

The circular cylinder is one of the simple but most important canonical shapes for the study of scattering of electromagnetic waves. The analysis of scattering by multiple circular cylinders of arbitrary radii and positions makes it possible to simulate the scattering from two-dimensional scatterers of arbitrary cross-section. Therefore scattering from the circular cylinders, has been a very attractive topic for the researchers.

Scientists had studied the problems involving circular cylinders composed of different materials, e.g., dielectric, negative refractive index materials (NRM), chiral, and nihility [1-41]. The scattering of electromagnetic plane waves from a single circular dielectric or conductor cylinder for both normal and oblique incidence had been studied for many years [1-5].

Scattering from multiple cylinders in free-space has been studied by many researchers [6-18]. Scattering by arbitrary cross sectioned layered lossy dielectric cylinders has been discussed by Wu and Tsai [6]. For the analysis of multiple cylinders, different techniques have been used to analyze the scattering between two nearby conducting circular cylinders [7]. Twersky [8] extended the multiple scattering problem to N number of cylinders for the first time. He expressed the total radiation field as an incident field plus a scattered field of various orders. Burke *et al.* [9] derived the multiple scattering solution for N cylinders as a series of Hankel functions. Ragheb and Hamid [10] studied the scattering of plane waves by N circular cylinders. They used conducting circular cylinders to simulate a cylindrical reflector [11]. Furthermore, a rigorous solution had been introduced to solve the scattering problem from an array of dielectric or conductor cylinders for a plane wave excitation of normal incidence [12]. Elsherbeni and Kishk [13] used the principle of equal volume model to study any two-dimensional cylindrical object of arbitrary cross section by an array of circular cylinders. Elsherbeni *et al.* [14] presented an iterative scattering of a gaussian beam by an array of circular conducting and dielectric cylinders. Elsherbeni gave a comparative study of two-dimensional multiple scattering techniques [15]. Yin *et al.* [16, 17] studied the scattering of electromagnetic waves by an array of circular bi-anisotropic cylinders in the case of normal incidence. The scattering of an obliquely incident plane wave on an array of parallel dielectric circular cylinders of arbitrary radii and positions, was considered by Henin *et al.* [18].

Electromagnetic scattering by coated circular cylinders is a classical problem in electromagnetics and was investigated by several researchers [19-30]. Scattering behavior becomes much more complicated if scattering obstacle is made of layers or sections of several materials. This is because of presence of unavoidable multiple scattering at the boundary surfaces, i.e., multiple reflection, refraction and interference. Tang [19, 20] found the theoretical and experimental results for the backscattering from coated cylinders where the thickness of the dielectric coating was comparable to the wavelength. Wang [21] converted the eigenfunction solution into a high frequency ray solution and expressed the scattered fields in terms of geometrical ray and two surface waves around the cylinder. Scattering of electromagnetic waves by an anisotropic plasma-coated conducting cylinder was considered by Chen and Cheng [22]. Electromagnetic scattering by an impedance cylinder coated eccentrically with a chiro-plasma cylinder was discussed by Shen [23]. Shen and Li [24] studied electromagnetic scattering by a conducting cylinder coated with materials having negative permittivity and permeability also known as double negative (DNG) material. The scattered field for two plane waves incident on a circular cylinder covered by a dielectric material, was investigated by Mushref [25]. A closed series solution of electromagnetic scattering by an eccentric coated cylinder in matrix form was achieved by Mushref [26]. While Sun *et al.* [27] analyzed the electromagnetic radiation of a line source scattered by an infinite conducting cylinder coated with a left handed material (LHM material). Irci and Ertürk [28] used the DNG and single negative (SNG) coated conducting cylinder to achieve transparency and scattering maximization. Ahmed and Naqvi studied the behavior of the coated nihility circular cylinder for the plane wave and a line source excitation [29, 30].

Buried object detection has also been an attractive topic for the researchers due to its applications in the remote sensing of the earth's subsurface and detection of landmines, pipes, and other buried objects of interest. Many techniques have been

used in this regard. Yakonov [31] discussed the diffraction of electromagnetic waves by a circular cylinder in a homogeneous half-space. Parry and Ward [32] solved the problem of electromagnetic scattering from cylinders of arbitrary cross-section in a conductive half-space. Howard [33] employed the mode-matching method to solve a two dimensional integral equation for the scattered field. Ogunade [34] extended an early work [29] allowing one to obtain numerical results in a more easy way. Mahmoud *et al.* [35] tackled the problem using a multipole expansion of the scattered field. Butler *et al.* [36] solved an integral equation for the induced current, discussing various forms of the kernel suitable for an efficient numerical evaluation. Hongo and Hamamura [37] treated the plane-wave scattering by a two-dimensional cylindrical obstacle in a dielectric half-space employing the Kobayashi potential concept. Moaveni *et al.* [38] discussed the plane wave scattering by gratings of conducting cylinders in an inhomogeneous and lossy dielectric. A corrected version of paper [37] has been reported in [39]. Scattering of obliquely incident, perpendicularly polarized plane wave by a dielectric circular cylinder, which is buried in a grounded dielectric layer had been considered by Naqvi and Rizvi [40]. Dielectric cylinder has low dielectric contrast from the host grounded dielectric layer. And Lambert [41] studied the scattering by a cylindrical dielectric obstacle buried in a half-space: a H-field-based solution method. Scattering of electromagnetic waves from a deeply buried circular cylinder has been discussed by Naqvi *et al.* [42]. Electromagnetic scattering from a dielectric cylinder buried beneath a slightly rough surface has been discussed by Lawrence and Sarabandi [43]. Ciambra *et al.* [44, 45] used the spectral domain solution for the scattering problem of a circular cylinder buried in a dielectric half-space. Scattering by a finite set of perfectly conducting cylinders buried in a dielectric half space, using a spectral-domain solution, had been discussed by Vico *et al.* [46].

Recent years have witnessed an increased interest in materials, such as DNG and SNG materials, as well as combinations of these with conventional double-positive

(DPS) materials [47-63]. Veselago [47] mentioned the unusual properties of DNG materials, which are characterized by a negative real part of the permittivity as well as the permeability. Pendry [48] gave the concept of the so called perfect lens consisting of a specific DNG slab which has attracted much attention. Shelby *et al.* [49] gave the experimental verification of a negative index of refraction. Ziolkowski and Heyman [50] studied the wave propagation in a double negative DNG medium, both analytically and numerically. Lakhtakia discussed an electromagnetic trinity from negative permittivity and negative permeability [51, 52]. Propagation of electromagnetic wave in media in which the effective relative permittivity and the effective relative permeability are allowed to take any value in the upper half of the complex plane has been studied by McCall *et al.* [53]. Moreover, combinations of DNG and DPS materials have lead to a new paradigm in the miniaturization of devices such as cavity resonators [54]. Depine and Lakhtakia [55] derived a new condition for the constitutive parameters of a linear isotropic dielectric-magnetic medium to have phase velocity that is opposite to the direction of power flow, and demonstrated its equivalence with previously derived conditions. Ziolkowski and Kipple [56], used the double negative materials to increase the power radiated by electrically small antennas. Alú and Engheta [57] used different combinations of different materials in the waveguides to study the guided modes. Eleftheriades and Balmain [58] discussed the fundamental principles and applications of the NRMs. Polarizabilities and effective parameters, for collections of spherical nano-particles formed by pairs of concentric double-negative (DNG), single-negative (SNG) and/or double-positive (DPS) material layers, were studied by Alú and Engheta [59]. Ziolkowski and Kipple [60] discussed the reciprocity between the effects of resonant scattering and enhanced radiated power by electrically small antennas in the presence of nested metamaterials shells. Caloz and Itoh [61] studied the role of NRMs in transmission line theory and microwave applications. Arslanagic *et al.* [62] presented the excitation of an electrically small DNG material-coated cylinder by an

arbitrarily located line source. The role of NRMs in the field of antennas is available in [63-65].

A new type of material which is known as perfect electromagnetic conductor (PEMC), has been introduced by Lindell and Sihvola [66], which displays truly special properties. PEMC is a very fundamental type of medium, at the same time extremely simple and very complex. It is a generalization of both perfect electric conductor (PEC) and perfect magnetic conductor (PMC) media for which the medium is labeled as PEMC. Due to the cross-components in addition to the co-components in the scattered field, it is bi-isotropic. Due to its particular property of short-circuiting a linear combination of the tangential electric and magnetic fields, the PEMC material offers a medium which can be exploited in different electromagnetic applications. The possible applications of this material include ground planes for low-profile antennas, field pattern purifiers for aperture antennas, polarization transformers, radar reflectors, and generalized high-impedance surfaces. Many researchers have worked on this material [67-83]. In the following sections the main features of the PEMC medium have been discussed.

1.1. Perfect electromagnetic conductor (PEMC)

To define PEMC, consider the constitutive relations between the electric field \mathbf{E} and magnetic field \mathbf{H} , electric displacement \mathbf{D} and magnetic displacement \mathbf{B} as mentioned in [72]

$$\mathbf{D} = M\mathbf{B}, \quad \mathbf{H} = -M\mathbf{E} \quad (1.1.1)$$

where M is a real scalar admittance parameter. At every spatial point within PEMC, a linear combination of fields vanishes ($\mathbf{H} + M\mathbf{E} = 0$) and also a combination of displacements is zero ($\mathbf{D} - M\mathbf{B} = 0$). For $M \rightarrow \pm\infty$ we get PEC case

$$\mathbf{E} = 0, \quad \mathbf{B} = 0$$

while $M = 0$, gives us the PMC case

$$\mathbf{H} = 0, \quad \mathbf{D} = 0$$

More common form of constitutive relations than (1.1.1), is to write the displacements in terms of the field quantities as

$$\begin{pmatrix} \mathbf{D} \\ \mathbf{B} \end{pmatrix} = \begin{pmatrix} \epsilon & \xi \\ \zeta & \mu \end{pmatrix} \begin{pmatrix} \mathbf{E} \\ \mathbf{H} \end{pmatrix} = C \begin{pmatrix} \mathbf{E} \\ \mathbf{H} \end{pmatrix} \quad (1.1.2)$$

where the material matrix C contains the four scalars $\epsilon, \xi, \zeta, \mu$. Equation (1.1.2) can be written as

$$\begin{pmatrix} \mathbf{D} \\ \mathbf{H} \end{pmatrix} = \frac{1}{\mu} \begin{pmatrix} \epsilon\mu - \xi\zeta & \xi \\ -\zeta & 1 \end{pmatrix} \begin{pmatrix} \mathbf{E} \\ \mathbf{B} \end{pmatrix} \quad (1.1.3)$$

Comparing relation (1.1.3) with (1.1.1), we get the PEMC constitutive matrix

$$C = q \begin{pmatrix} M & 1 \\ 1 & 1/M \end{pmatrix}, \quad \text{with} \quad q \rightarrow \infty \quad (1.1.4)$$

which leads to infinite values for $\epsilon, \xi, \zeta, \mu$ unless M is zero or infinite. The parameter q is only introduced to show the relation between the four infinite parameters. The four parameters satisfy the relation

$$\mu\epsilon - \xi\zeta = 0 \quad (1.1.5)$$

in spite of their infinite magnitudes. Also, we have the relation

$$M^2 = \epsilon/\mu \quad (1.1.6)$$

The conditions arising from (1.1.4) are

$$\mathbf{D} = q(M\mathbf{E} + \mathbf{H}), \quad \mathbf{B} = q(\mathbf{E} + \mathbf{H}/M) \quad (1.1.7)$$

Equation (1.1.7) imply $\mathbf{D} = M\mathbf{B}$ for any q . The second condition $\mathbf{H} = -M\mathbf{E}$ arises only by requiring $q \rightarrow \pm\infty$ and finite \mathbf{D} and \mathbf{B} .

1.2. Realization of a planar PEMC boundary

The PEMC medium can be realized and has been reported in [68]. On a conducting plane, a uniaxially gyrotropic layer with a certain resonating thickness is grown. The permittivity and permeability components of the layer have to be large in the direction of the normal to the plane. The gyrotropy (the off-diagonal parts of the permeability tensor) are controlled by an external (or internal) static magnetic field which also then determines the M parameter of the PEMC medium. The essential point here is that the electric and magnetic boundary conditions at the surface of such a structure are equal to those of PEMC for all possible fields. Then the structure is indistinguishable from perfect electromagnetic conductor. Obviously, the PEMC condition

$$\mathbf{H} = -M\mathbf{E} \quad (1.2.1)$$

and the tangential continuity of the fields across a surface require the following boundary condition

$$\mathbf{n} \times (\mathbf{H} + M\mathbf{E}) = 0 \quad (1.2.2)$$

where \mathbf{n} is unit normal vector with respect to the boundary. Therefore, in order to fabricate an artificial PEMC sample, it is sufficient to be able to create a structure with the following surface impedance \tilde{Z}_s , [72]

$$\mathbf{n} \times \mathbf{E} = \tilde{Z}_s \cdot \mathbf{H}, \quad \tilde{Z}_s = -\frac{1}{M} \mathbf{n} \times \tilde{\mathbf{I}} \quad (1.2.3)$$

where $\tilde{\mathbf{I}}$ is the unit dyadic.

1.3. PEMC boundary

For fields satisfying the PEMC medium conditions (1.1.1), both the energy density and Poynting vector obviously vanish [69]

$$\mathbf{E} \times \mathbf{H} = 0, \quad \mathbf{D} \cdot \mathbf{E} + \mathbf{B} \cdot \mathbf{H} = 0 \quad (1.3.1)$$

Thus, even if the PEMC medium allows some nonzero fields, it rejects electromagnetic energy propagation and acts as a boundary to electromagnetic waves just like the PEC and PMC media. Denoting the unit normal between air and PEMC boundary by \mathbf{n} , from the continuity of tangential \mathbf{E} and \mathbf{H} fields it follows that the tangential component of the field $\mathbf{H} + M\mathbf{E}$ is also continuous through the PEMC air interface. Because this vanishes in the PEMC medium, the boundary condition becomes

$$\mathbf{n} \times (\mathbf{H} + M\mathbf{E}) = 0 \quad (1.3.2)$$

Also, because the normal component of the field $\mathbf{D} - M\mathbf{B}$, is continuous through any boundary, another condition at the PEMC boundary reads

$$\mathbf{n} \cdot (\mathbf{D} - M\mathbf{B}) = 0 \quad (1.3.3)$$

Because the normal component of the Poynting vector at the PEMC boundary vanishes

$$\begin{aligned} \mathbf{n} \cdot (\mathbf{E} \times \mathbf{H}) &= -\mathbf{E} \cdot (\mathbf{n} \times \mathbf{H}) \\ &= M\mathbf{E} \cdot (\mathbf{n} \times \mathbf{E}) = 0 \end{aligned} \quad (1.3.4)$$

PEMC serves as an example of an ideal boundary. As a check, the PMC and PEC boundary conditions are obtained as the two limits

$$M \rightarrow 0(\text{PMC}) : \quad \mathbf{n} \times \mathbf{H} = 0, \quad \mathbf{n} \cdot \mathbf{D} = 0 \quad (1.3.5)$$

$$M \rightarrow \pm\infty(\text{PEC}) : \quad \mathbf{n} \times \mathbf{E} = 0, \quad \mathbf{n} \cdot \mathbf{B} = 0 \quad (1.3.6)$$

Conditions (1.3.2) and (1.3.3) are valid for any medium with a PEMC boundary. If the medium is air (vacuum) with the parameters $\epsilon = \epsilon_0$, $\mu = \mu_0$, $\xi_0 = \zeta_0$, (1.3.3) can be written as

$$\mathbf{n} \cdot (\mathbf{E} - M\eta_0^2\mathbf{H}) = 0 \quad (1.3.7)$$

While the condition (1.3.2) can also be expressed as

$$\mathbf{n} \times \mathbf{E} = \tilde{Z}_s \cdot \mathbf{H} \quad (1.3.8)$$

\tilde{Z}_s is a two-dimensional surface impedance dyadic satisfying $\mathbf{n} \cdot \tilde{Z}_s = \tilde{Z}_s \cdot \mathbf{n} = 0$. Comparison with (1.3.2), shows us that for the PEMC boundary has the simple anti-symmetric form

$$\tilde{Z}_s = -\frac{1}{M} \mathbf{n} \times \tilde{\mathbf{I}} \quad (1.3.9)$$

This means that the PEMC boundary is nonreciprocal, except in the PMC and PEC limiting cases $M = 0, \pm\infty$. One can also ask about conditions on making the boundary passive or active. PEMC boundary conditions being the generalized forms of those of PEC and PMC boundaries. So PEMC boundary is not active (i.e., it does not give energy to the exterior field) if $\mathbf{n} \cdot \Re\{\mathbf{E} \times \mathbf{H}\} \leq 0$ is satisfied for any electromagnetic field at the boundary. Inserting (1.3.2) leads to the condition

$$\begin{aligned} -\Re\{\mathbf{E} \cdot (\mathbf{n} \times \mathbf{H})^*\} &= \Re\{M^* \mathbf{E} \cdot (\mathbf{n} \times \mathbf{E})^*\} \\ &= -\Re\{M^* \mathbf{n} \cdot (\mathbf{E} \times \mathbf{E}^*)\} \leq 0 \end{aligned} \quad (1.3.10)$$

which must be valid for any complex field vector \mathbf{E} . Since changing the sense of rotation of an elliptically polarized field \mathbf{E} corresponds to replacing \mathbf{E} by \mathbf{E}^* , the expression in (1.3.10) (if not zero) can have either sign. Thus, the only possibility is either less than or equal to (\leq) is actually equal to ($=$). Because $\mathbf{n} \cdot (\mathbf{E} \times \mathbf{E}^*)$ has zero real part, this requires that be real. Thus, excluding the possibility that PEMC be active for some fields, it must be lossless like PEC and PMC boundaries, i.e., it does not absorb or emit energy. Negative time dependence $e^{-j\omega t}$, is used and has been suppressed in the entire work.

1.4. Reflection from a planar PEMC boundary

Because the PEMC medium does not allow electromagnetic energy to enter, an interface of such a medium serves as an ideal boundary to the electromagnetic field. Let us consider the boundary of PEMC medium and air with unit normal vector \mathbf{n} . Because tangential components of the \mathbf{E} and \mathbf{H} fields are continuous at any interface

of two media, one of the boundary conditions for the medium in the air side is given in (1.3.2), because a similar term vanishes in the PEMC medium side. The other condition is based on the continuity of the normal component of the \mathbf{D} and \mathbf{B} fields which gives another boundary condition as expressed by (1.3.3), which may also be expressed as [66]

$$M\mathbf{E} = -\mathbf{H} + (1 + M^2\eta_0^2)\mathbf{nn}\cdot\mathbf{H} \quad (1.4.1)$$

As an application, let us consider plane-wave reflection from a PEMC boundary plane at $z = 0$. For simplicity, the incident and reflected plane waves in the region $z < 0$ are assumed polarized parallel to the boundary. The total fields are

$$\mathbf{E}(z) = \mathbf{E}^i e^{-jk_0 z} + \mathbf{E}^r e^{jk_0 z} \quad (1.4.2)$$

$$\eta_0 \mathbf{H}(z) = \mathbf{u}_z \times \mathbf{E}^i e^{-jk_0 z} - \mathbf{u}_z \times \mathbf{E}^r e^{jk_0 z} \quad (1.4.3)$$

Inserting these into (1.4.1) at $z = 0$ with $\mathbf{n} = -\mathbf{u}_z$, it is found that

$$M\eta_0(\mathbf{E}^i + \mathbf{E}^r) = -\mathbf{u}_z \times (\mathbf{E}^i - \mathbf{E}^r) \quad (1.4.4)$$

$$(\mathbf{u}_z \times \tilde{\mathbf{I}} - M\eta_0\tilde{\mathbf{I}}) \cdot \mathbf{E}^r = (\mathbf{u}_z \times \tilde{\mathbf{I}} + M\eta_0\tilde{\mathbf{I}})\mathbf{E}^i \quad (1.4.5)$$

with $\tilde{\mathbf{I}} = u_x u_x + u_y u_y$. Multiplying above equation by the dyadic $(\mathbf{u}_z \times \tilde{\mathbf{I}} + M\eta_0\tilde{\mathbf{I}})$, the reflected field is then

$$\mathbf{E}^r = -\frac{1}{1 + M^2\eta_0^2} [(-1 + M^2\eta_0^2)\mathbf{E}^i + 2M\eta_0\mathbf{u}_z \times \mathbf{E}^i] \quad (1.4.6)$$

This equation shows that for a linearly polarized incident field, the field reflected from a PEMC boundary contains co-polarized component and cross-polarized components. For $M = 0$ (PMC case) and $M\eta_0 \rightarrow \pm\infty$ (PEC case) the cross-polarized component vanishes. For the special PEMC case $M = 1/\eta_0$, (1.4.6) becomes

$$\mathbf{E}^r = -\mathbf{u}_z \times \mathbf{E}^i$$

which means that the reflected field appears totally cross-polarized. Thus, the boundary acts as a twist polarizer which is a nonreciprocal device.

Before starting work on PEMC circular cylinders it is necessary to first analyze whether the PEMC boundary conditions (1.3.2) and (1.3.3) are satisfied on the surface of cylindrical structures. Therefore realization of a cylindrical PEMC structure is required for this purpose which is discussed in the following section.

1.5. Realization of a cylindrical PEMC boundary

Let us define two problems, labeled I and II. In Problem I, the region $\rho \leq a$ is occupied by a PEC, the region $b \geq \rho \geq a$ by a canonical nonreciprocal Tellegen medium with constitutive relations

$$\mathbf{D} = \epsilon \mathbf{E} + \xi \mathbf{H} \quad (1.5.1)$$

$$\mathbf{B} = \mu \mathbf{H} + \xi \mathbf{E} \quad (1.5.2)$$

and the region $\rho > b$ by free space

$$\mathbf{D} = \epsilon_0 \mathbf{E}$$

$$\mathbf{B} = \mu_0 \mathbf{H}$$

In Problem II, the region $\rho \leq b$ is occupied by a special admittance M medium, and the region $\rho \geq b$ by free space.

To set up the fields in the region $\rho \geq b$ for problem I, it is assumed that the incident EM wave is travelling along x axis with its electric field vector parallel to the z axis. Hence the fields may be written as

$$\mathbf{E}_{out}(\rho, \phi) = E_0/k_0 \sum_{-\infty}^{\infty} j^n \left[\mathbf{N}_n^{(1)}(k_0, \rho, \phi) + a_n \mathbf{N}_n^{(4)}(k_0, \rho, \phi) + b_n \mathbf{M}_n^{(4)}(k_0, \rho, \phi) \right]$$

where $k_0 = \omega\sqrt{\mu_0\epsilon_0}$, the coefficients a_n and b_n may be obtained by solving the boundary value problem, whereas the remaining functions are defined as

$$\begin{aligned}\mathbf{M}_n^{(l)} &= \nabla \times \left[\hat{z}\psi_n^{(l)}(k, \rho, \phi) \right], \quad l \in \{1, 4\} \\ \mathbf{N}_n^{(l)} &= 1/k\nabla \times \mathbf{M}_n^{(l)}(k, \rho, \phi), \quad l \in \{1, 4\}\end{aligned}$$

where

$$\begin{aligned}\psi_n^{(1)}(k, \rho, \phi) &= J_n(k\rho)e^{jn\phi} \\ \psi_n^{(4)}(k, \rho, \phi) &= H_n^{(1)}(k\rho)e^{jn\phi}\end{aligned}$$

where $J_n(\cdot)$ and $H_n^{(1)}(\cdot)$ are the Bessel and Hankel functions of first kind, respectively. The corresponding magnetic field $\mathbf{H}_{out}(\rho, \phi)$ may be found by using the Maxwell equations for free space.

Now the fields in the coating layer i.e., in the Tellegen medium may be set up as

$$\begin{aligned}\mathbf{E}_{in}(\rho, \phi) &= E_0/k_0 \sum_{-\infty}^{\infty} j^n \left\{ c_n \left[\mathbf{M}_n^{(1)}(k, \rho, \phi) + \mathbf{N}_n^{(1)}(k, \rho, \phi) \right] \right. \\ &\quad + d_n \left[\mathbf{M}_n^{(4)}(k, \rho, \phi) + \mathbf{N}_n^{(4)}(k, \rho, \phi) \right] \\ &\quad + e_n \left[\mathbf{M}_n^{(1)}(k, \rho, \phi) - \mathbf{N}_n^{(1)}(k, \rho, \phi) \right] \\ &\quad \left. + f_n \left[\mathbf{M}_n^{(4)}(k, \rho, \phi) - \mathbf{N}_n^{(4)}(k, \rho, \phi) \right] \right\}, \quad b \geq \rho \geq a\end{aligned}$$

where $k = \omega\sqrt{\mu\epsilon - \xi^2}$. Again Maxwell equations are used to find out the corresponding magnetic field $\mathbf{H}_{in}(\rho, \phi)$ in the Tellegen layer. Now the boundary conditions at the two interfaces $\rho = a$ and $\rho = b$ are listed below

$$\begin{aligned}\hat{z} \cdot \mathbf{E}_{in}(a, \phi) &= 0 \\ \hat{\phi} \cdot \mathbf{E}_{in}(a, \phi) &= 0\end{aligned}$$

$$\hat{z} \cdot \mathbf{E}_{in}(b, \phi) = \hat{z} \cdot \mathbf{E}_{out}(b, \phi)$$

$$\hat{\phi} \cdot \mathbf{E}_{in}(b, \phi) = \hat{\phi} \cdot \mathbf{E}_{out}(b, \phi)$$

$$\hat{z} \cdot \mathbf{H}_{in}(b, \phi) = \hat{z} \cdot \mathbf{H}_{out}(b, \phi)$$

$$\hat{\phi} \cdot \mathbf{H}_{in}(b, \phi) = \hat{\phi} \cdot \mathbf{H}_{out}(b, \phi)$$

The coefficients a_n, b_n, c_n, d_n, e_n , and f_n are calculated by solving the above boundary conditions with the application of the orthogonality relationship

$$\int_0^{2\pi} e^{j(n-m)\phi} d\phi \propto \delta_{mn}$$

and hence the coefficients “ a_n ” and “ b_n ”, are

$$a_n = \frac{2M_n}{\eta_0 V_n} J'_n(k_0 b) \quad (1.5.3)$$

$$b_n = \frac{1}{2j H_n^{(1)}(k_0 b)} \left[\frac{W_n}{\eta_0 V_n} J'_n(k_0 b) - 2j J_n(k_0 b) \right] \quad (1.5.4)$$

where prime denotes the derivative w. r. t. entire argument of the function, $j = \sqrt{-1}$

and

$$W_n = 4\pi(ka)jH_n^{(1)'}(k_0b)C_nG_n + 2j\eta\frac{R_nU_n}{S_n}$$

$$V_n = \frac{2\pi(ka)}{\eta}H_n^{(1)'}(k_0b)F_nG_n - \eta\frac{R_nT_n}{S_n}$$

$$U_n = 2J_nM_n - 2\pi(ka)C_nG_nL_n$$

$$T_n = 2M_nQ_n + 2\pi(ka)F_nG_nL_n$$

$$S_n = L_nP_n + 2M_nN_n$$

$$R_n = \frac{2}{\eta_0}M_nH_n^{(1)}(k_0b) + \frac{2}{\eta}P_nH_n^{(1)'}(k_0b)$$

$$Q_n = \pi(ka)B_nF_n + 2jF_n$$

$$P_n = -K_n + \pi(ka)C_nG_n$$

$$N_n = -E_n + \pi(ka)B_nC_n$$

$$M_n = -2jH_n + \pi(ka)F_nG_n$$

$$L_n = -2jD_n + \pi(ka)B_nF_n$$

$$J_n = 2jD_n - \pi(ka)B_nC_n$$

$$K_n = H_n^{(1)}(ka)H_n^{(1)}(kb)$$

$$H_n = H_n^{(1)}(ka)H_n^{(1)'}(kb)$$

$$G_n = H_n^{(1)}(ka)H_n^{(1)'}(kb)$$

$$F_n = J_n(ka)H_n^{(1)'}(kb) - J_n'(kb)H_n^{(1)}(ka)$$

$$E_n = J_n(ka)H_n^{(1)}(kb) + J_n(kb)H_n^{(1)}(ka)$$

$$D_n = J_n'(kb)H_n^{(1)}(ka) + J_n(ka)H_n^{(1)'}(kb)$$

$$C_n = J_n(ka)H_n^{(1)}(kb) - J_n(kb)H_n^{(1)}(ka)$$

$$B_n = J_n'(ka)H_n^{(1)}(ka) + J_n(ka)H_n^{(1)'}(ka)$$

When the coating of the Tellegen medium is removed that is by inserting $b = a, k = k_0$, in the equations (1.5.3) and (1.5.4) give

$$a_n = 0 \tag{1.5.5}$$

$$b_n = -\frac{J_n(ka)}{H_n^{(1)}(ka)} \tag{1.5.6}$$

which is the case of an uncoated PEC cylinder.

At this point \mathbf{E}_{out} and \mathbf{H}_{out} for Problem I are known. Now consider Problem II to find out a condition on a, b, ϵ, μ and ξ that allows the satisfaction of

$$\begin{pmatrix} \hat{z} \cdot \mathbf{H}_{out}(b, \phi) \\ \hat{\phi} \cdot \mathbf{H}_{out}(b, \phi) \end{pmatrix} = - \begin{pmatrix} M_{zz} & M_{z\phi} \\ M_{\phi z} & M_{\phi\phi} \end{pmatrix} \begin{pmatrix} \hat{z} \cdot \mathbf{E}_{out} \\ \hat{\phi} \cdot \mathbf{E}_{out} \end{pmatrix} \tag{1.5.7}$$

We focus on $M_{\phi z}$ and try to find out whether the condition

$$\left\{ \sum_{-\infty}^{\infty} [\hat{\phi} \cdot \mathbf{H}_{out}^{(n)}(b, \phi)] \right\} + M_{\phi z} \left\{ \sum_{-\infty}^{\infty} [\hat{z} \cdot \mathbf{E}_{out}^{(n)}(b, \phi)] \right\} = 0 \tag{1.5.8}$$

is satisfied.

Using the values of a_n and b_n , \mathbf{E}_{out} and \mathbf{H}_{out} can be obtained for the coated geometry and it is found that

$$\hat{z} \cdot \mathbf{E}_{out}(b, \phi) = E_0 \sum_{n=-\infty}^{\infty} \left[J_n(k_0 b) + b_n H_n^{(1)}(k_0 b) \right] \quad (1.5.9)$$

$$\hat{\phi} \cdot \mathbf{H}_{out}(b, \phi) = -\frac{E_0}{j\eta_0} \sum_{n=-\infty}^{\infty} \left[J_n'(k_0 b) + b_n H_n^{(1)'}(k_0 b) \right] \quad (1.5.10)$$

Now to find out the value of the the admittance parameter $M_{\phi z}$, for which the condition (1.5.8) is satisfied, the values of a, b, ϵ, μ and ξ are fixed and small arguments approximations (retaining only squared terms) for the Bessel and Hankel functions i.e.,

$$\begin{aligned} J_0(\alpha) &= 1 - \frac{\alpha^2}{4} & Y_0(\alpha) &= \frac{2}{\pi} \ln\left(\frac{\alpha}{2}\right) \\ J_1(\alpha) &= \frac{\alpha}{2} & Y_1(\alpha) &= -\frac{2}{\pi\alpha} \\ J_0'(\alpha) &= -\frac{\alpha}{2} & Y_0'(\alpha) &= \frac{2}{\pi\alpha} \\ J_1'(\alpha) &= \frac{1}{2} - \frac{3\alpha^2}{16} & Y_1'(\alpha) &= \frac{2}{\pi\alpha^2} \end{aligned}$$

and hence $H_n^{(1)}(\alpha) = J_n(\alpha) + jY_n(\alpha)$ and $H_n^{(1)'}(\alpha) = J_n'(\alpha) + jY_n'(\alpha)$, are used. Using the above values of the Bessel and Hankel functions in (1.5.8) and solving for $M_{\phi z}$, it is observed that the (1.5.8) is satisfied for different combinations of the parameters a, b, ϵ, μ and ξ . That is for every combination of quantities a, ϵ, μ and ξ , there exists a particular value of b such that condition (1.5.8) is satisfied. For example: for $k_0 a = 0.025$, $k_0 b = 0.075$, $\epsilon_r = 5 - j0.001$, $\mu_r = 0.0001 - j0.0221$, $\xi = 1 \times 10^{-9}$ while in this case $M_{\phi z} = \xi/\mu = 0.0001629 + j0.0359892$, the PEMC condition (1.5.8) is satisfied. Now consider an other example of relatively larger radii with $k_0 a = 1.25$, $k_0 b = 3.015$ condition (1.5.8) is satisfied when $\epsilon_r = 5 - j0.001$, $\mu_r = 0.1286 + j0.000088$, $\xi = 1 \times 10^{-9}$ and $M_{\phi z} = 0.006188 - 4.2458 \times 10^{-6}$ and $|n| \leq 10$.

Due to the unusual and impressive properties of the PEMC material it has been chosen as topic of research. Two dimensional cylindrical structures of PEMC material

have been considered for the analysis. We are interested to find out the answers of the questions like: How would PEMC material affect the forward and backward scattering cross-section of circular cylinders? What is the difference between a coated and an uncoated PEMC circular cylinder, regarding monostatic and bistatic echo widths? How would a PEMC cylinder respond when it is coated by a DPS, epsilon-negative (ENG), mu-negative (MNG) or a DNG layer? How would the dissipative and dispersive DNG coating layer affect the scattering behaviors of the coated geometries? Is it possible to achieve transparency and scattering maximization in the case of a coated PEMC cylinder? What would be the response of a coated PEMC cylinder when many plane waves strike it? How would a coated geometry behave when the PEC core is replaced by a PEMC one? To answer these questions we have proceeded in the following manner.

In chapter I, the previous works related to our topics have been mentioned. Then introduction to PEMC medium, realization of both planar and cylindrical PEMC surfaces, and behavior of PEMC boundary are discussed.

In chapter II, firstly scattering of electromagnetic waves from a single PEMC circular cylinder in free space is considered, the problem is solved by using scalar field expressions instead of vector wave functions discussed by Ruppin [70]. Numerical results thus obtained are compared with those given in [70] and are found in good agreement with them. Then the discussion is extended to N parallel PEMC circular cylinders and iterative procedure has been used to study the scattered field patterns from assemblies of parallel cylinders. In response to the incident field each cylinder scatters both the co- and cross-polarized fields, which is referred to as the initial or zeroth order scattered field of each cylinder. Then the zeroth order scattered field from $N - 1$ cylinders are considered as the incident field on the remaining cylinder. Thus a first order scattered field is generated. This process is repeated for each cylinder. Results under special conditions are comparable with the published literature.

Electromagnetic scattering from a rectangular PEMC strip and PEMC strip grating with finite number of PEMC strips simulated from PEMC circular cylinders are also analyzed in this chapter. Effects of variation of the angle of incidence, number of strips in the grating, and the admittance of the PEMC material have been noted on the scattered fields.

Chapter III contains the discussion on electromagnetic scattering from an infinitely long PEMC circular cylinder coated with homogeneous, isotropic, and linear material ENG, MNG or DNG layer. The effect of dissipative and dispersive DNG coating layer on the scattered field from the coated PEMC cylinder is also analyzed. Firstly source of excitation is taken to be a single plane wave and then many plane waves in the analysis. Electric vector of the incident plane wave is taken parallel (E-polarized) as well as perpendicular (H-polarized) to the axis of the PEMC cylinder. The method of eigenfunction expansion is used in the theoretical study. The problem is formulated assuming fields in two regions, i.e., free space outside the coating and the coating layer. Appropriate boundary conditions are applied at the two interfaces. The monostatic and bistatic echo widths in the far-zone are calculated by using the large argument approximation of Hankel function. To verify the correctness of the analytical formulation and the numerical code, the numerical results are compared with the published work for the special cases.

Chapter IV presents the radiation characteristics of a lossless and, dissipative and dispersive DNG material coated PEMC cylinder when a line source is introduced as a source of excitation. The problem is formulated with three regions, i.e., free space and the DNG material layer. Appropriate boundary conditions are applied at the interfaces. The far-zone scattered field patterns are calculated by using the large argument approximations of Hankel functions. The numerical results obtained are compared with the published work for the special cases to verify the correctness of the analytical formulation and the numerical code.

In chapter V, the analytical solution for a perfect PEMC cylinder buried beneath a dielectric half space, is presented. The solution is obtained by employing the plane wave representation of the fields and adding the successive reflections from the interface and the scattered fields from the buried cylinder. All the multiple interactions are accounted for in this analysis. Numerical results are obtained for co- and cross-polarized components of far-zone scattered field above the dielectric half space for both E-polarized and H-polarized cases.

Chapter VI deals with conclusions made during the discussion and possible extensions of the work presented in this thesis.

CHAPTER II

Electromagnetic scattering from parallel PEMC cylinders

Scattering of electromagnetic waves from parallel PEMC circular cylinders of infinite length in free space, is studied in this chapter. As first consideration, analytic theory for the electromagnetic scattering from a single PEMC cylinder is given. Secondly, based on this theory scattering of electromagnetic waves from parallel PEMC circular cylinders is discussed. Then the PEMC cylinders are arranged to form strip and strip grating. In order to obtain the unknown field expansion coefficients, iterative procedure utilizes the boundary conditions on the surface of each cylinder. Plane wave has been used as a source of excitation. Both the near and far fields, due to any number of interactions between the cylinders, are determined. Numerical results obtained for E-polarized and H-polarized cases are compared with the published literature, under special conditions.

2.1. Single PEMC cylinder

Consider a circular PEMC cylinder with radius a as shown in Fig. 2.1. Cylinder is excited by either an E-polarized or H-polarized uniform plane wave. The E-polarized

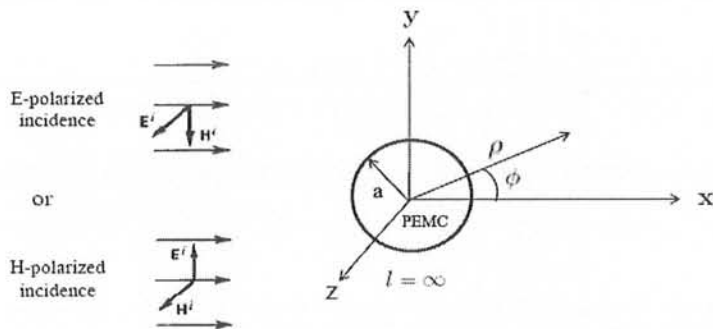


Figure 2.1. PEMC circular cylinder of infinite length in free space.

incident field in terms of scalar cylindrical functions may be expressed as

$$E_z^i = E_0 \sum_{n=-\infty}^{\infty} j^n J_n(k_0 \rho) e^{jn\phi} \quad (2.1.1)$$

where E_0 is the amplitude of the incident plane wave. Using following Maxwell equation

$$\mathbf{H} = \frac{1}{j\omega\mu_0} \nabla \times \mathbf{E} \quad (2.1.2)$$

corresponding ϕ component of incident magnetic field is obtained as

$$H_\phi^i = -\frac{E_0}{j\eta_0} \sum_{n=-\infty}^{\infty} j^n J'_n(k_0 \rho) e^{jn\phi} \quad (2.1.3)$$

In the above equation prime denotes the derivative with respect to the entire argument. $\eta_0 = \sqrt{\mu_0/\epsilon_0}$ is the impedance of the free space.

The PEMC nature of the cylinder allows the occurrence of cross-polarized component in the scattered field in addition to co-polarized one. Co-polarized components of the scattered field in terms of unknowns are expressed as

$$E_z^s = E_0 \sum_{n=-\infty}^{\infty} j^n b_n H_n^{(1)}(k_0 \rho) e^{jn\phi} \quad (2.1.4)$$

$$H_\phi^s = -\frac{E_0}{j\eta_0} \sum_{n=-\infty}^{\infty} j^n b_n H_n^{(1)'}(k_0 \rho) e^{jn\phi} \quad (2.1.5)$$

and cross-polarized component of the magnetic field in terms of unknown scattering coefficient is

$$H_z^s = -\frac{jE_0}{\eta_0} \sum_{n=-\infty}^{\infty} j^n c_n H_n^{(1)}(k_0 \rho) e^{jn\phi} \quad (2.1.6)$$

Using following Maxwell's equation

$$\mathbf{E} = -\frac{1}{j\omega\epsilon_0} \nabla \times \mathbf{H} \quad (2.1.7)$$

corresponding ϕ component of the scattered electric field may be obtained as

$$E_{\phi}^s = -E_0 \sum_{n=-\infty}^{\infty} j^n c_n H_n^{(1)'}(k_0 \rho) e^{jn\phi} \quad (2.1.8)$$

where b_n and c_n are the unknown scattering coefficients of the co-polarized and cross-polarized scattered fields respectively. Which are to be determined from the imposition of the boundary conditions at the surface of the PEMC cylinder, i.e., at $\rho = a$. The boundary conditions for the circular PEMC cylinder are given by [66]

$$H_t^i + ME_t^i + H_t^s + ME_t^s = 0 \quad (2.1.9)$$

$$\epsilon_0 E_{\rho}^i - M\mu_0 H_{\rho}^i + \epsilon_0 E_{\rho}^s - M\mu_0 H_{\rho}^s = 0 \quad (2.1.10)$$

where M is the admittance of the PEMC cylinder and the subscript t stands for the tangential components. Using tangential components of the fields in (2.1.9) and solving resulting expressions yield coefficients b_n and c_n as given below

$$b_n = -\frac{H_n^{(1)}(k_0 a) J_n'(k_0 a) + M^2 \eta_0^2 J_n(k_0 a) H_n^{(1)'}(k_0 a)}{(1 + M^2 \eta_0^2) H_n^{(1)}(k_0 a) H_n^{(1)'}(k_0 a)} \quad (2.1.11)$$

$$c_n = \frac{2M\eta_0}{\pi k_0 a (1 + M^2 \eta_0^2) H_n^{(1)}(k_0 a) H_n^{(1)'}(k_0 a)} \quad (2.1.12)$$

These coefficients also satisfy the other boundary condition given by (2.1.10). The H-polarized case has not been discussed in analytical formulation but the numerical results are given for both the E-polarized and H-polarized cases.

2.1.1. Numerical results and discussion

In this section, we have reproduced the results given by Ruppin [70] and presented some new results to give better insight of the PEMC nature of the circular cylinder. Fig. 2.2(a) shows the behavior of the co- and cross-polarized components of the normalized monostatic scattering width versus the parameter $M\eta_0$, for E-polarized case. Fig. 2.2(b) shows the corresponding behavior of monostatic scattering width for the case of H-polarization. From these two figures, it is observed that the behavior of the

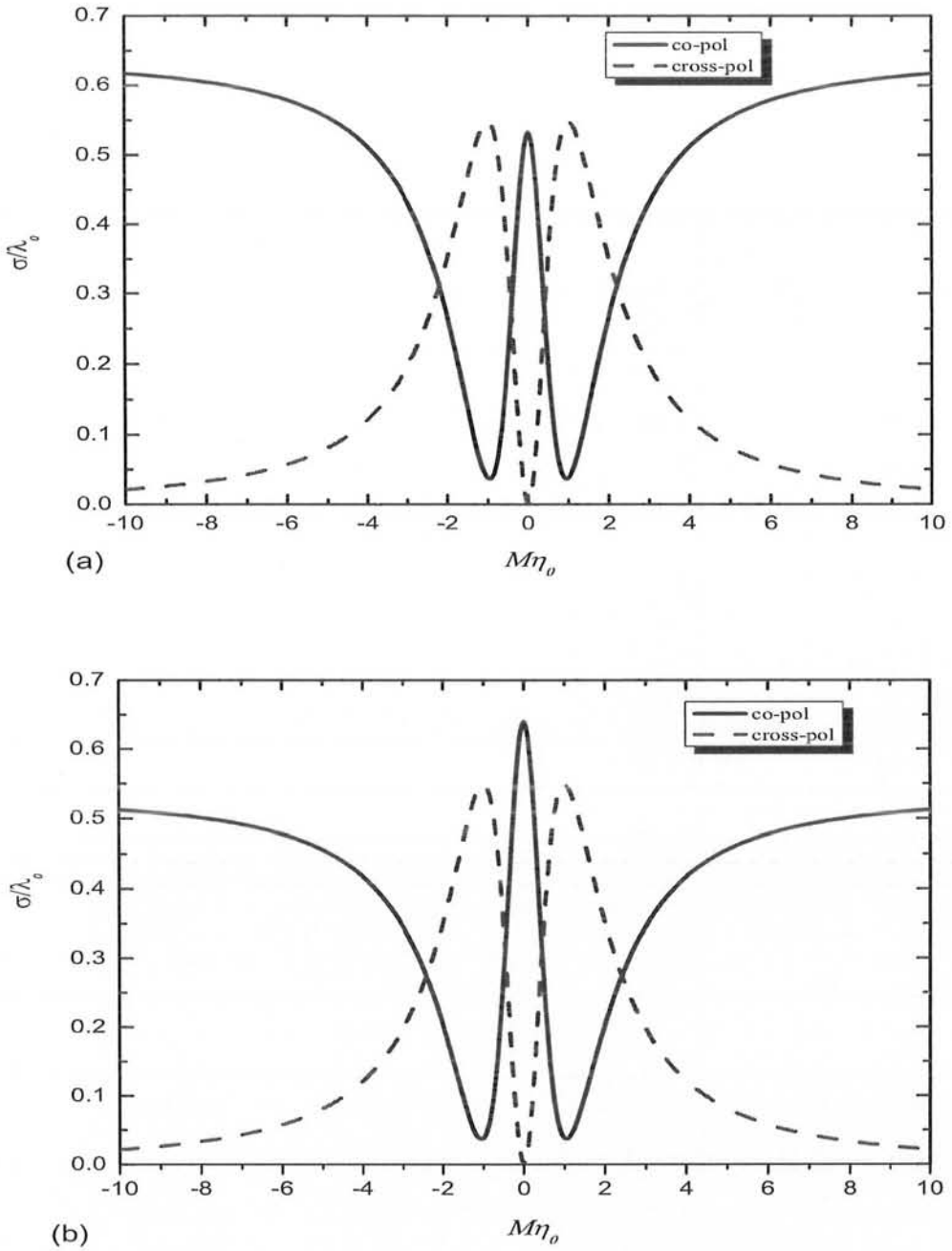
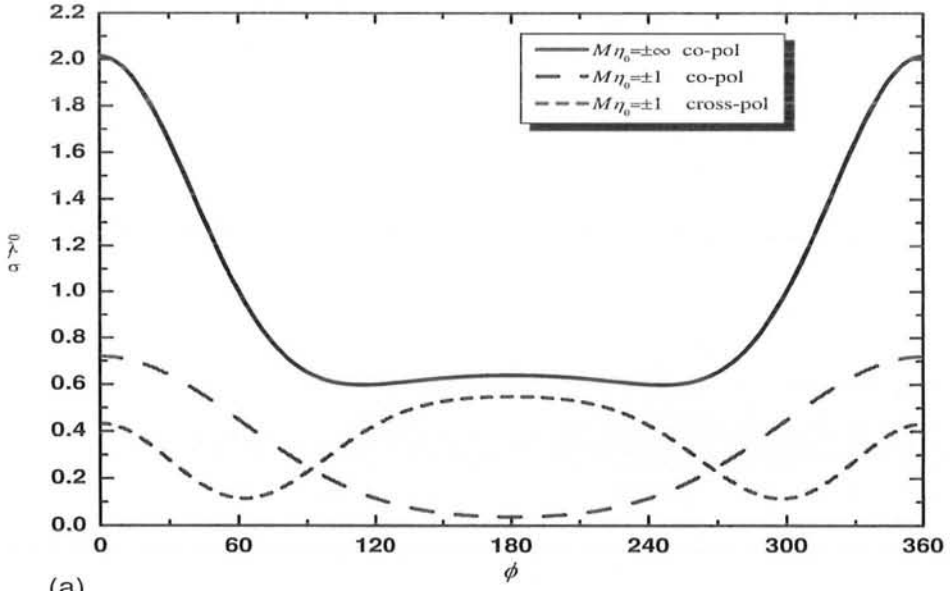
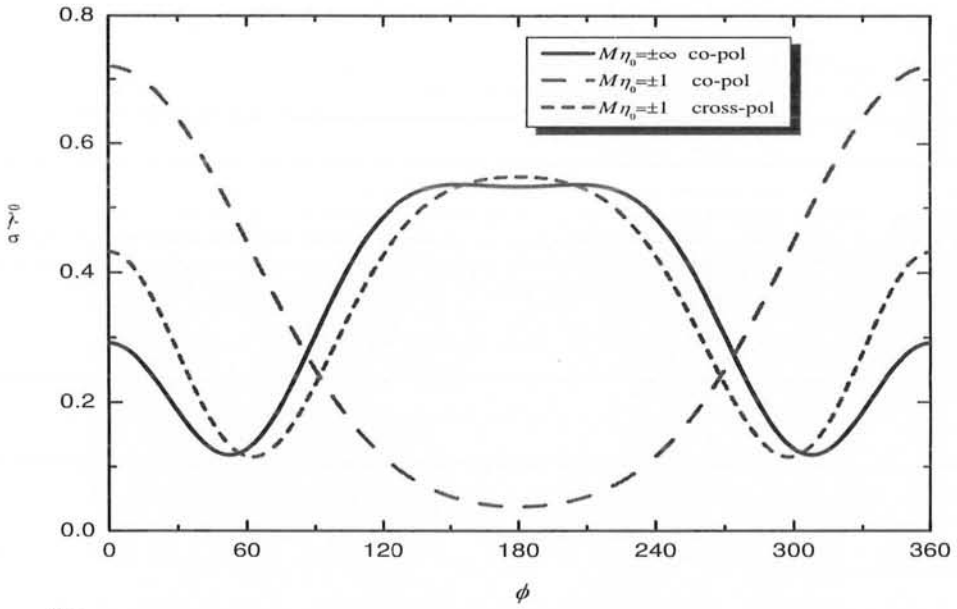


Figure 2.2. Normalized monostatic scattering width of a PEMC cylinder versus $M\eta_0$ with $a = 5$ cm and $f = 1$ GHz. (a) E-pol case, (b) H-pol case.



(a)



(b)

Figure 2.3. Comparison of normalized bistatic scattering width of PEMC ($M\eta_0 = \pm 1$) cylinder with bistatic scattering width of a PEC ($M\eta_0 \rightarrow \pm\infty$) cylinder with, $a = 5$ cm and $f = 1$ GHz. (a) E-pol case, (b) H-pol case.

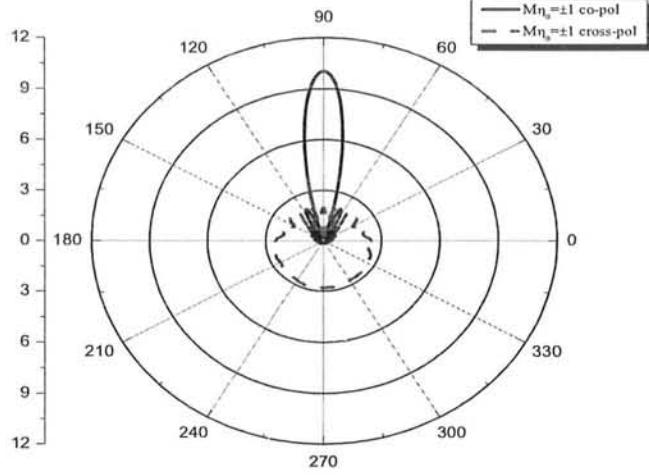


Figure 2.4. Scattered co- and cross-polarized fields from a single PEMC circular cylinder with $k_0 a = 10$.

monostatic scattering width for both co- and cross-polarized components is the same for two types of polarizations. Moreover the cross-polarized component of scattering width shows its maximum value at $M\eta_0 = \pm 1$ while the co-polarized component is minimum there. If we look at the figure 2.2, we see that the scattering width has the same values at every point for both the positive and negative values of $M\eta_0$. Therefore for an uncoated PEMC cylinder it is observed that the behavior of the co- and cross-polarized components does not depend on the sign of the factor $M\eta_0$. For $|M\eta_0| > 1$, the cross-polarized component decreases to zero at $M\eta_0 \rightarrow \pm\infty$, while the co-polarized component increases to a constant value for this variation in $M\eta_0$. Figs. 2.3a and (b) show the comparison of normalized bistatic scattering width of a PEMC cylinder with a PEC cylinder for E-polarized and H-polarized cases respectively. From Fig. 2.3, it is observed that the results obtained for a PEMC cylinder for $M\eta_0 \rightarrow \pm\infty$ are in good agreement with those obtained for a PEC cylinder for both the polarizations. It is noted that PEC cylinder exhibits different behavior for E-polarized H-polarized cases.

However in case of a PEMC cylinder with $M\eta_0 = \pm 1$, it is observed from Fig. 2.3, that both co- and cross-polarized components of the bistatic scattering width show similar behavior for both E-polarized and H-polarized incidences [70]. The radius of the PEMC cylinder is $a = 5\text{cm}$ and the frequency of the incident wave is $f = 1\text{GHz}$ for Figs. 2.2 and 2.3. Fig. 2.4 shows the co- and cross-polarized components of the far-zone scattered field for a large radius parameter, i.e., $k_0a = 10$ and $M\eta_0 = \pm 1$. These field plots are the same as given in [70].

2.2. Parallel PEMC cylinders

Consider N-number of parallel PEMC circular cylinders as shown in Fig. 2.5. These cylinders are placed in free-space defined by permittivity ϵ_0 and permeability μ_0 . Cylinders are supposed to be numbered from 1 to N, while each cylinder is defined by its radius and its location with respect to the local as well as global coordinate systems.

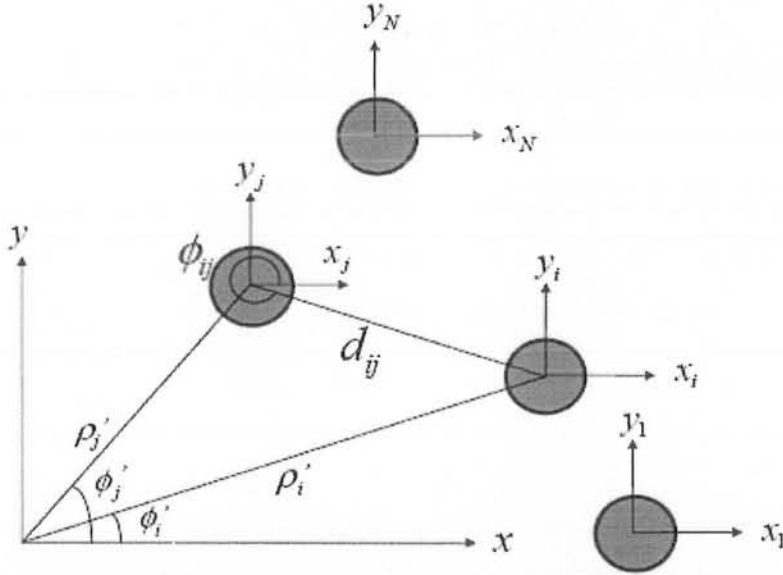


Figure 2.5. Geometry of the parallel PEMC circular cylinders.

Let us take an E-polarized plane wave as incident on the i th cylinder whose center with respect to global coordinates is located at (ρ'_i, ϕ'_i) . Incident field in terms of local

coordinates (ρ_i, ϕ_i) of the i th cylinder is given as

$$\begin{aligned} E_{zi}^{inc}(\rho_i, \phi_i) &= E_0 e^{jk_0 \rho'_i \cos(\phi'_i - \phi_0)} e^{jk_0 \rho_i \cos(\phi_i - \phi_0)} \\ &= e^{jk_0 \rho'_i \cos(\phi'_i - \phi_0)} \sum_{n=-\infty}^{\infty} j^n J_n(k_0 \rho_i) e^{jn(\phi_i - \phi_0)} \end{aligned} \quad (2.2.1)$$

$$H_{\phi i}^{inc}(\rho_i, \phi_i) = -\frac{E_0}{j\eta_0} e^{jk_0 \rho'_i \cos(\phi'_i - \phi_0)} \sum_{n=-\infty}^{\infty} j^n J'_n(k_0 \rho_i) e^{jn(\phi_i - \phi_0)} \quad (2.2.2)$$

where ϕ_0 is the angle of incidence of the plane wave with respect to the positive x-axis. Also (ρ'_i, ϕ'_i) are the coordinates of the i th cylinder with respect to the global coordinates. In response to the incident field, both the co- and cross-polarized field components are scattered by the i th PEMC cylinder.

The co-polarized components of scattered field may be assumed in terms of unknown coefficients as

$$E_{zi}^s = E_0 \sum_{n=-\infty}^{\infty} B_{in} H_n^{(1)}(k_0 \rho_i) e^{jn\phi_i} \quad (2.2.3)$$

$$H_{\phi i}^s = -\frac{E_0}{j\eta_0} \sum_{n=-\infty}^{\infty} B_{in} H_n^{(1)'}(k_0 \rho_i) e^{jn\phi_i} \quad (2.2.4)$$

While the cross-polarized components of the scattered field may be expressed

$$H_{zi}^s = -j \frac{E_0}{\eta_0} \sum_{n=-\infty}^{\infty} C_{in} H_n^{(1)}(k_0 \rho_i) e^{jn\phi_i} \quad (2.2.5)$$

$$E_{\phi i}^s = -E_0 \sum_{n=-\infty}^{\infty} C_{in} H_n^{(1)'}(k_0 \rho_i) e^{jn\phi_i} \quad (2.2.6)$$

where B_{in} and C_{in} are the unknown scattering coefficients for co-polarized and cross-polarized scattered fields respectively, related to of the i th cylinder.

2.2.1. Solution of the unknown scattering coefficients

The unknown scattering coefficients B_{in} and C_{in} may be determined by applying the boundary conditions (2.1.9) and (2.1.10) at the surface of i th PEMC cylinder. For the tangential z -component, boundary condition (2.1.9) yields

$$ME_0 e^{jk_0 \rho'_i \cos(\phi'_i - \phi_0)} \sum_{n=-\infty}^{\infty} j^{-n} J_n(k_0 a_i) e^{jm(\phi_i - \phi_0)} + \frac{E_0}{j\eta_0} \sum_{n=-\infty}^{\infty} C_{in}^{(0)} H_n^{(1)}(k_0 a_i) + ME_0 \sum_{n=-\infty}^{\infty} B_{in}^{(0)} H_n^{(1)}(k_0 a_i) = 0 \quad (2.2.7)$$

And for tangential ϕ -component, equation (2.1.9) yields the following

$$-\frac{E_0}{j\eta_0} e^{jk_0 \rho'_i \cos(\phi'_i - \phi_0)} \sum_{n=-\infty}^{\infty} j^{-n} J'_n(k_0 a_i) e^{jm(\phi_i - \phi_0)} - \frac{E_0}{j\eta_0} \sum_{n=-\infty}^{\infty} B_{in}^{(0)} H_n^{(1)}(k_0 a_i) - ME_0 \sum_{n=-\infty}^{\infty} C_{in}^{(0)} H_n^{(1)}(k_0 a_i) = 0 \quad (2.2.8)$$

The superscript "0" on the scattering coefficients has been used to indicate that the scattering from the i th cylinder is considered due to the incident plane wave only and no interaction with the $N - 1$ cylinders is considered. This scattered field has been termed as the zeroth (0th) order scattered field. After simplification these scattering coefficients may be written as

$$B_{il}^{(0)} = B^I e^{jk_0 \rho'_i \cos(\phi'_i - \phi_0)} j^{-l} e^{-jl\phi_0} \quad (2.2.9)$$

$$C_{il}^{(0)} = C^I e^{jk_0 \rho'_i \cos(\phi'_i - \phi_0)} j^{-l} e^{-jl\phi_0} \quad (2.2.10)$$

where

$$B^I = -\frac{J'_l(k_0 a_i) H_l^{(1)}(k_0 a_i) + M^2 \eta_0^2 J_l(k_0 a_i) H_l'^{(1)}(k_0 a_i)}{(1 + M^2 \eta_0^2) H_l^{(1)}(k_0 a_i) H_l'^{(1)}(k_0 a_i)}$$

$$C^I = \frac{2M\eta_0}{\pi k_0 a_i (1 + M^2 \eta_0^2) H_l^{(1)}(k_0 a_i) H_l'^{(1)}(k_0 a_i)}$$

It can be verified that the coefficients $B_{in}^{(0)}$ and $C_{in}^{(0)}$ also satisfy the boundary condition for the normal component given in (2.1.10).

After evaluating the zeroth order scattered field from all the cylinders separately, interaction between the cylinders is calculated by considering that the interaction is due to mutual scattering among the cylinders. To calculate the first order scattered field from the i th cylinder, the zeroth order scattered fields from rest of the cylinders are considered as the incident fields on i th cylinder. The incident co-polarized fields on the i th cylinder for the first order interaction may be written as

$$E_{zi}^{inc} = E_0 \sum_{\substack{j=1 \\ j \neq i}}^N \sum_{n=-\infty}^{\infty} B_{jn}^{(0)} H_n^{(1)}(k_0 \rho_j) e^{jn\phi_j} \quad (2.2.11)$$

$$H_{\phi i}^{inc} = -\frac{E_0}{j\eta_0} \sum_{\substack{j=1 \\ j \neq i}}^N \sum_{n=-\infty}^{\infty} B_{jn}^{(0)} H_n^{(1)'}(k_0 \rho_j) e^{jn\phi_j} \quad (2.2.12)$$

Similarly the incident cross-polarized fields on the i th cylinder for the first order interaction can be expressed as

$$H_{zi}^{inc} = -j \frac{E_0}{\eta_0} \sum_{\substack{j=1 \\ j \neq i}}^N \sum_{n=-\infty}^{\infty} C_{jn}^{(0)} H_n^{(1)}(k_0 \rho_j) e^{jn\phi_j} \quad (2.2.13)$$

$$E_{\phi i}^{inc} = -E_0 \sum_{\substack{j=1 \\ j \neq i}}^N \sum_{n=-\infty}^{\infty} C_{jn}^{(0)} H_n^{(1)'}(k_0 \rho_j) e^{jn\phi_j} \quad (2.2.14)$$

In response to this co- and cross-polarized incident fields coming from $N-1$ PEMC cylinders, the i th cylinder scatters the first order co- and cross-polarized field components. The first order scattered co-polarized field components are expressed as

$$E_{zi}^{s1} = E_0 \sum_{n=-\infty}^{\infty} B_{in}^{(1)} H_n^{(1)}(k_0 \rho_i) e^{jn\phi_i} \quad (2.2.15)$$

$$H_{\phi i}^{s1} = -\frac{E_0}{j\eta_0} \sum_{n=-\infty}^{\infty} B_{in}^{(1)} H_n^{(1)'}(k_0 \rho_i) e^{jn\phi_i} \quad (2.2.16)$$

While the cross-polarized components of the first order scattered field from the i th cylinder may be expressed

$$H_{zi}^{s1} = -j \frac{E_0}{\eta_0} \sum_{n=-\infty}^{\infty} C_{in}^{(1)} H_n^{(1)}(k_0 \rho_i) e^{jn\phi_i} \quad (2.2.17)$$

$$E_{\phi i}^{s1} = -E_0 \sum_{n=-\infty}^{\infty} C_{in}^{(1)} H_n^{(1)'}(k_0 \rho_i) e^{jn\phi_i} \quad (2.2.18)$$

In order to solve for the first order scattering coefficients $B_{in}^{(1)}$ and $C_{in}^{(1)}$, boundary condition (2.1.9) is applied, taking (2.2.11)-(2.2.14) as the incident field while (2.2.15)-(2.2.18) as the scattered field. Resulting expression for tangential z - component is

$$\begin{aligned} & -j \frac{E_0}{\eta_0} \sum_{\substack{j=1 \\ j \neq i}}^N \sum_{n=-\infty}^{\infty} C_{jn}^{(0)} H_n^{(1)}(k_0 \rho_j) e^{jn\phi_j} \\ & + ME_0 \sum_{\substack{j=1 \\ j \neq i}}^N \sum_{n=-\infty}^{\infty} B_{jn}^{(0)} H_n^{(1)}(k_0 \rho_j) e^{jn\phi_j} \\ & - j \frac{E_0}{\eta_0} \sum_{n=-\infty}^{\infty} C_{in}^{(1)} H_n^{(1)}(k_0 \rho_i) e^{jn\phi_i} \\ & - ME_0 \sum_{n=-\infty}^{\infty} B_{in}^{(1)} H_n^{(1)}(k_0 \rho_i) e^{jn\phi_i} = 0 \end{aligned} \quad (2.2.19a)$$

And for tangential ϕ -component, we get

$$\begin{aligned} & - \frac{E_0}{j\eta_0} \sum_{\substack{j=1 \\ j \neq i}}^N \sum_{n=-\infty}^{\infty} B_{jn}^{(0)} H_n^{(1)'}(k_0 \rho_j) e^{jn\phi_j} \\ & - ME_0 \sum_{\substack{j=1 \\ j \neq i}}^N \sum_{n=-\infty}^{\infty} C_{jn}^{(0)} H_n^{(1)'}(k_0 \rho_j) e^{jn\phi_j} \\ & - \frac{E_0}{j\eta_0} \sum_{n=-\infty}^{\infty} B_{in}^{(1)} H_n^{(1)'}(k_0 \rho_i) e^{jn\phi_i} \\ & - ME_0 \sum_{n=-\infty}^{\infty} C_{in}^{(1)} H_n^{(1)'}(k_0 \rho_i) e^{jn\phi_i} = 0 \end{aligned} \quad (2.2.19b)$$

Unknown scattering coefficients $B_{in}^{(1)}$ and $C_{in}^{(1)}$ can not be calculated from set of equations (2.2.19) as the scattered field from N-1 cylinders is in terms of their local coordinates. It is then required to express the 0th order scattered field from all the N-1 cylinders in terms of the local coordinates of the i th cylinder. For the transformation of the field components, from j th coordinate system to the i th coordinate system, we have to use addition theorem of Hankel functions [14]. Addition theorem of Hankel functions is given below

$$H_n^{(1)}(k\rho_j)e^{jm\phi_j} = \sum_{m=-\infty}^{\infty} J_m(k\rho_i)H_{m-n}^{(1)}(kd_{ij})e^{jm\phi_i}e^{-j(m-n)\phi_{ij}} \quad (2.2.20)$$

where

$$d_{ij}^2 = \rho_i'^2 + \rho_j'^2 - 2\rho_i'\rho_j'\cos(\phi_i' - \phi_j')$$

$$\phi_{ij} = \begin{cases} \cos^{-1} \left[\frac{\rho_j' \cos \phi_j' - \rho_i' \cos \phi_i'}{d_{ij}} \right], & \rho_j' \sin \phi_j' \geq \rho_i' \sin \phi_i' \\ -\cos^{-1} \left[\frac{\rho_j' \cos \phi_j' - \rho_i' \cos \phi_i'}{d_{ij}} \right], & \rho_j' \sin \phi_j' < \rho_i' \sin \phi_i' \end{cases}$$

After some mathematical calculations the first order scattering coefficients $B_{in}^{(1)}$ and $C_{in}^{(1)}$ for the i th cylinder are

$$B_{il}^{(1)} = B^I \sum_{\substack{j=1 \\ j \neq i}}^N \sum_{n=-\infty}^{\infty} B_{jn}^{(0)} H_{l-n}^{(1)}(k_0 d_{ij}) e^{-j(l-n)\phi_{ij}} \\ + C^{II} \sum_{\substack{j=1 \\ j \neq i}}^N \sum_{n=-\infty}^{\infty} C_{jn}^{(0)} H_{l-n}^{(1)}(k_0 d_{ij}) e^{-j(l-n)\phi_{ij}} \quad (2.2.21)$$

$$C_{il}^{(1)} = B^{II} \sum_{\substack{j=1 \\ j \neq i}}^N \sum_{n=-\infty}^{\infty} C_{jn}^{(0)} H_{l-n}^{(1)}(k_0 d_{ij}) e^{-j(l-n)\phi_{ij}} \\ + C^I \sum_{\substack{j=1 \\ j \neq i}}^N \sum_{n=-\infty}^{\infty} B_{jn}^{(0)} H_{l-n}^{(1)}(k_0 d_{ij}) e^{-j(l-n)\phi_{ij}} \quad (2.2.22)$$

where

$$B^{\text{II}} = -\frac{J_l(k_0 a_i) H_l'^{(1)}(k_0 a_i) + M^2 \eta_0^2 J_l'(k_0 a_i) H_l^{(1)}(k_0 a_i)}{(1 + M^2 \eta_0^2) H_l^{(1)}(k_0 a_i) H_l'^{(1)}(k_0 a_i)}$$

$$C^{\text{II}} = -\frac{2M\eta_0}{\pi k_0 a_i (1 + M^2 \eta_0^2) H_l^{(1)}(k_0 a_i) H_l'^{(1)}(k_0 a_i)}$$

After solving for the unknown first order scattering coefficients, for all the N cylinders, we can continue on to find the coefficients of the second order interaction. A recurrence relation is developed, where the coefficients in the p th interaction depend on the coefficients of the $(p - 1)$ th interaction. Application of boundary condition (2.1.9) on the z - components of the fields, for p th order scattering coefficients yields

$$ME_0 \sum_{\substack{j=1 \\ j \neq i}}^N \sum_{n=-\infty}^{\infty} B_{jn}^{(p-1)} J_l(k_0 a_i) H_{l-n}^{(1)}(k_0 d_{ij}) e^{-j(l-n)\phi_{ij}}$$

$$+ ME_0 \sum_{n=-\infty}^{\infty} B_{in}^{(p)} H_n^{(1)}(k_0 a_i) e^{jn\phi_i}$$

$$- j \frac{E_0}{\eta_0} \sum_{\substack{j=1 \\ j \neq i}}^N \sum_{n=-\infty}^{\infty} C_{jn}^{(p-1)} J_l(k_0 a_i) H_{l-n}^{(1)}(k_0 d_{ij}) e^{-j(l-n)\phi_{ij}}$$

$$- j \frac{E_0}{\eta_0} \sum_{n=-\infty}^{\infty} C_{in}^{(p)} H_n^{(1)}(k_0 a_i) e^{jn\phi_i} = 0 \quad (2.2.23a)$$

And for tangential ϕ -component, equation (2.1.9) gets the form

$$- ME_0 \sum_{\substack{j=1 \\ j \neq i}}^N \sum_{n=-\infty}^{\infty} B_{jn}^{(p-1)} J_l'(k_0 a_i) H_{l-n}^{(1)}(k_0 d_{ij}) e^{-j(l-n)\phi_{ij}}$$

$$- ME_0 \sum_{n=-\infty}^{\infty} B_{in}^{(p)} H_n'^{(1)}(k_0 a_i) e^{jn\phi_i}$$

$$- \frac{E_0}{j\eta_0} \sum_{\substack{j=1 \\ j \neq i}}^N \sum_{n=-\infty}^{\infty} C_{jn}^{(p-1)} J_l'(k_0 a_i) H_{l-n}^{(1)}(k_0 d_{ij}) e^{-j(l-n)\phi_{ij}}$$

$$- \frac{E_0}{j\eta_0} \sum_{n=-\infty}^{\infty} C_{in}^{(p)} H_n'^{(1)}(k_0 a_i) e^{jn\phi_i} = 0 \quad (2.2.23b)$$

Solving above set of equations simultaneously gives the unknown scattering coefficients

$$\begin{aligned}
 B_{il}^{(p)} &= B^I \sum_{\substack{j=1 \\ j \neq i}}^N \sum_{n=-\infty}^{\infty} B_{jn}^{(p-1)} H_{l-n}^{(1)}(k_0 d_{ij}) e^{-j(l-n)\phi_{ij}} \\
 &+ C^{II} \sum_{\substack{j=1 \\ j \neq i}}^N \sum_{n=-\infty}^{\infty} C_{jn}^{(p-1)} H_{l-n}^{(1)}(k_0 d_{ij}) e^{-j(l-n)\phi_{ij}} \quad (2.2.24)
 \end{aligned}$$

$$\begin{aligned}
 C_{il}^{(p)} &= B^{II} \sum_{\substack{j=1 \\ j \neq i}}^N \sum_{n=-\infty}^{\infty} C_{jn}^{(p-1)} H_{l-n}^{(1)}(k_0 d_{ij}) e^{-j(l-n)\phi_{ij}} \\
 &+ C^I \sum_{\substack{j=1 \\ j \neq i}}^N \sum_{n=-\infty}^{\infty} B_{jn}^{(p-1)} H_{l-n}^{(1)}(k_0 d_{ij}) e^{-j(l-n)\phi_{ij}} \quad (2.2.25)
 \end{aligned}$$

From above results, it is obvious that the p th scattering coefficients depend on the $(p-1)$ th scattering coefficients and the physical nature of the material of the interacting cylinders. Performing the same procedure for rest of the cylinders it is possible to write these coefficients in a matrix form, such that

$$[B^p] = [TB] [B^{p-1}] + [RB] [C^{p-1}] \quad (2.2.26)$$

$$[C^p] = [TC] [B^{p-1}] + [RC] [C^{p-1}] \quad (2.2.27)$$

where the B and C are given in the vector form

$$\begin{aligned}
 [B^p] &= \begin{pmatrix} [B_1^p] \\ [B_i^p] \\ [B_N^p] \end{pmatrix}, & [B^{p-1}] &= \begin{pmatrix} [B_1^{p-1}] \\ [B_i^{p-1}] \\ [B_N^{p-1}] \end{pmatrix}, & [C^{p-1}] &= \begin{pmatrix} [C_1^{p-1}] \\ [C_i^{p-1}] \\ [C_N^{p-1}] \end{pmatrix} \\
 [C^p] &= \begin{pmatrix} [C_1^p] \\ [C_i^p] \\ [C_N^p] \end{pmatrix}, & [B^{p-1}] &= \begin{pmatrix} [B_1^{p-1}] \\ [B_i^{p-1}] \\ [B_N^{p-1}] \end{pmatrix}, & [C^{p-1}] &= \begin{pmatrix} [C_1^{p-1}] \\ [C_i^{p-1}] \\ [C_N^{p-1}] \end{pmatrix}
 \end{aligned}$$

The matrices TB, RB, TC and RC, all get the following form

$$[T] = \begin{pmatrix} [0] & \cdot & [T_{1,j}] & \cdot & [T_{1,N}] \\ [T_{2,1}] & \cdot & [T_{2,j}] & \cdot & [T_{2,N}] \\ \cdot & \cdot & \cdot & [T_{i,j}] & \cdot \\ \cdot & \cdot & \cdot & [0] & \cdot \\ [T_{N,1}] & \cdot & [T_{N,j}] & \cdot & [0] \end{pmatrix}$$

where

$$[T_{i,j}] = \begin{pmatrix} T_{i,j}^{1,1} & \cdot & \cdot & \cdot & \cdot & T_{i,j}^{1,n} \\ \cdot & \cdot & \cdot & \cdot & T_{i,j}^{1,n} & \cdot \\ \cdot & \cdot & \cdot & \cdot & \cdot & \cdot \\ T_{i,j}^{m,1} & \cdot & \cdot & \cdot & \cdot & T_{i,j}^{m,n} \\ \cdot & \cdot & \cdot & \cdot & \cdot & \cdot \end{pmatrix}$$

with

$$i \in (1, N)$$

$$j \in (1, N)$$

$$m \in (1, 2Q_i + 1)$$

$$n \in (1, 2Q_j + 1)$$

and

$$TB_{ij}^{l,n} = B^I H_{l-n}^{(1)}(k_0 d_{ij}) e^{-j(l-n)\phi_{ij}}$$

$$RB_{ij}^{l,n} = C^I H_{l-n}^{(1)}(k_0 d_{ij}) e^{-j(l-n)\phi_{ij}}$$

$$TC_{ij}^{l,n} = C^I H_{l-n}^{(1)}(k_0 d_{ij}) e^{-j(l-n)\phi_{ij}}$$

$$RC_{ij}^{l,n} = B^I H_{l-n}^{(1)}(k_0 d_{ij}) e^{-j(l-n)\phi_{ij}}$$

Here the matrix $[T]$ is a square matrix with diagonal sub matrices $[0]$. The sub matrices $[T_{i,j}]$ depend on the radii and type of the cylinders. We have used the cylinders of the same radii and material, i.e., PEMC circular cylinders.

Thus the total unknown scattering coefficients may be written as

$$B_{in}^{tot} = \sum_{p=1}^Q B_{in}^p, \quad C_{in}^{tot} = \sum_{p=1}^Q C_{in}^p \quad (2.2.28)$$

where Q is an arbitrary large number which satisfies the relation $3 \leq Q_i \leq 3k_0a_i + 3$, in order to have a convergent solution. The co- and cross-polarized field components of the total scattered field are given by

$$E_{zi}^s = E_0 \sum_{i=1}^N \sum_{n=-\infty}^{\infty} B_{in}^{tot} H_n^{(1)}(k_0\rho) e^{jn\phi} \quad (2.2.29)$$

$$E_{\phi i}^s = -E_0 \sum_{i=1}^N \sum_{n=-\infty}^{\infty} C_{in}^{tot} H_n^{(1)'}(k_0\rho) e^{jn\phi} \quad (2.2.30)$$

Far field scattering patterns of the co- and cross-polarized components may be obtained by using the asymptotic expressions of the Hankel functions and their derivatives for large arguments and are given [2] as

$$H_n^{(1)}(\alpha) \simeq \sqrt{\frac{2}{\pi\alpha}} j^{-n} e^{j\alpha - j\pi/4}, \quad \alpha \rightarrow \infty \quad (2.2.31a)$$

$$H_n^{(1)'}(\alpha) \simeq \sqrt{\frac{2}{\pi\alpha}} j^{-n+1} e^{j\alpha - j\pi/4}, \quad \alpha \rightarrow \infty \quad (2.2.31b)$$

Transforming the scattered fields from all the cylinders into global coordinates and applying (2.2.31) on the scattered field, the far-zone scattered field is given by

$$E_z^s = E_0 \sqrt{\frac{2j}{\pi k_0\rho}} e^{jk_0\rho} P_{\parallel}(\phi) \quad (2.2.32)$$

$$E_{\phi}^s = -E_0 \sqrt{\frac{2j}{\pi k_0\rho}} e^{jk_0\rho} P_{\perp}(\phi) \quad (2.2.33)$$

where

$$P_{\parallel}(\phi) = \sum_{i=1}^N e^{jk_0\rho_i' \cos(\phi_i' - \phi)} \sum_{n=-\infty}^{\infty} j^{-n} B_n^{tot} e^{j(n\phi - \pi/4)}$$

$$P_{\perp}(\phi) = \sum_{i=1}^N e^{jk_0\rho_i' \cos(\phi_i' - \phi)} \sum_{n=-\infty}^{\infty} j^{-n+1} C_n^{tot} e^{j(n\phi - \pi/4)}$$

Equations (2.2.32) and (2.2.33) represent the far-zone co- and cross-polarized components of the scattered field due to all the cylinders, taking into account all the interactions among them. The H-polarized incidence case can be deduced from E-polarized case using the duality theorem. The expressions of H_z and E_{ϕ} fields in H-polarized case correspond to the E_z and H_{ϕ} field expressions in the E-polarized incidence case.

2.2.2. Numerical results and discussion

Five PEMC circular cylinders of equal radii ($a_i = 0.1\lambda_0$) with $d = 0.75\lambda_0$ as spacing between their centers have been considered. Cylinders are arranged in four different shapes, i.e., horizontally, vertically, star-like and corner reflector, both the E-polarized and H-polarized excitations have been used. It is observed that the co- and cross-polarized components of the scattered field due to multiple PEMC cylinders show similar behavior for both E-polarized and H-polarized cases at $M\eta_0 = \pm 1$. Therefore the plots for the H-polarized case are given for $M\eta_0 = \pm 1.5$. In all the plots, solid line shows co-polarized component for the case of $M\eta_0 \rightarrow \pm\infty$. The dashed line is for the co-polarized component while the short dashed line exhibits the cross-polarized component taking $M\eta_0 = \pm 1$. Fig. 2.6 shows the co- and cross-polarized components of the far-zone scattered field, for the five horizontally lying PEMC circular cylinders. Fig. 2.6(a) shows the co- and cross-polarized components of the far-zone scattered field for horizontally lying PEMC circular cylinders with different $M\eta_0$, while Fig. 2.6(b) shows the co-polarized component of the far-zone scattered field for $M\eta_0 = 0$. In Fig. 2.6(c) this configuration has been analyzed for the H-polarized case with $M\eta_0 = \pm 1.5$.

In Fig. 2.7, the variations of co- and cross-polarized components are shown for five vertically oriented PEMC cylinders. Fig. 2.7(a) shows the co- and cross-polarized components of the far-zone scattered field when different values of $M\eta_0$ are taken and Fig. 2.7(b) shows the co-polarized component of the far-zone scattered field for $M\eta_0 = 0$. In Fig. 2.7(c) the same geometry has been analyzed for the H-polarized case with $M\eta_0 = \pm 1.5$.

Fig. 2.8 exhibits the variations of co- and cross-polarized components for five PEMC cylinders in a star-like geometry. Fig. 2.8(a) shows the co- and cross-polarized components of the far-zone scattered field for different $M\eta_0$ while Fig. 2.8(b) shows the co-polarized component of the far-zone scattered field when $M\eta_0 = 0$. And Fig. 2.8(c)

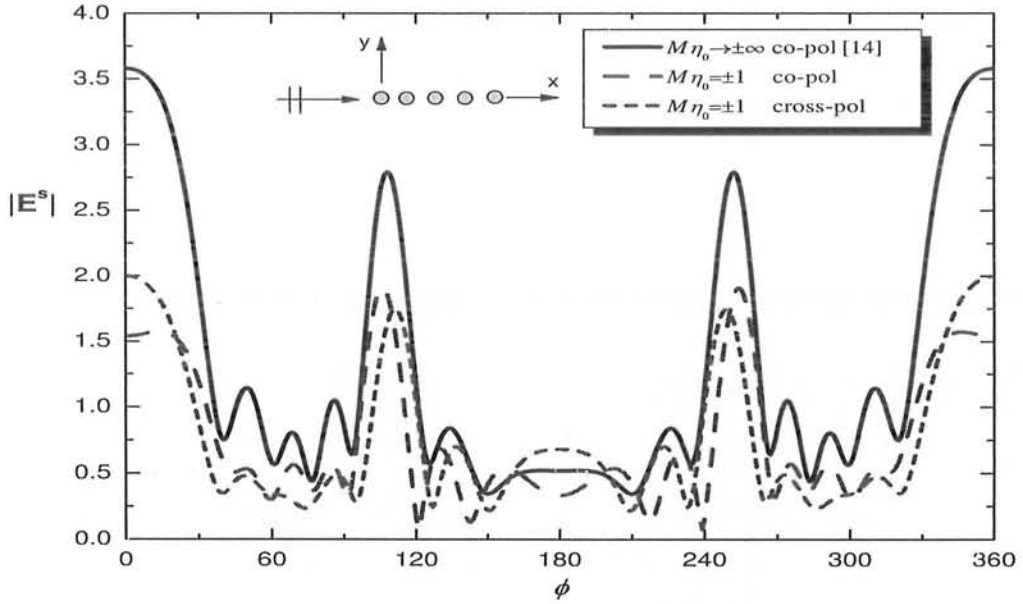


Figure 2.6(a). Co- and cross-polarized components (E-pol) of the Far-zone scattered field due to five horizontally lying PEMC circular cylinders for different $M\eta_0$.

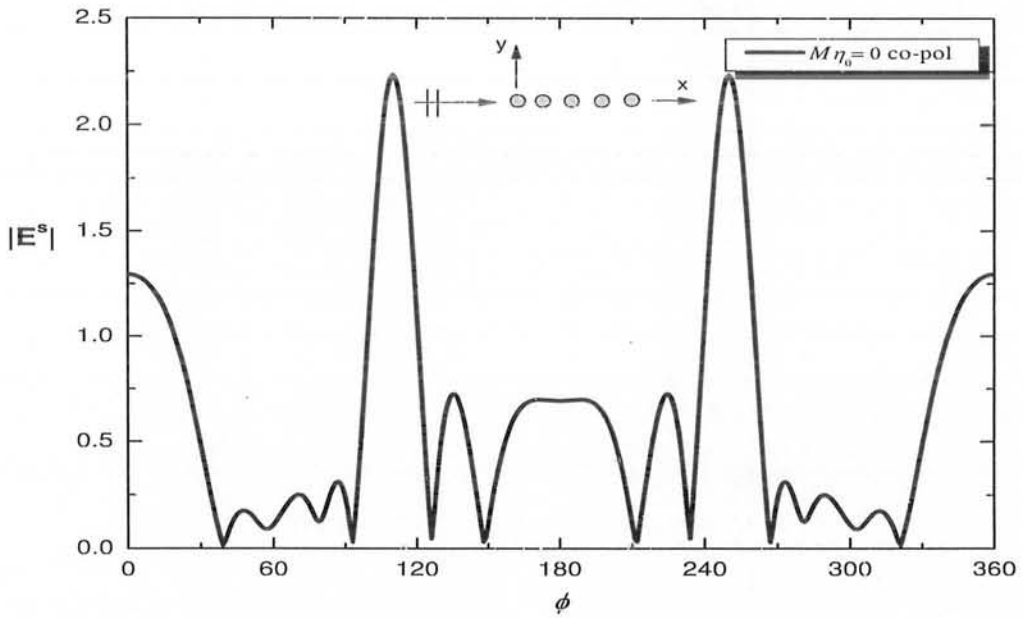


Figure 2.6(b). Co-polarized components (E-pol) of the Far-zone scattered field due to five horizontally lying PEMC circular cylinders, for $M\eta_0 = 0$.

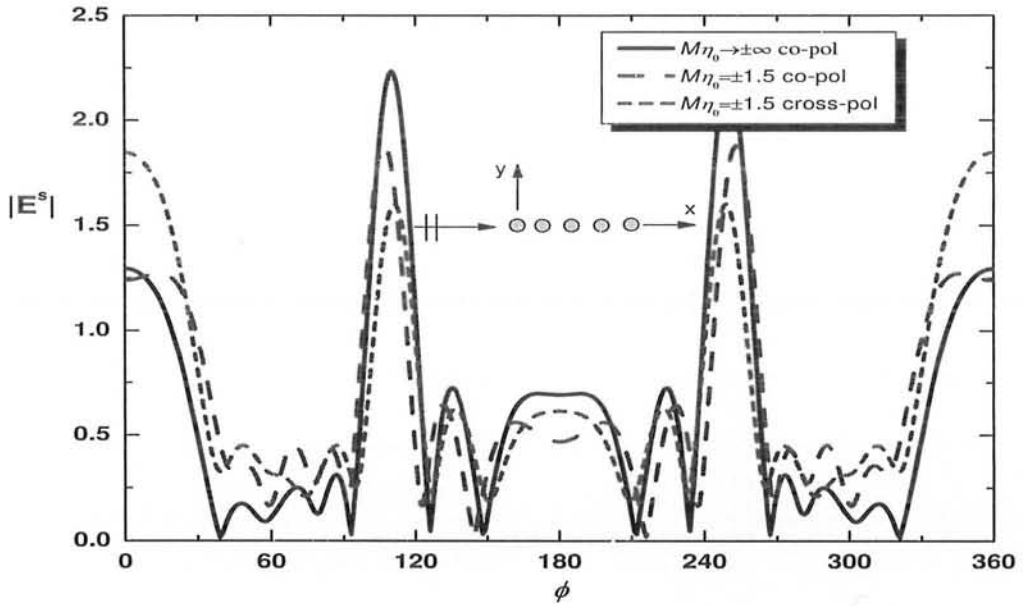


Figure 2.6(c). Co- and cross-polarized components (H-pol) of the Far-zone scattered field due to five horizontally lying PEMC circular cylinders for different $M\eta_0$.

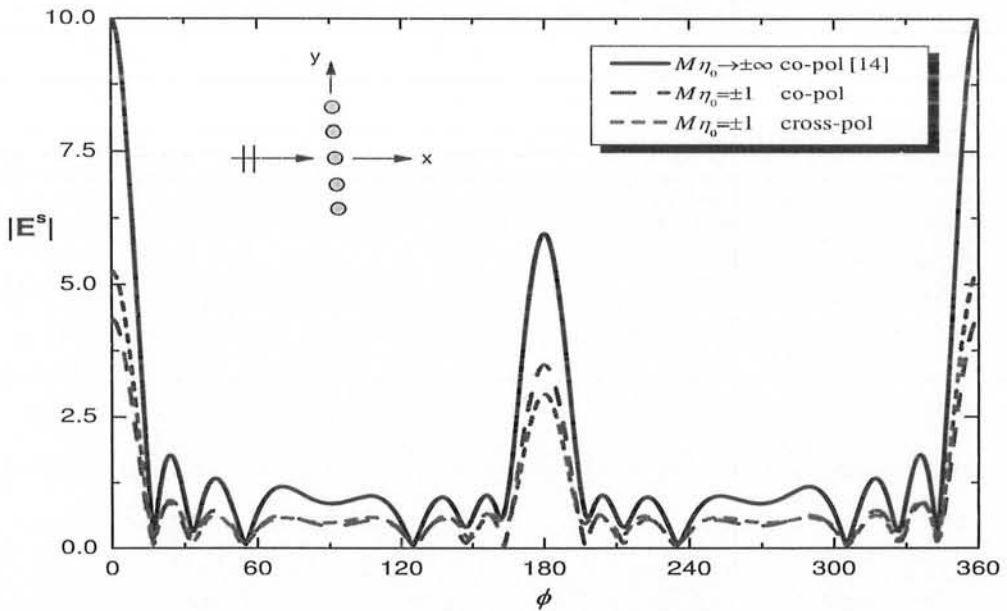


Figure 2.7(a). Co- and cross-polarized components (E-pol) of the Far-zone scattered field due to five vertically oriented PEMC circular cylinders for different $M\eta_0$.

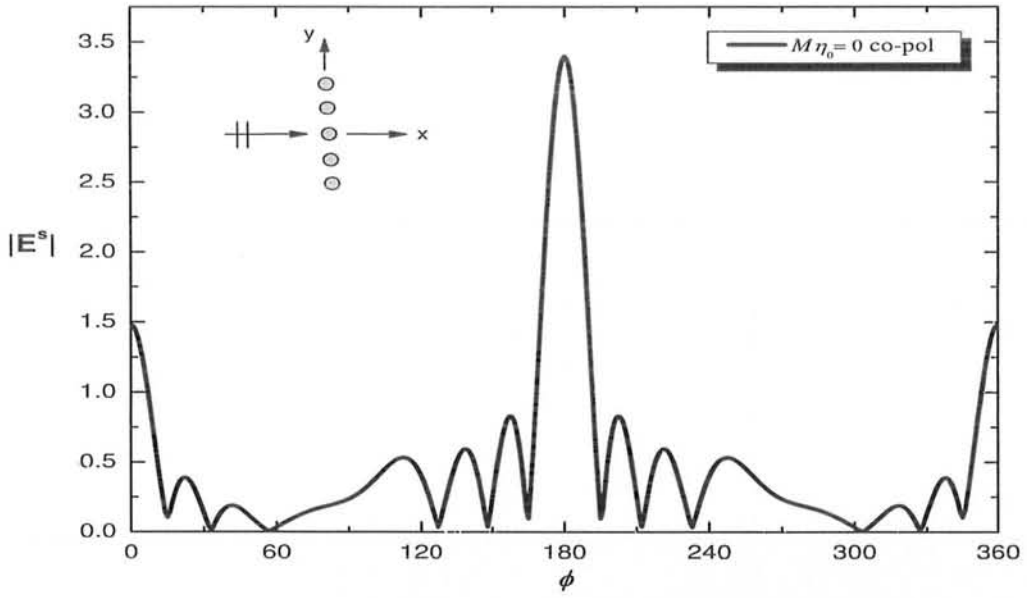


Figure 2.7(b). Co-polarized components (E-pol) of the Far-zone scattered field due to five vertically oriented PEMC circular cylinders for $M\eta_0 = 0$.

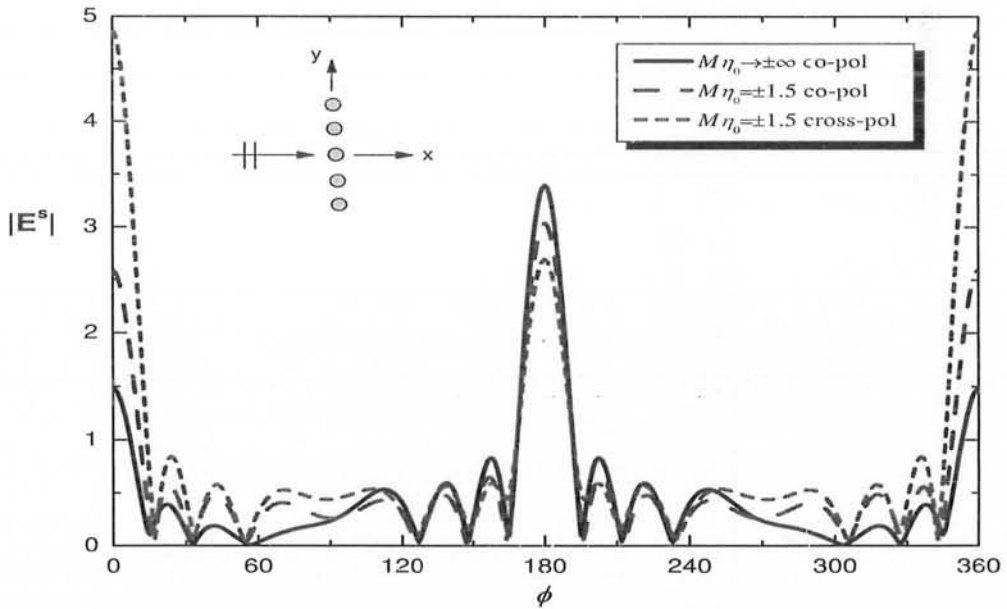


Figure 2.7(c). Co- and cross-polarized components (H-pol) of the Far-zone scattered field due to vertically oriented PEMC circular cylinders for different $M\eta_0$.

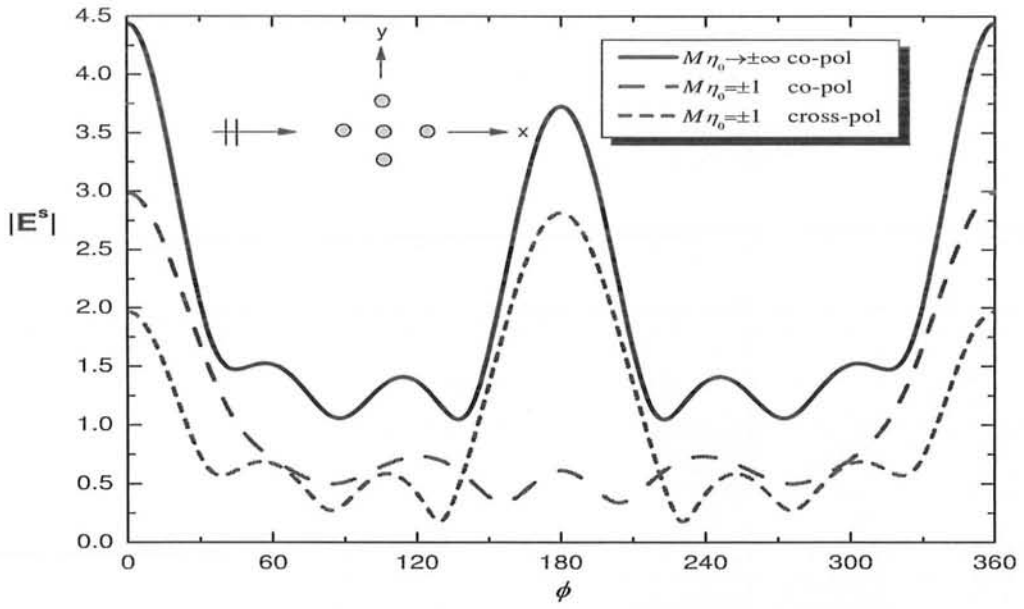


Figure 2.8(a). Co- and cross-polarized components (E-pol) of the Far-zone scattered field of a star-like configuration of PEMC circular cylinders for different $M\eta_0$.

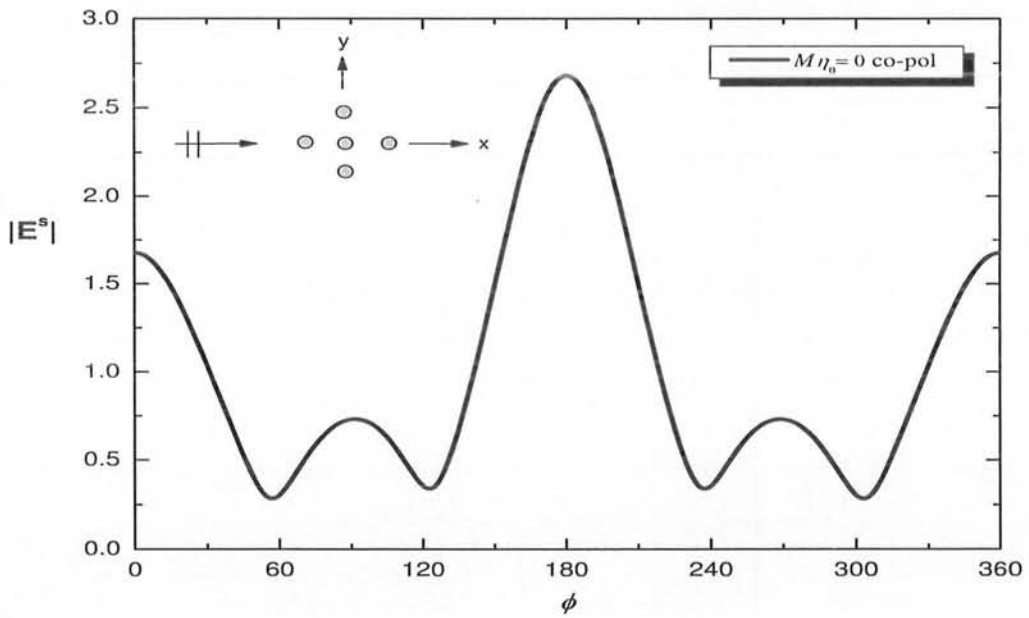


Figure 2.8(b). Co-polarized components (E-pol) of the Far-zone scattered field of a star-like configuration of PEMC circular cylinders for $M\eta_0 = 0$.

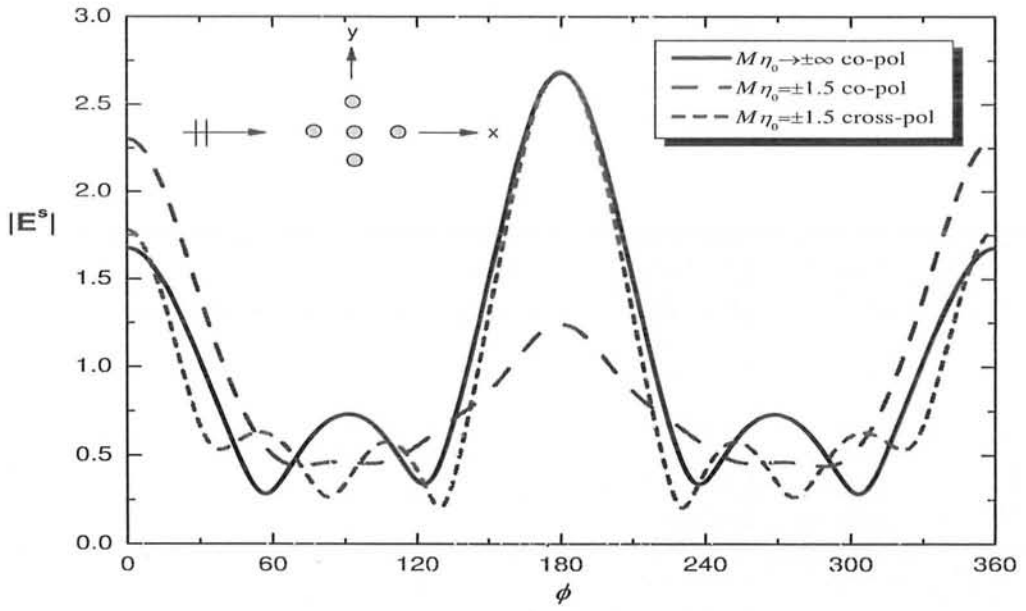


Figure 2.8(c). Co- and cross-polarized components (H-pol) of the Far-zone scattered field of a star-like configuration of PEMC circular cylinders for different $M\eta_0$.

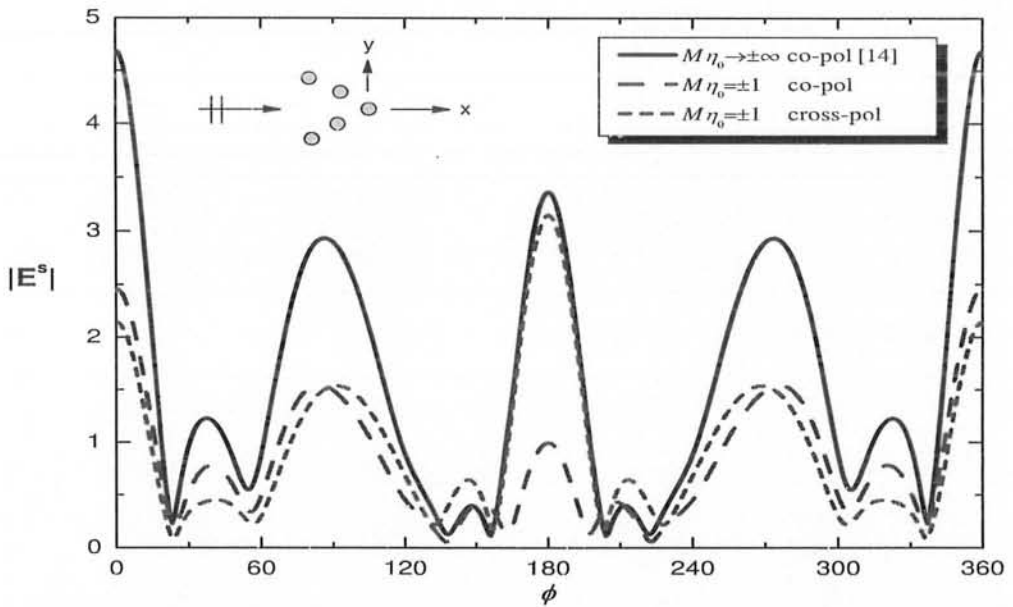


Figure 2.9(a). Co- and cross-polarized components (E-pol) of the Far-zone scattered field of a PEMC corner reflector made by circular cylinders for different $M\eta_0$.

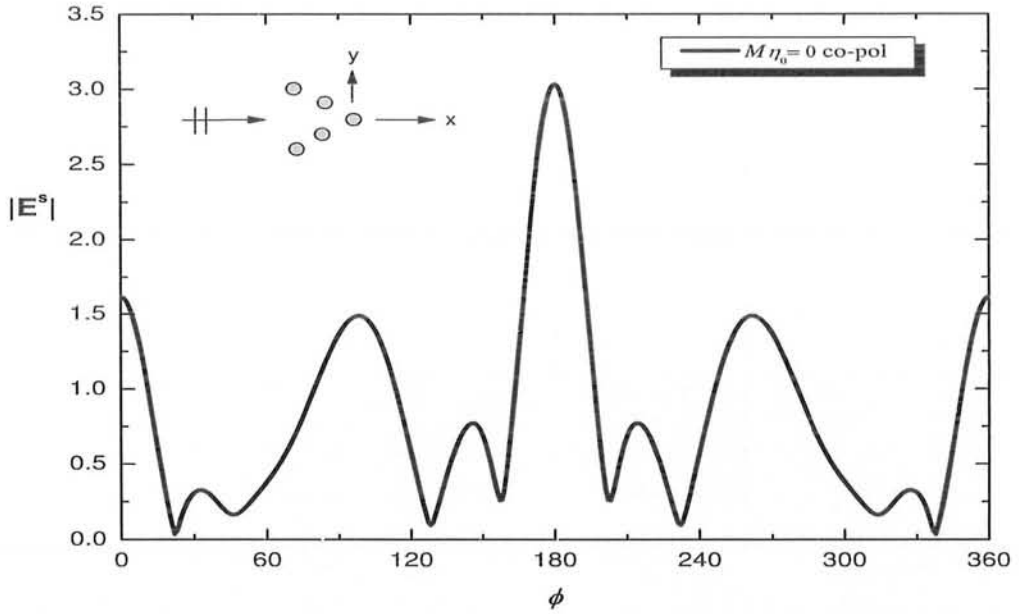


Figure 2.9(b). Co-polarized components (E-pol) of the Far-zone scattered field of a PEMC corner reflector made by circular cylinders for $M\eta_0 = 0$.

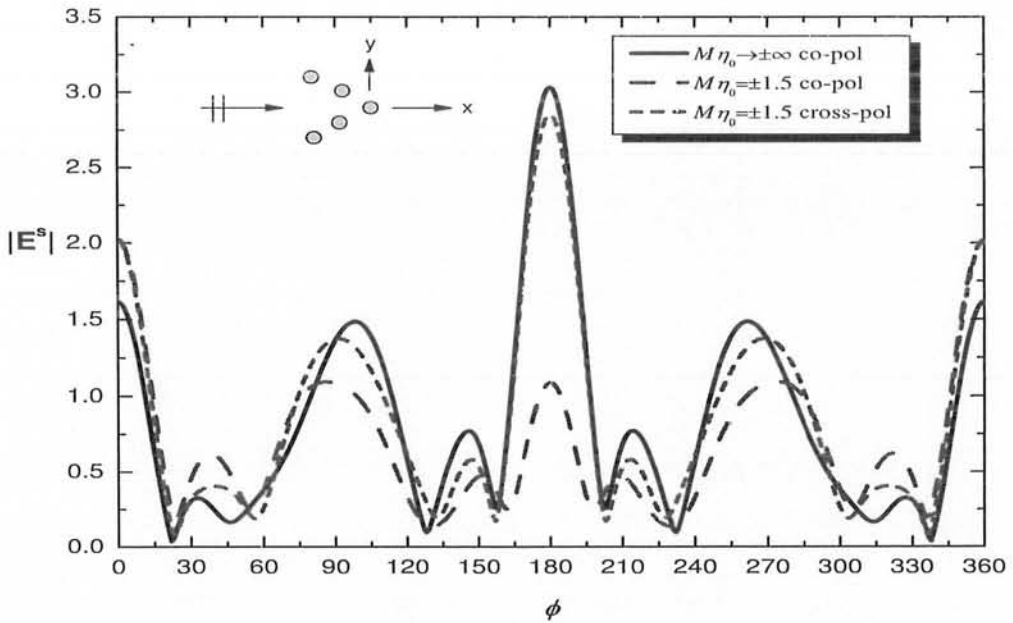


Figure 2.9(c). Co- and cross-polarized components (H-pol) of the Far-zone scattered field of a PEMC corner reflector made by circular cylinders for different $M\eta_0$.

gives the behavior of the same arrangement of the cylinders in response to H-polarized case when $M\eta_0 = \pm 1.5$ has been chosen.

Fig. 2.9 shows the behaviors of the co- and cross-polarized components due to corner reflector made by PEMC circular cylinders, for different $M\eta_0$. Figs. 2.9(a) and (b) show the co- and cross-polarized components of the far-zone scattered field in case of E-polarization for different $M\eta_0$ and $M\eta_0 = 0$, respectively. Fig. 2.9(c) presents the scattering characteristics of the same configuration for the H-polarization with $M\eta_0 = \pm 1.5$. It is observed from these figures that the forward and backward scattering patterns of the field scattered from different combinations of PEMC cylinders are different from those of PEC cylinders. This behavior may be exploited in the defence technology.

2.3. Two dimensional rectangular PEMC strip and strip grating

Two dimensional rectangular PEMC strip and PEMC strip grating, simulated by parallel PEMC circular cylinders, have been analyzed in this section. The diameters of the cylinders is taken equal to the thickness of the strip. The width of the strip determines the number of cylinders used for the simulation. In this section, only the numerical results are presented. Both the PEMC strip and strip grating are made by

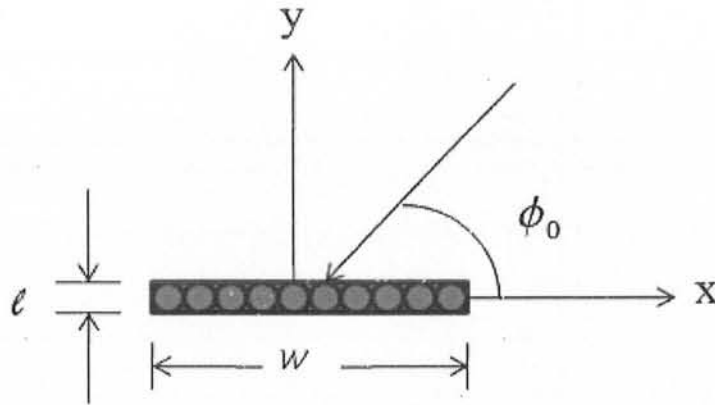


Figure 2.10(a) Rectangular PEMC strip simulated by circular cylinders.

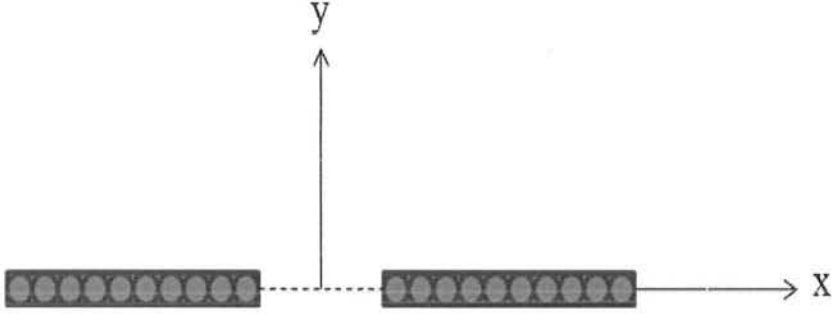


Figure 2.10(b) Two rectangular PEMC strips simulated by circular cylinders.

joining the circular cylinders together as shown in Fig. 2.10(a). Two or more strips of this kind have been used to form a PEMC strip grating as shown in Fig. 2.10(b).

2.3.1. Numerical results and discussion

In this section some numerical results are presented for E-polarized scattering by a PEMC strip and PEMC strip grating, simulated by PEMC circular cylinders with radii $a = 0.05\lambda_0$. In all the plots presented here, the thickness of the strip has been kept constant which is $w = 0.1\lambda_0$ and 20 PEMC circular cylinders are used to simulate it. Also the angles of incidence have been taken as $\phi_i = 0^0, 60^0$ and 90^0 in figures for the PEMC strip. Fig. 2.11(a) shows the co-polarized component of the diffracted field of a PEMC strip with $M\eta_0 = 0$, i.e., the PMC case. Fig. 2.11(b) presents the co-polarized components of the diffracted field of a PEMC strip with $M\eta_0 \rightarrow \pm\infty$, i.e., the PEC case. In these two figures, the cross-polarized component is zero. The co- and cross-polarized components of the diffracted field of a PEMC strip, for $M\eta_0 = \pm 1$, have been presented in Fig. 2.12. Co-polarized component of the diffracted field of a PEMC strip with $M\eta_0 = \pm 1$ has been shown in Fig. 2.12(a). While the cross-polarized component of the diffracted field of a PEMC strip with $M\eta_0 = \pm 1$ is shown in Fig. 2.12(b).

Figs. 2.13-2.15, show the co- and cross-polarized components of the diffracted field

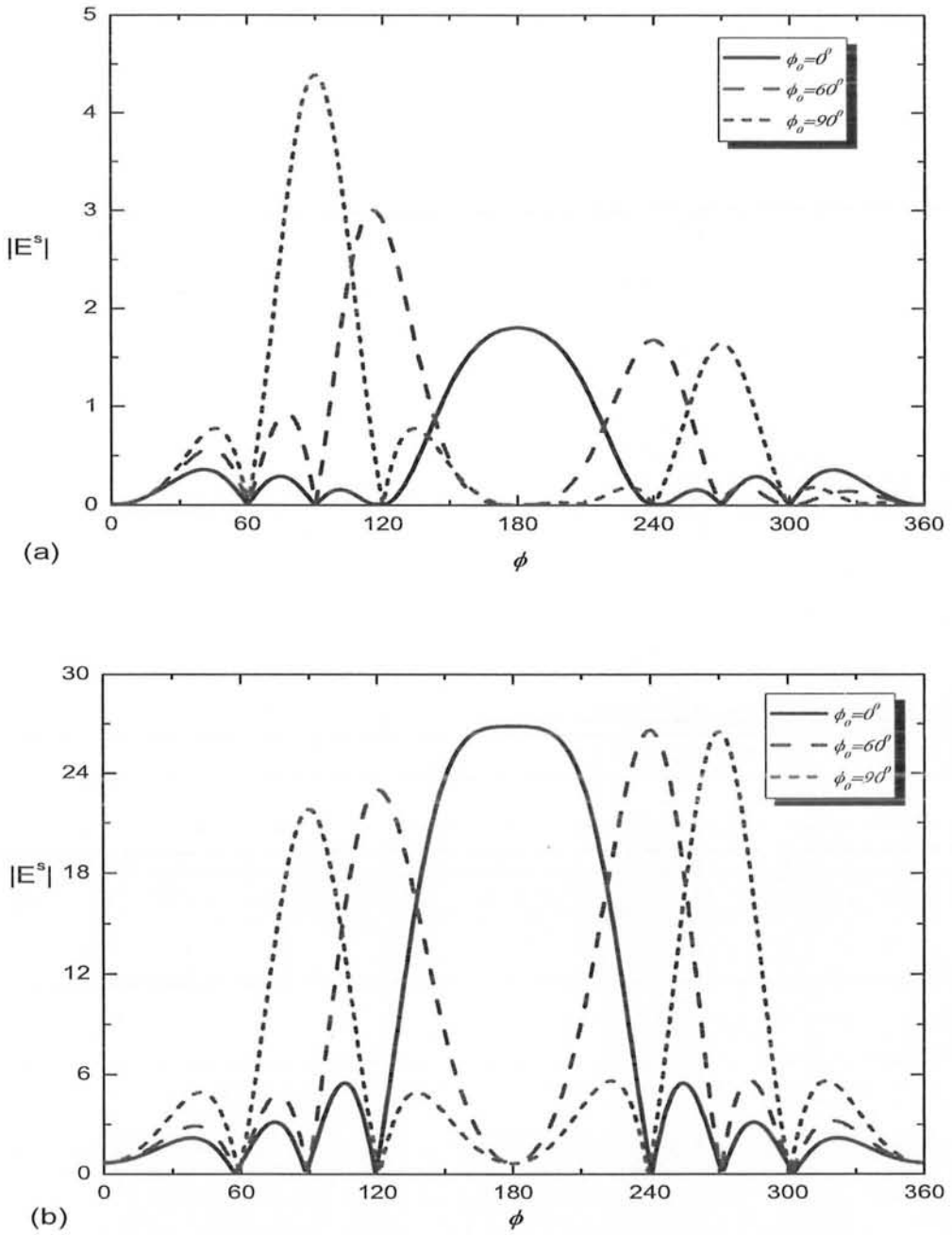


Figure 2.11. Co-pol component (E-pol) of far-zone scattered field from a PEMC strip simulated by 20 PEMC circular cylinders, with $a = 0.05\lambda_0$ and $l = 0.1\lambda_0$. (a) $M\eta_0 = 0$ (b) $M\eta_0 \rightarrow \pm\infty$.

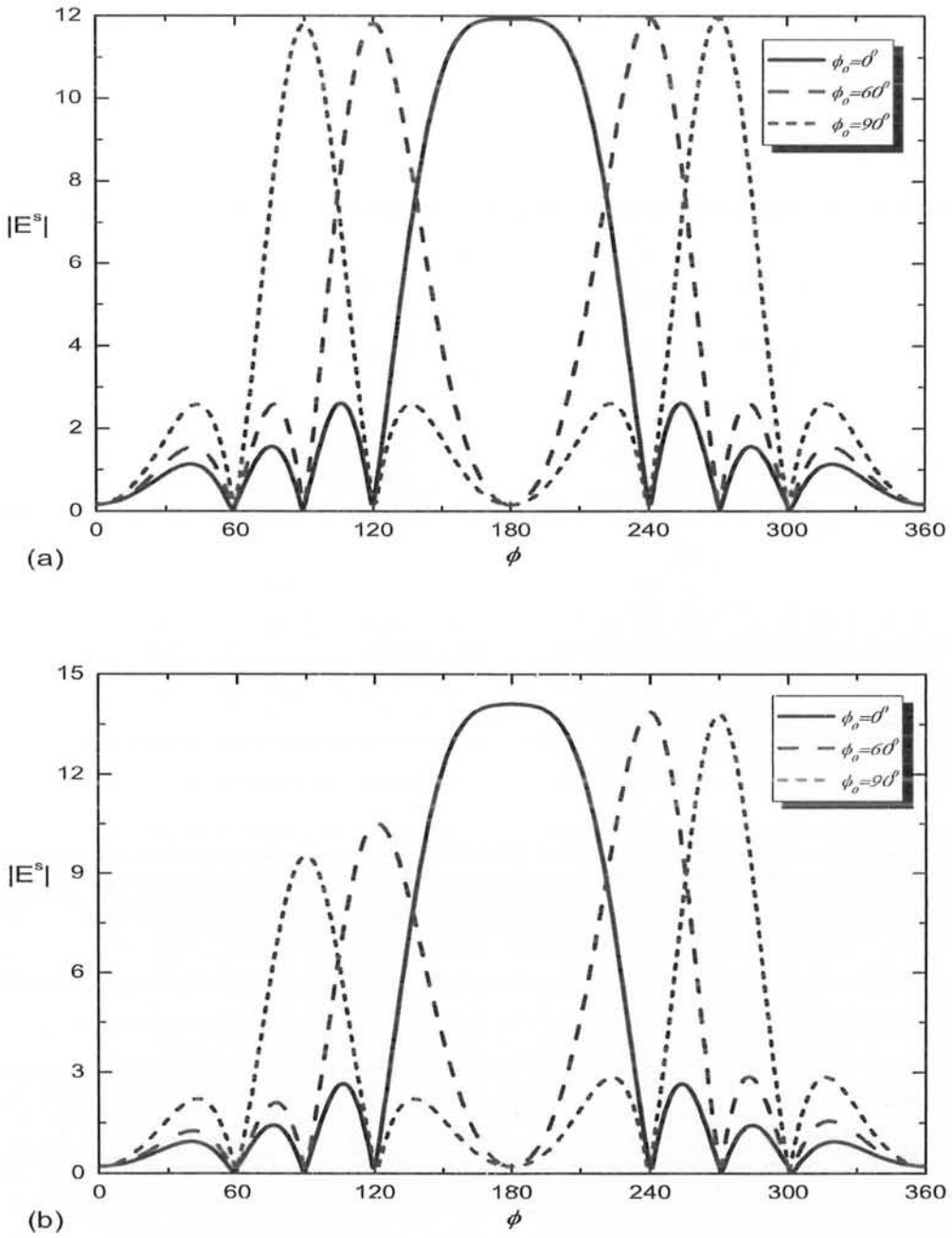


Figure 2.12. Far-zone scattered field (E-pol) from a PEMC strip simulated by 20 PEMC circular cylinders, with $a = 0.05\lambda_0$, $l = 0.1\lambda_0$ and $M\eta_0 = \pm 1$. (a) Co-pol component (b) cross-pol component.

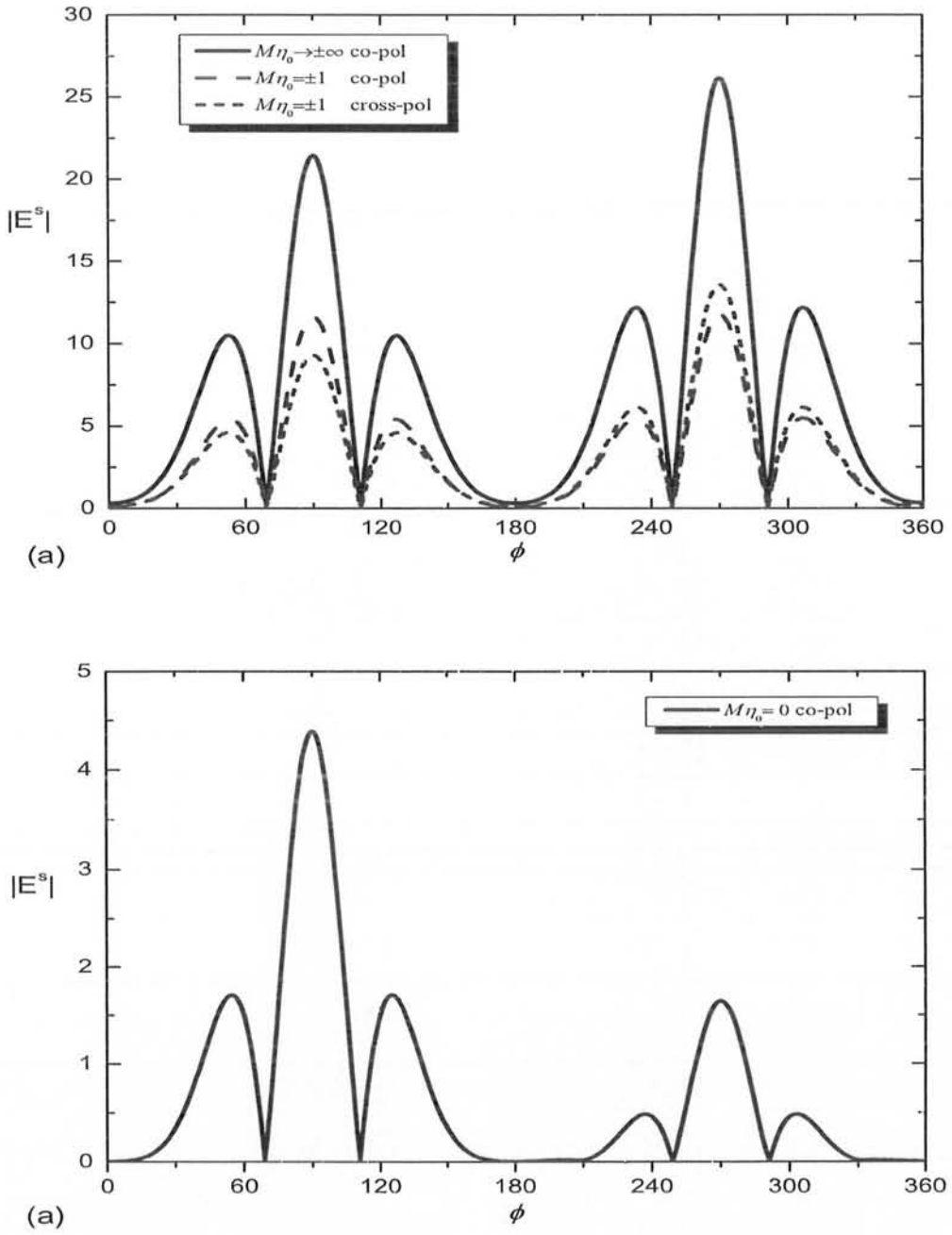


Figure 2.13. Far-zone scattered co- and cross-polarized field components (E -pol), for two PEC strips, (a) for different $M\eta_0$ (b) $M\eta_0 = 0$.

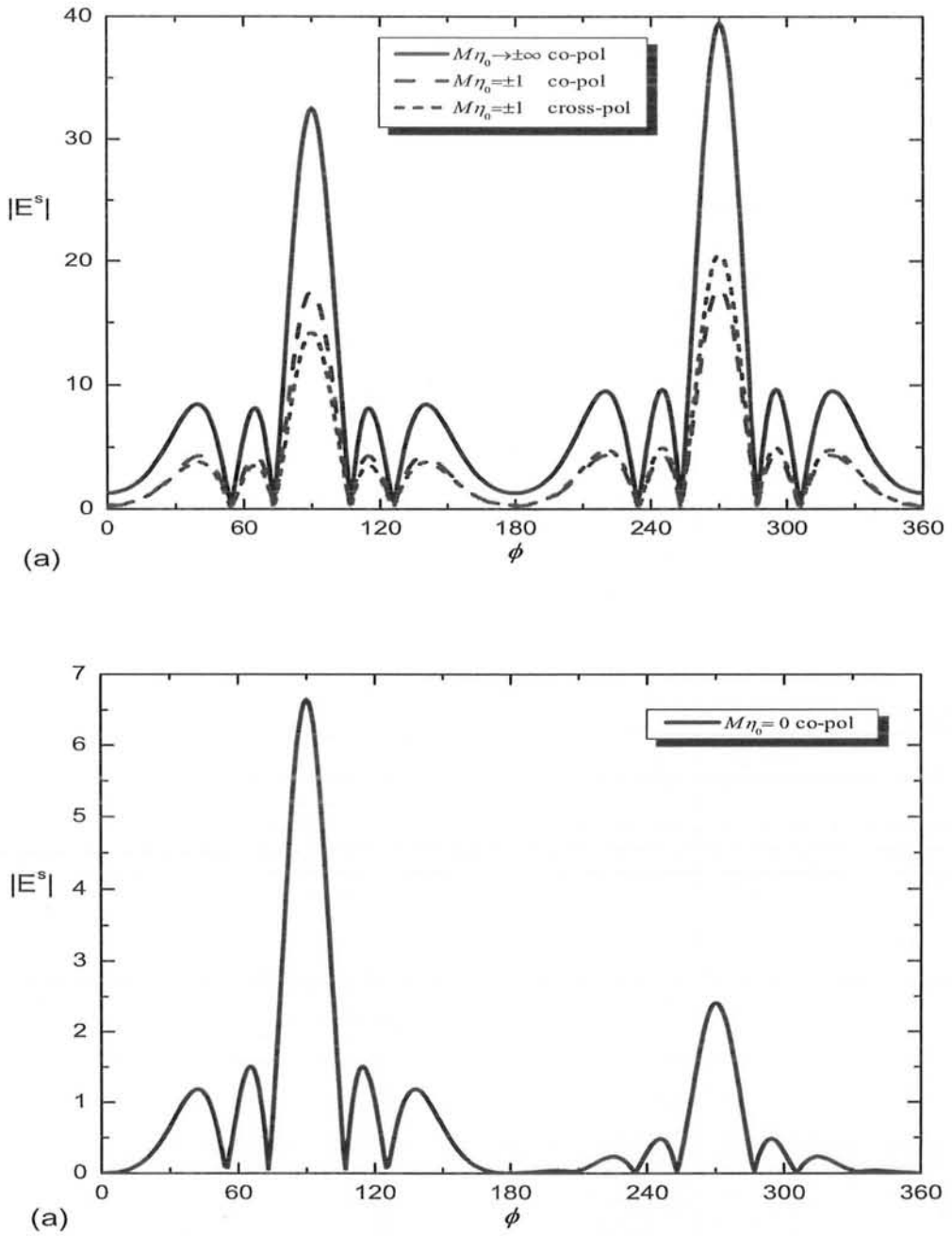


Figure 2.14. Far-zone scattered co- and cross-polarized field components ($E-pol$), for three PEMC strips, (a) for different $M\eta_0$ (b) $M\eta_0 = 0$.

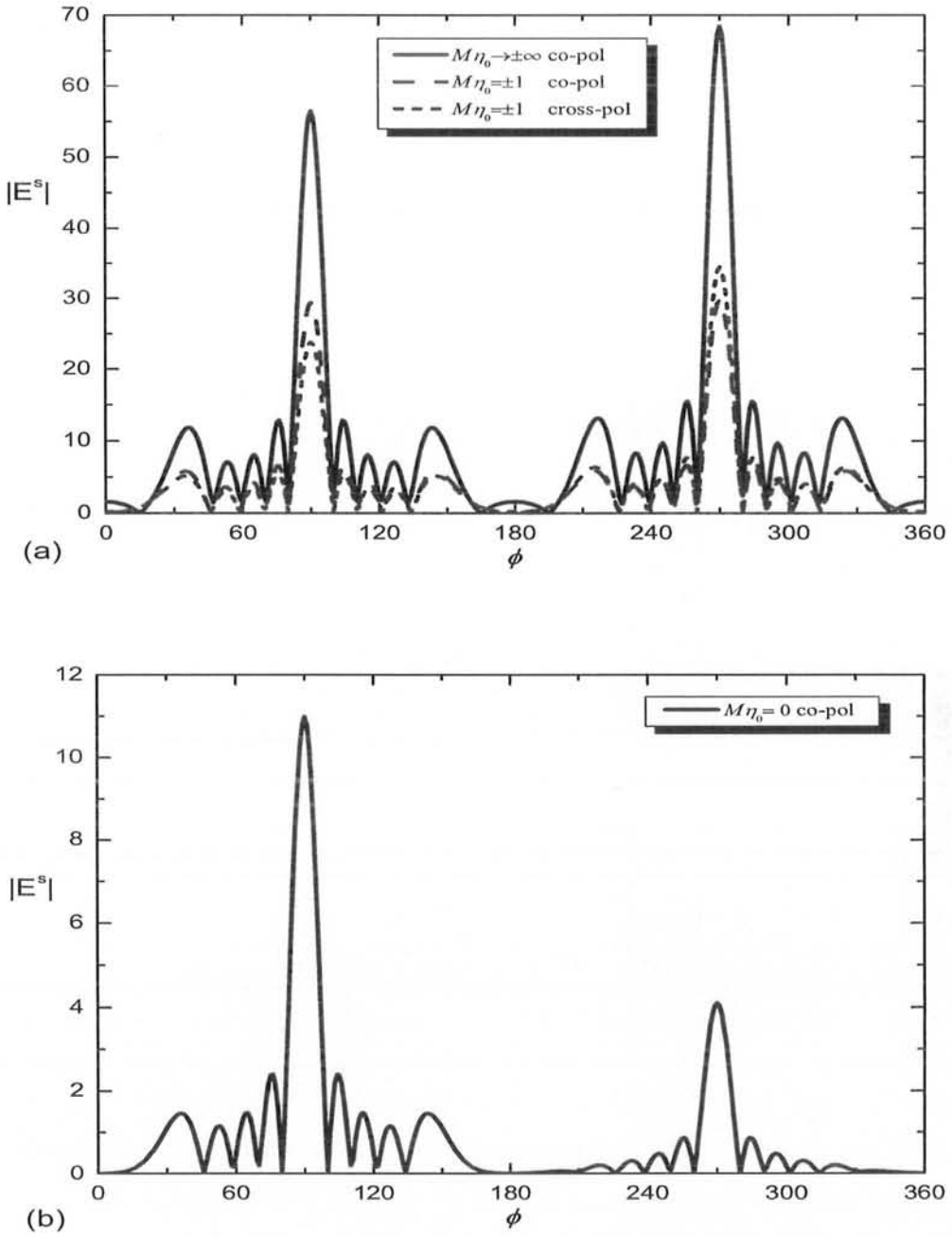


Figure 2.15. Far-zone scattered co- and cross-polarized field components (E -pol), for five PEMC strips, (a) for different $M\eta_0$ (b) $M\eta_0 = 0$.

by PEMC strip grating. In Fig. 2.13(a) the co-and cross-polarized components of two strips are analyzed for different $M\eta_0$ while in Fig.2.13(b), the co-polarized component has been presented taking $M\eta_0 = 0$. Fig. 2.14 gives the diffracted field patterns of three PEMC strips when $M\eta_0$ has different values given in Fig. 2.14(a) and $M\eta_0 = 0$, shown in Fig. 2.14(b). Figs. 2.15(a) and (b) present the far-field behaviors of five PEMC strips. In Fig. 2.15(a) co- and cross-polarized components are shown for different $M\eta_0$ while Fig. 2.15(b) shows the co-polarized component for $M\eta_0 = 0$.

CHAPTER III

Electromagnetic scattering from a metamaterial coated PEMC cylinder

In this chapter, scattering of electromagnetic waves from a coated PEMC circular cylinder is investigated analytically. The discussion has been divided into two parts. In the first part, scattering of single electromagnetic plane wave has been considered while in the second part scattering of two or more electromagnetic plane waves is discussed. The coating layer is taken as a lossless DPS, ENG, MNG or DNG and dissipative and dispersive DNG. Results under special conditions are compared with the published literature.

3.1. Scattering of single plane wave from a coated PEMC cylinder

The geometry of the scattering problem is shown in Fig. 3.1. It contains a PEMC circular cylinder which has been coated with a layer of uniform thickness. The coating layer has negative permittivity and/or permeability. The coated cylinder is supposed to be of infinite extent and radius of PEMC cylinder is a while radius of PEMC cylinder with coating is b . The external medium $\rho > b$, which is free space with wave number $k_0 = \omega\sqrt{\mu_0\epsilon_0}$, has been mentioned as region 0 in Fig. 3.1. The material with wave number $k_1 = \omega\sqrt{\mu_1\epsilon_1}$ occupies the region $a < \rho < b$ and is named as region 1. The polarization of the incident electric field is taken parallel to the axis of the cylinder. The incident electric field is given by

$$E_{0z}^{inc}(\rho, \phi) = E_0 e^{jk_0 \rho \cos \phi} \quad (3.1.1)$$

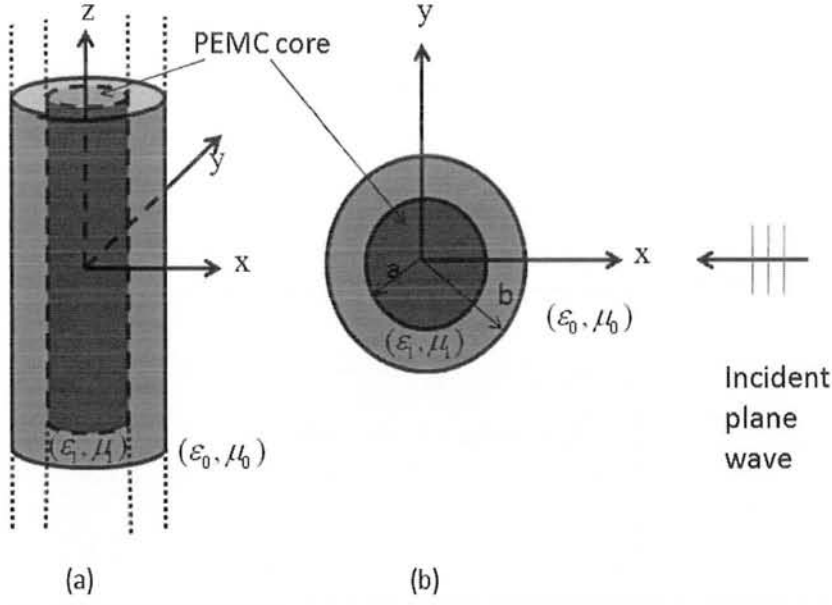


Figure 3.1. An infinite PEMC circular cylinder coated with metamaterial, (a) 3D view (b) top view.

Using the wave transformation, the incident electric and magnetic fields may be written in terms of an infinite Fourier-Bessel series as

$$E_{0z}^{inc}(\rho, \phi) = E_0 \sum_{n=-\infty}^{\infty} j^n J_n(k_0 \rho) e^{jn\phi} \quad (3.1.2)$$

$$H_{0\phi}^{inc}(\rho, \phi) = -\frac{E_0}{j\eta_0} \sum_{n=-\infty}^{\infty} j^n J'_n(k_0 \rho) e^{jn\phi} \quad (3.1.3)$$

As the core material is a PEMC cylinder so the scattered field contains a cross-polarized component in addition to the co-polarized component of the scattered field.

Using Maxwell's equations, the scattered fields in region 0 can be written as

$$E_{0z}^s = E_0 \sum_{n=-\infty}^{\infty} j^n a_n H_n^{(1)}(k_0 \rho) e^{jn\phi} \quad (3.1.4)$$

$$H_{0\phi}^s = -\frac{1}{j\eta_0} E_0 \sum_{n=-\infty}^{\infty} j^n a_n H_n^{(1)'}(k_0 \rho) e^{jn\phi} \quad (3.1.5)$$

$$H_{0z}^s = -\frac{j}{\eta_0} E_0 \sum_{n=-\infty}^{\infty} j^n b_n H_n^{(1)}(k_0 \rho) e^{jn\phi} \quad (3.1.6)$$

$$E_{0\phi}^s = -E_0 \sum_{n=-\infty}^{\infty} j^n b_n H_n^{(1)'}(k_0 \rho) e^{jn\phi} \quad (3.1.7)$$

Region 1 is bounded by two interfaces at $\rho = a$ and $\rho = b$, therefore the total field in this region can be expressed in terms of oppositely traveling cylindrical waves as given below

$$E_{1z} = E_0 \sum_{n=-\infty}^{\infty} j^n [c_n H_n^{(2)}(k_1 \rho) + d_n H_n^{(1)}(k_1 \rho)] e^{jn\phi} \quad (3.1.8)$$

$$H_{1\phi} = -\frac{1}{j\eta_1} E_0 \sum_{n=-\infty}^{\infty} j^n [c_n H_n^{(2)'}(k_1 \rho) + d_n H_n^{(1)'}(k_1 \rho)] e^{jn\phi} \quad (3.1.9)$$

$$H_{1z} = -\frac{j}{\eta_1} E_0 \sum_{n=-\infty}^{\infty} j^n [e_n H_n^{(2)}(k_1 \rho) + f_n H_n^{(1)}(k_1 \rho)] e^{jn\phi} \quad (3.1.10)$$

$$E_{1\phi} = -E_0 \sum_{n=-\infty}^{\infty} j^n [e_n H_n^{(2)'}(k_1 \rho) + f_n H_n^{(1)'}(k_1 \rho)] e^{jn\phi} \quad (3.1.11)$$

where in all the above expressions $J_n(x)$ and $Y_n(x)$ are the Bessel functions of first and second kinds while $H_n^{(1)}(x)$ and $H_n^{(2)}(x)$ are the Hankel functions of first and second kinds respectively. Also in the above expressions $a_n, b_n, c_n, d_n, e_n,$ and f_n are the unknown scattering coefficients, which are to be determined. These unknowns can be found by using appropriate boundary conditions at the interfaces $\rho = a$ and $\rho = b$. The boundary conditions at the interface $\rho = a$ are

$$H_{1z} + M E_{1z} = 0, \quad \rho = a, \quad 0 \leq \phi \leq 2\pi \quad (3.1.12)$$

$$H_{1\phi} + M E_{1\phi} = 0, \quad \rho = a, \quad 0 \leq \phi \leq 2\pi \quad (3.1.13)$$

While the boundary conditions at the interface $\rho = b$ are

$$E_{0z} = E_{1z}, \quad \rho = b, \quad 0 \leq \phi \leq 2\pi \quad (3.1.14)$$

$$H_{0\phi} = H_{1\phi}, \quad \rho = b, \quad 0 \leq \phi \leq 2\pi \quad (3.1.15)$$

$$H_{0z}^s = H_{1z}, \quad \rho = b, \quad 0 \leq \phi \leq 2\pi \quad (3.1.16)$$

$$E_{0\phi}^s = E_{1\phi}, \quad \rho = b, \quad 0 \leq \phi \leq 2\pi \quad (3.1.17)$$

where

$$E_{0z} = E_{0z}^{inc} + E_{0z}^s$$

$$H_{0\phi} = H_{0\phi}^{inc} + H_{0\phi}^s$$

Applying these boundary conditions at $\rho = a$ and $\rho = b$, a linear matrix equation is obtained in terms of the unknown scattering coefficients. Solution of the matrix equation yields the values of all the unknown scattering coefficients in the matrix equation. Co- and cross-polarized components of the scattered field due to a coated PEMC cylinder are obtained by using the values of a_n and b_n . Far-zone scattered field is obtained by using the asymptotic form of Hankel functions.

The backscattering cross-section is defined as the ratio of the total power scattered by the scatterer to the incident power per unit area on the scatterer and is given as

$$\sigma = 2\pi\rho \frac{W^{sca}}{W^{inc}} = 2\pi\rho \frac{|E^s|^2}{|E^{inc}|^2} \quad (3.1.18)$$

where W^{inc} is the incident power density and W^{sca} is the power density of the far-zone scattered field. The normalized bistatic scattering width of co-polarized and cross-polarized field components, in the case of E-polarized plane wave incidence, can be written in the following form:

$$\sigma_{co}/\lambda_0 = \frac{2}{\pi} \left| \sum_{n=-\infty}^{\infty} a_n e^{jn\phi} \right|^2 \quad (3.1.19)$$

$$\sigma_{cross}/\lambda_0 = \frac{4}{\pi} \left| \sum_{n=-\infty}^{\infty} b_n e^{jn\phi} \right|^2 \quad (3.1.20)$$

where a_n and b_n are the scattering coefficients of the co- and cross-polarized field components respectively.

3.1.1. Numerical results and discussion

Numerical results on the basis of analytical formulation in section 3.1 are presented in this section. Plots show the behavior of the normalized monostatic and bistatic scattering widths of a coated PEMC circular cylinder. Throughout the discussion radius of the core cylinder is taken as $a = 5$ cm and the frequency of the incident wave in case of lossless coating layers is taken as $f = 1$ GHz. In order to verify the analytical formulation and the numerical code, the results obtained are compared with the results given in published literature and the comparison is found to be in good agreement.

For the numerical discussion, different types of coating layer have been considered; DPS, i.e., permittivity and permeability both are positive, DNG, i.e., both permittivity and permeability are negative, epsilon negative (ENG) and mu negative (MNG). Fig. 3.2 gives the behavior of the co-polarized component of the monostatic scattering width of a DPS and DNG coated PEMC cylinder when $b = 7$ cm, with the variation in the parameter $M\eta_1$. Figs. 3.2(a) and (b) show the variations in the co-polarized component for E-polarized and H-polarized cases respectively. In both the cases, the solid line is for the DPS coating while dashed line is for DNG coating. It is seen from these two figures that, the behavior of the co-polarized component of the monostatic scattering width changes with the change of polarization and type of the coating layer. Fig. 3.3 gives the behavior of the cross-polarized component of the monostatic scattering width of a DPS/DNG coated PEMC cylinder when $b = 7$ cm, with the variation in the parameter $M\eta_1$, for both type of polarizations. Fig. 3.3 shows that the cross-polarized component of the monostatic scattering width does not depend on the type of polarization but it depends upon the type of the coating layer. It is observed from Figs. 3.2 and 3.3, that the maximum (minimum) value of the cross-polarized component (co-polarized component) of the monostatic scattering width does not occur at $M\eta_1 = \pm 1$, as it happened for the case of an uncoated PEMC cylinder. If we look at

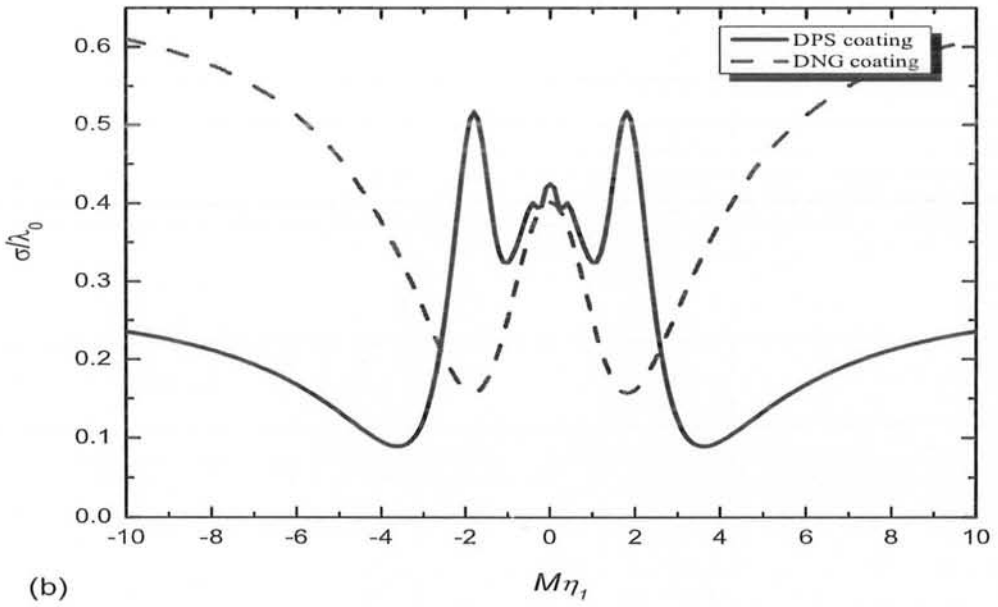
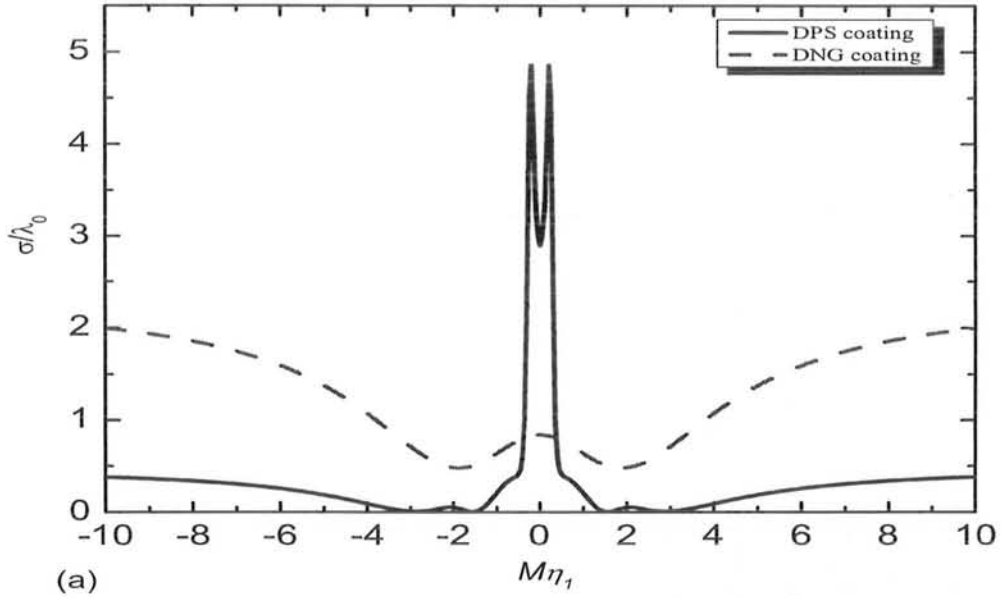


Figure 3.2. Co-polarized component of normalized monostatic scattering width versus $M\eta_1$ with $a = 5$ cm, $b = 7$ cm, and $f = 1$ GHz. (a) E-pol case (b) H-pol case.

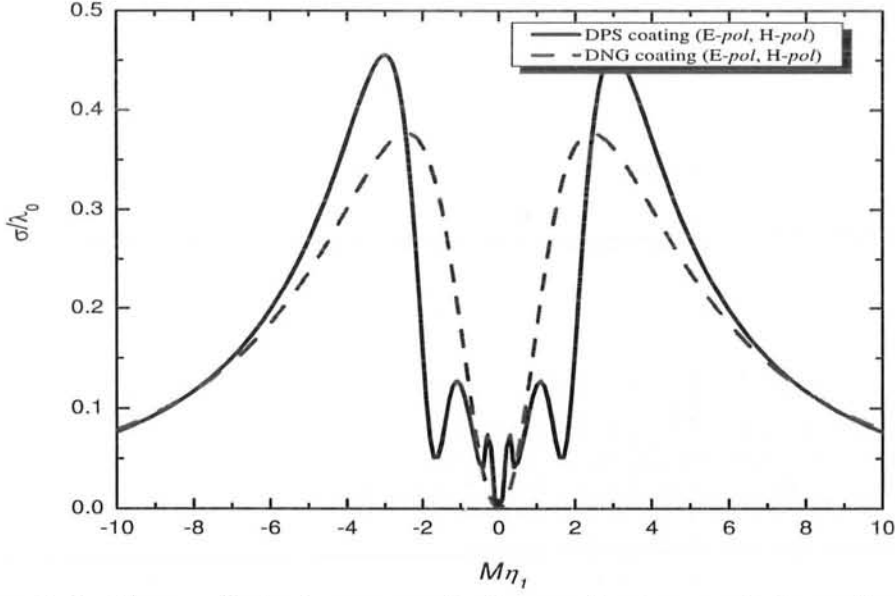


Figure 3.3. Cross-polarized component of normalized monostatic scattering width versus $M\eta_1$ with $a = 5$ cm, $b = 7$ cm and $f = 1$ GHz.

the figures 3.2 and 3.3, it is observed that the scattering width of a coated PEMC cylinder does not depend upon the sign of the factor $M\eta_1$.

In Fig. 3.4, scattering characteristics of a DPS, DNG, ENG and MNG coated PEMC cylinder for $b = 7$ cm, are analyzed for the E-polarized case. Figs. 3.4(a) and (b), show the co- and cross-polarized components of the monostatic scattering width for different values of ϵ_r when $\mu_r = 1$ and $\mu_r = -1$, respectively. Fig. 3.5 shows the scattering from a coated PEMC cylinder when $b = 7$ cm, for H-polarization. Figs. 3.5(a) and (b) show the co- and cross-polarized components of the monostatic scattering width for different μ_r when $\epsilon_r = 1$ and $\epsilon_r = -1$, respectively. From Figs. 3.4 and 3.5, it is seen that the co-polarized component of the monostatic scattering width of the coated PEMC cylinder for $M\eta_1 \rightarrow \pm\infty$ shows a good comparison with that of a coated PEC cylinder which has been presented by Irci and Ertürk [28]. While co- and cross-polarized components of a coated PEMC cylinder for $M\eta_0 = \pm 1$, exhibit entirely

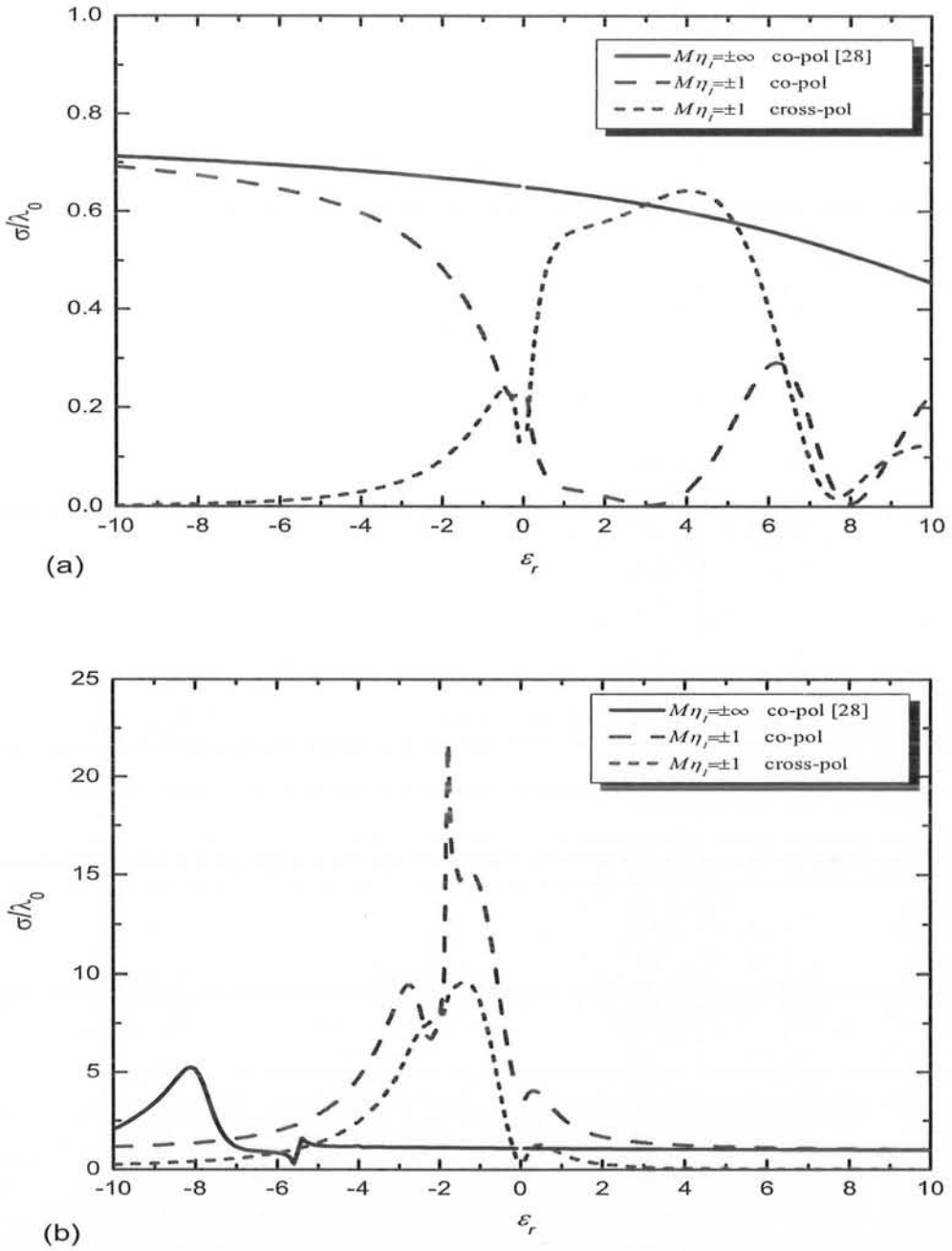


Figure 3.4. Normalized monostatic scattering width of a coated PEMC cylinder (E-pol case) with $a = 5$ cm, $b = 7$ cm and $f = 1$ GHz. (a) $\mu_r = 1$, (b) $\mu_r = -1$.

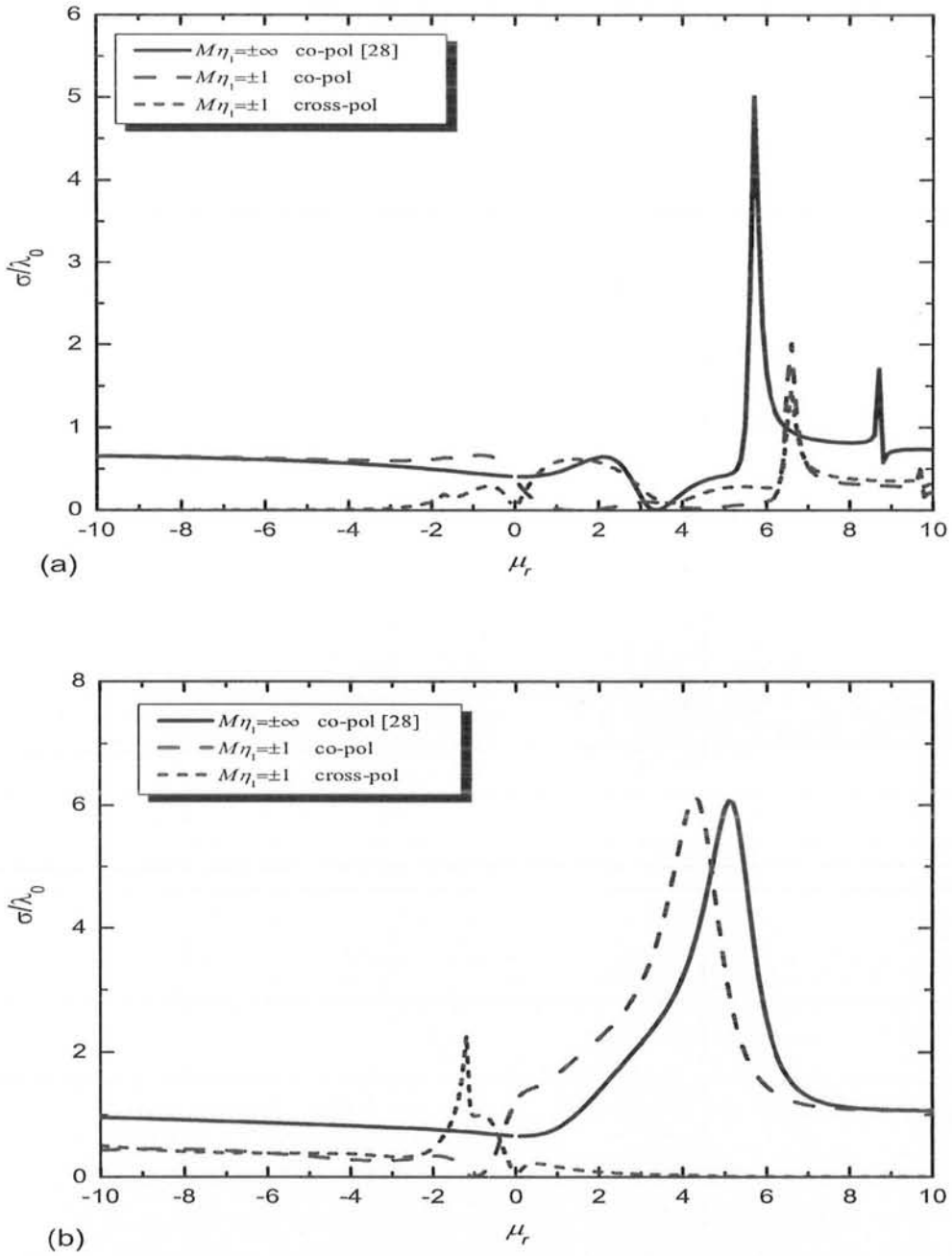


Figure 3.5. Normalized monostatic scattering width of a coated PEMC cylinder (H-pol case) with $a = 5$ cm, $b = 7$ cm and $f = 1$ GHz. (a) $\epsilon_r = 2.2$, (b) $\epsilon_r = -2.2$.

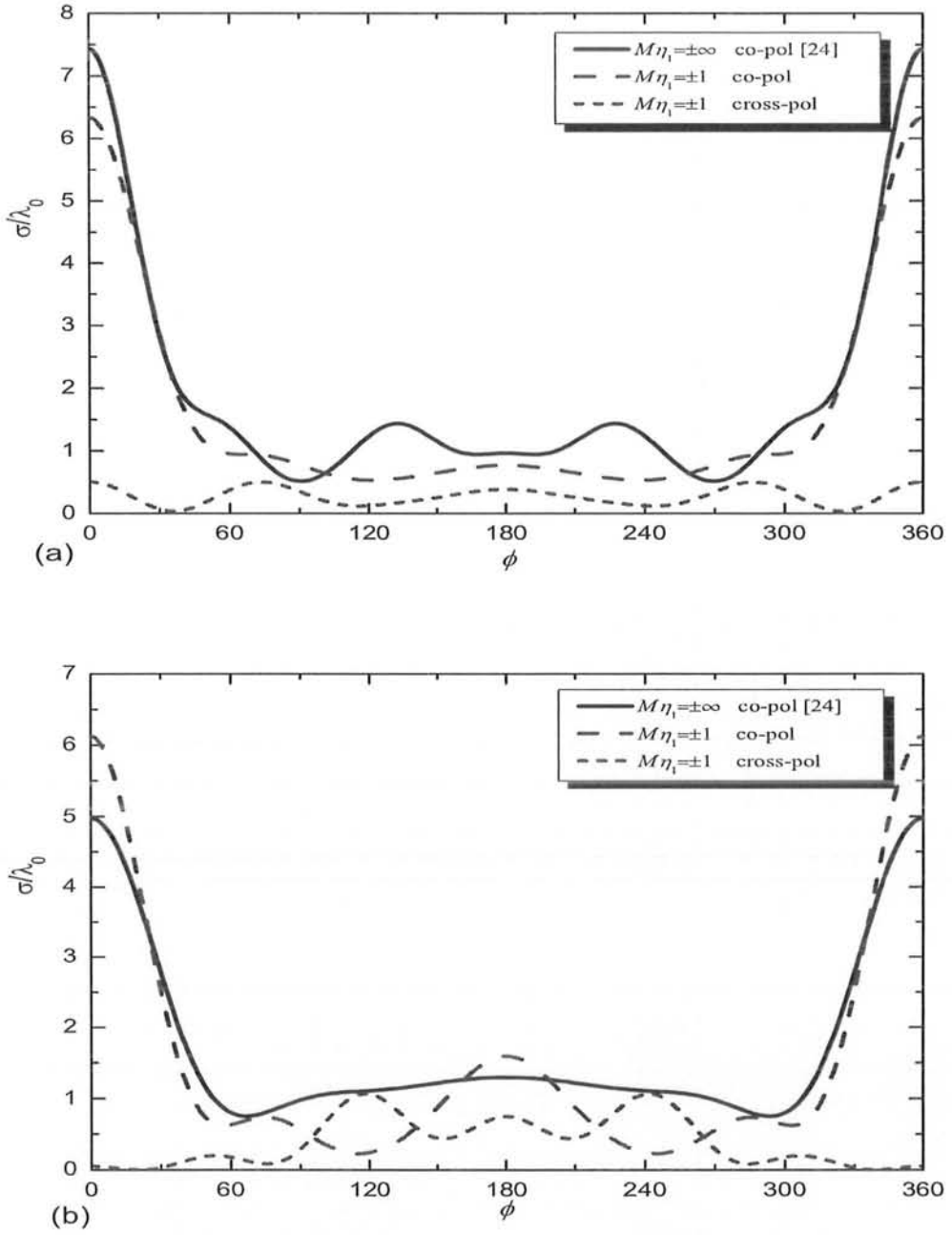


Figure 3.6. Normalized bistatic scattering width of a coated PEMC cylinder (E-pol case) with $a = 5$ cm, $b = 10$ cm and $f = 1$ GHz. (a) DPS coating with $\epsilon_r = 9.8$, $\mu_r = 1$, (b) DNG coating with $\epsilon_r = -9.8$, $\mu_r = -1$.

different behaviors as compared to a coated PEC cylinder, for the same configurations. Especially these plots show that the transparency is achievable in case of a coated PEMC cylinder for both E-polarization and H-polarization which has been observed only for H-polarization in case of coated PEC cylinder. Also the cross-polarized component of the monostatic scattering width of the coated PEMC cylinder vanishes for $M\eta_1 \rightarrow \pm\infty$, in all the four plots.

Normalized bistatic scattering width of a coated PEMC circular cylinder, with $b = 10$ cm, coated with a DPS layer having $\epsilon_r = 9.8$ and $\mu_r = 1$ is presented in Figs. 3.6. While Fig. 3.7 shows the bistatic scattering width for the PEMC cylinder coated with DNG layer with $\epsilon_r = -9.8$ and $\mu_r = -1$. Figs. 3.6(a) and (b) give the co- and cross-polarized components of the normalized bistatic scattering width of the PEMC cylinder, coated by DPS and DNG materials respectively, for the case of E-polarization. While Figs. 3.7(a) and (b) show the behavior of the co- and cross-polarized components of the normalized bistatic scattering width of the PEMC cylinder, coated by a DPS and a DNG material respectively, for the case of H-polarization. From Figs. 3.6 and 3.7, it is obvious that the co-polarized component of the bistatic scattering width of the coated PEMC cylinder for $M\eta_1 \rightarrow \pm\infty$ is in agreement with the bistatic scattering width of a coated PEC cylinder, discussed by Shen and Li [24]. While the cross-polarized component of the bistatic scattering width disappears as $M\eta_1 \rightarrow \pm\infty$, in all the four plots. Also it is observed that co-polarized components of the normalized bistatic scattering width, show relatively different behaviors for the same configurations when $M\eta_1 = \pm 1$. While the cross-polarized component, shows similar behavior for the two polarizations for different coating layers when $M\eta_1 = \pm 1$. For $M\eta_1 = \pm 1$, interchanging the values of ϵ_r and μ_r , it is noted that E-polarization case reduces to H-polarization case and vice versa. These are shown in Figs. 3.6 and 3.7.

Figs. 3.8 and 3.9 show the co- and cross-polarized components of the normalized

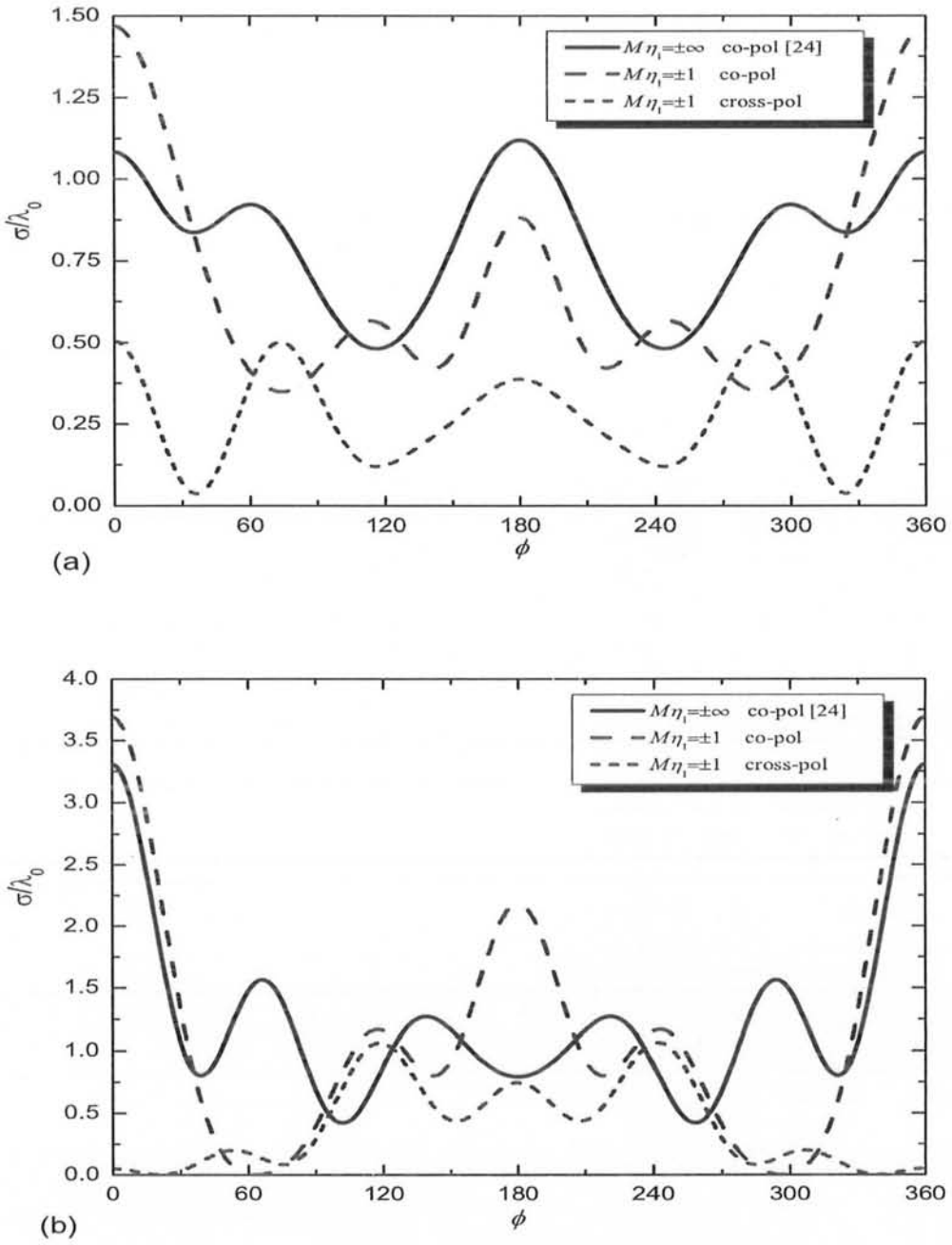


Figure 3.7. Normalized bistatic scattering width of a coated PEMC cylinder (H-pol case) with $a = 5$ cm, $b = 10$ cm and $f = 1$ GHz. (a) DPS coating with $\epsilon_r = 9.8, \mu_r = 1$, (b) DNG coating with $\epsilon_r = -9.8, \mu_r = -1$.

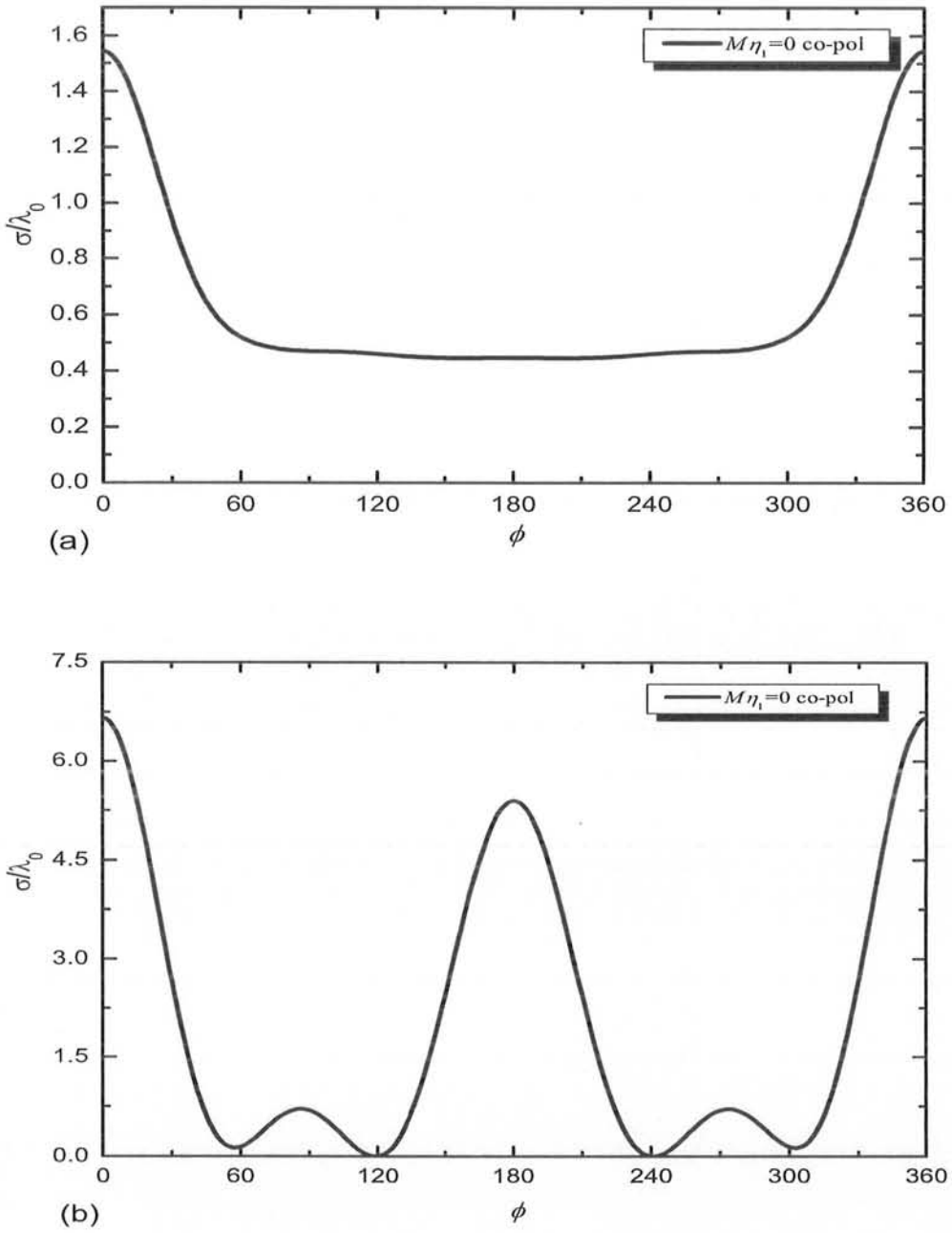


Figure 3.8. Normalized bistatic scattering width of a coated PEMC cylinder (E-pol case) with $a = 5$ cm, $b = 10$ cm and $f = 1$ GHz. (a) DPS coating with $\epsilon_r = 9.8$, $\mu_r = 1$, (b) DNG coating with $\epsilon_r = -9.8$, $\mu_r = -1$.

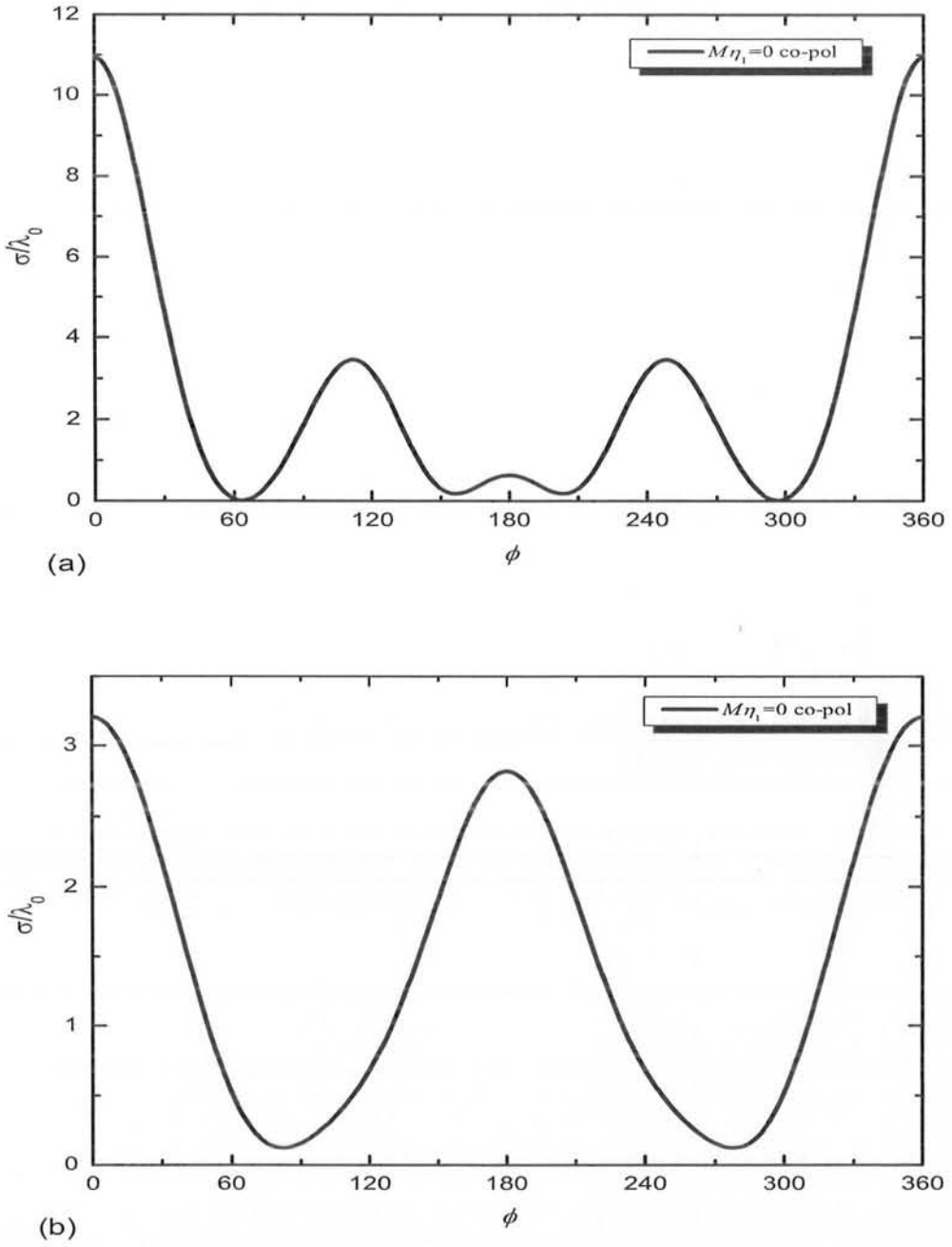


Figure 3.9. Normalized bistatic scattering width of a coated PEMC cylinder (H-pol case) with $a = 5$ cm, $b = 10$ cm and $f = 1$ GHz. (a) DPS coating with $\epsilon_r = 9.8$, $\mu_r = 1$, (b) DNG coating with $\epsilon_r = -9.8$, $\mu_r = -1$.

bistatic scattering width of a coated PEMC cylinder for E-polarized and H-polarized cases respectively, with $M\eta_1 = 0$. Figs. 3.8(a) and (b) give co- and cross-polarized components of the normalized bistatic scattering width of the PEMC cylinder, coated by DPS and DNG materials respectively, for the case of E-polarization. And Figs. 3.9(a) and (b) describe the variation in the co- and cross polarized components of the normalized bistatic scattering width of the PEMC cylinder with DPS and DNG material coating respectively, for the case of H-polarization. From these two figures, it is observed that the cross-polarized component vanishes for $M\eta_1 = 0$ while the co-polarized component is present in this case. E-polarized and H-polarized case of a coated PMC cylinder given in Figs. 3.8 and 3.9, can be verified by interchanging the values of ϵ_r and μ_r in the H-polarized and E-polarized case of coated PEC cylinder, given in Figs. 3.6 and 3.7 and vice versa.

Now the coating layer is considered to be dispersive and dissipative material for which ϵ_r and μ_r are written as [50, 53, 55]

$$\epsilon_r = \epsilon_{Re} + j\epsilon_{Im} \quad (3.1.21)$$

$$\mu_r = \mu_{Re} + j\mu_{Im} \quad (3.1.22)$$

Imaginary part of ϵ and μ relate directly to the absorption of electromagnetic radiation within that material. For DNG medium, equations for ϵ_r and μ_r may also be written as [53],

$$\epsilon_r = |\epsilon_r|e^{j(\phi_{\epsilon_r})} \quad \pi/2 < \phi_{\epsilon_r} \leq \pi$$

$$\mu_r = |\mu_r|e^{j(\phi_{\mu_r})} \quad \pi/2 < \phi_{\mu_r} \leq \pi$$

so

$$n = |n|e^{j(\phi_n)} \quad \pi/2 < \phi_n \leq \pi$$

For small losses imaginary parts of ϵ_r and μ_r have the limits

$$0 \ll \epsilon_{Im} \ll \epsilon_{Re}$$

$$0 \ll \mu_{Im} \ll \mu_{Re}$$

then

$$n = \mp \sqrt{|\epsilon_{Re}\mu_{Re}|} [1 - j1/2(\epsilon_{Im}/|\epsilon_{Re}|) + \mu_{Im}/|\mu_{Re}|] \quad (3.1.23)$$

and for the lossless limit

$$n = \mp \sqrt{|\epsilon_{Re}\mu_{Re}|}$$

For the DNG material dispersion relations for ϵ_r and μ_r can be written as

$$\epsilon_r(w) = \left[1 - \frac{w_{pe}^2}{(w^2 + jw\gamma_e - w_{0e}^2)} \right] \quad (3.1.24)$$

$$\mu_r(w) = \left[1 - \frac{w_{pm}^2}{(w^2 + jw\gamma_m - w_{0m}^2)} \right] \quad (3.1.25)$$

where $w_{pe/m}$ are plasma frequencies, $w_{0e/m}$ are the resonance frequencies and $\gamma_{e/m}$ are the corresponding widths given as

$$w_{0e/m}^2 = \gamma_{e/m1}\gamma_{e/m2}$$

$$\gamma_{e/m} = \gamma_{e/m1} + \gamma_{e/m2}$$

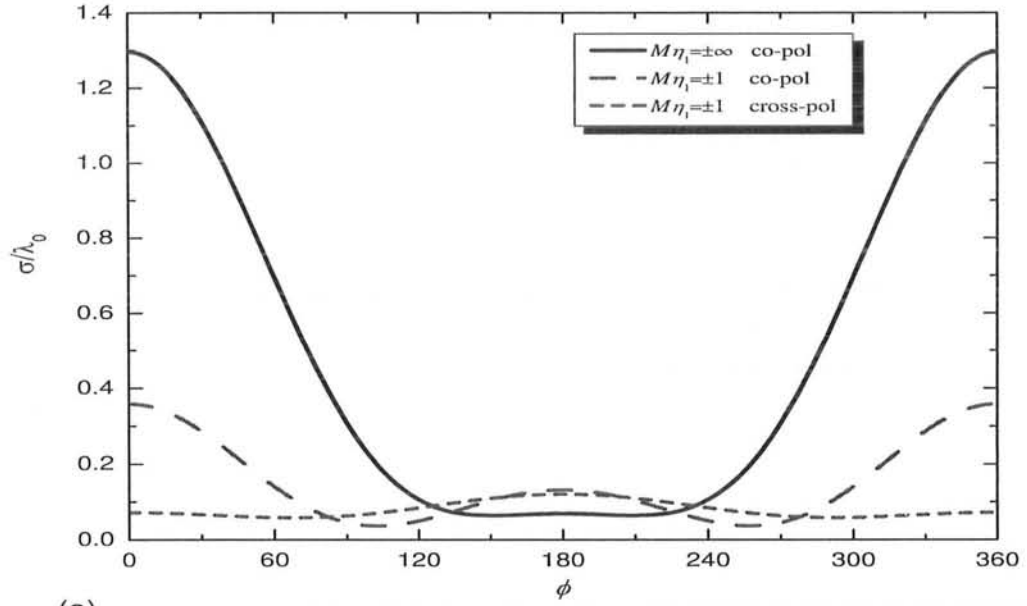
The symbol "e" is related to electric part and the symbol "m" to magnetic part. The real parts of ϵ and μ both are negative under the condition that

$$w_{pe/m}^2 > \gamma_{e/m}^2 + 2\gamma_{e/m}w_{0e/m}$$

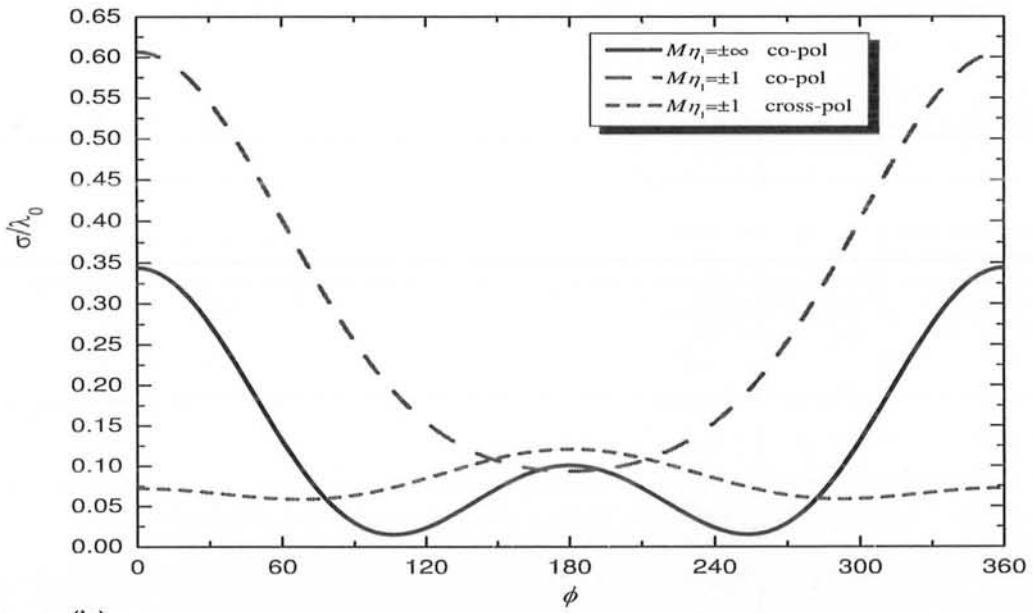
in the interval $[w_{le/m}, w_{ue/m}]$ where

$$w_{le/m} = \left[\frac{(2w_{0e/m}^2 + w_{pe/m}^2 - \gamma_{e/m}^2)}{2} - \frac{(w_{pe/m}^4 + \gamma_{e/m}^4 - 2w_{pe/m}^2\gamma_{e/m}^2 - 4\gamma_{e/m}^2w_{0e/m}^2)^{1/2}}{2} \right]^{1/2} \quad (3.1.26)$$

$$w_{ue/m} = \left[\frac{(2w_{0e/m}^2 + w_{pe/m}^2 - \gamma_{e/m}^2)}{2} + \frac{(w_{pe/m}^4 + \gamma_{e/m}^4 - 2w_{pe/m}^2\gamma_{e/m}^2 - 4\gamma_{e/m}^2w_{0e/m}^2)^{1/2}}{2} \right]^{1/2} \quad (3.1.27)$$



(a)



(b)

Figure 3.10. Normalized bistatic scattering width of a PEMC cylinder coated with a dissipative and dispersive DNG coating layer with $\epsilon_r = -0.40 + j0.26$, $\mu_r = -1.40 + j0.62$ and $a = 5$ cm, $b = 10$ cm. (a) E-pol case, (b) H-pol case.

where the symbols "l" and "u" denote the lower and upper limits of the angular frequencies. When $\gamma_{e/m} = 0$, it is found that

$$w_{le/m} = w_{0e/m}$$

$$w_{ue/m} = \sqrt{w_{0e/m}^2 + w_{pe/m}^2}$$

These are the simple expressions for the lower and upper boundaries of the interval.

Figs. 3.10(a) and (b) present the bistatic scattering width of a PEMC cylinder coated by a dissipative and dispersive DNG material with $\epsilon_r = -0.40 + j0.26$ and $\mu_r = -1.40 + j0.62$, for parallel and perpendicular polarizations respectively. In this figure the radii of uncoated and coated cylinders have been taken as $a = 5$ cm and $b = 10$ cm, respectively. It is observed that the bistatic scattering width has been reduced for dissipative and dispersive DNG and its co-polarized component is different while the cross-polarized component has the same behavior in case of $M\eta_1 = \pm 1$, for parallel and perpendicular polarizations.

3.2. Scattering of two or more plane waves by a coated PEMC cylinder

Electromagnetic scattering of two or more incident plane waves has been investigated for a PEMC circular cylinder, coated with a material having negative index of refraction. In the numerical results, both the E-polarized and H-polarized cases are considered for the analysis. The scattered fields are calculated by the application of appropriate boundary conditions at the interfaces. The numerical results are compared with the published literature, and are found to be in good agreement.

Geometry of the problem is shown in Fig. 3.11. Both the cylinder and uniform coating layer are supposed to be infinite along the axis and of circular cross section. The radius of the PEMC cylinder is a and PEMC cylinder with the coating layer is b . Region $\rho > b$ has been mentioned as Region 0 is free space and the coating region

$a < \rho < b$, is named as Region 1. In the E-polarized case of the incident plane waves the electric vector of all the waves is parallel to the axis of the cylinder.

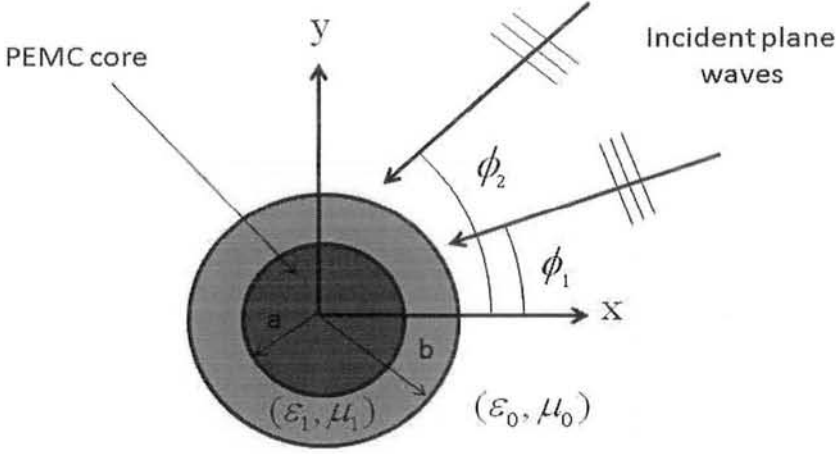


Figure 3.11. Infinite PEMC circular cylinder coated by a DPS or a DNG material.

The incident electric fields in terms of the cylindrical coordinates (ρ, ϕ) , can be expressed as

$$E_{0z}^{inc(l)}(\rho, \phi) = E_{0l} e^{jk_0 \rho \cos(\phi - \phi_l)} \quad (3.2.1)$$

where $l = 1, 2, 3, \dots$, which represents the number of incident plane waves. Therefore the total incident wave is the sum of the all the incident plane waves. Using the wave transformation, the total incident field components may be written in terms of an infinite Fourier-Bessel series as

$$E_{0z}^{inc}(\rho, \phi) = \sum_{n=-\infty}^{\infty} j^n J_n(k_0 \rho) e^{jn\phi} \sum_{l=1}^N E_{0l} e^{-jn\phi_l} \quad (3.2.2)$$

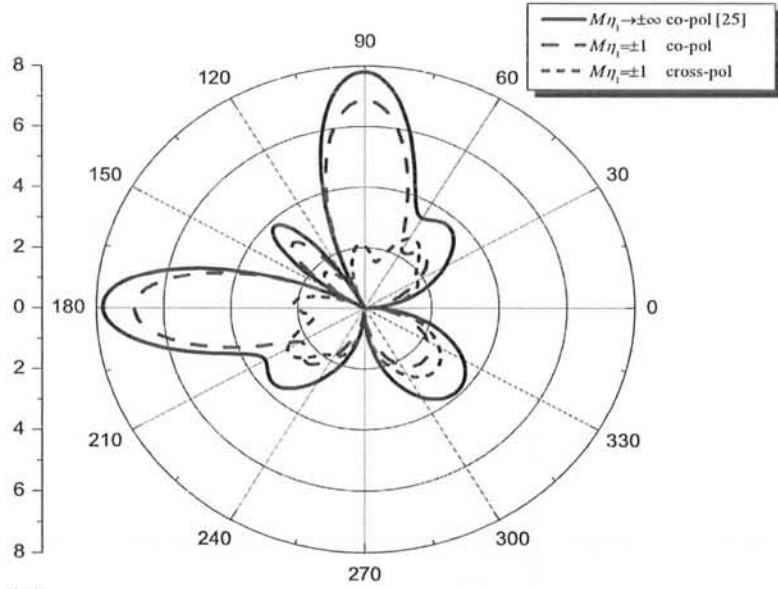
$$\begin{aligned} H_{0\phi}^{inc}(\rho, \phi) &= \frac{1}{-j\eta_0 k_0} \frac{\partial E_{0z}^{inc}(\rho, \phi)}{\partial \rho} \\ &= -\frac{1}{j\eta_0} \sum_{n=-\infty}^{\infty} j^n J'_n(k_0 \rho) e^{jn\phi} \sum_{l=1}^N E_{0l} e^{-jn\phi_l} \end{aligned} \quad (3.2.3)$$

Taking these incident field and applying the formulation of section 3.1, the problem is solved analytically. Only the numerical results are presented here in this section.

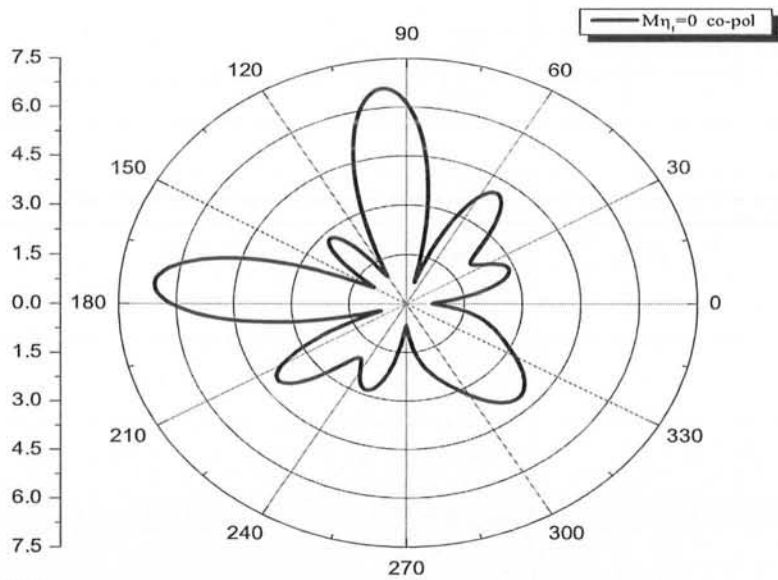
3.2.1. Numerical results and discussion

This section presents some numerical results for co- and cross-polarized scattered field patterns in the far-zone by a PEMC circular cylinder coated with metamaterial. To verify the analytical formulation and the numerical code, few examples are given under some special conditions and the results obtained are compared with the published literature. The comparisons are in good agreement with the published results [25]. In Fig. 3.12, the components of the far-zone scattered field patterns are given for a coated PEMC cylinder when $k_0a = 5$, $k_0b = 5.1$, $\epsilon_r = 5$ and $\mu_r = 1$. Also two waves are considered to be incident on the configuration, with the angles of incidence $\phi_1 = -90^0$, $\phi_2 = 0^0$ and amplitudes $E_{01} = E_{02} = 1$, for this figure. Fig. 3.12(a) shows the co- and cross-polarized components of the scattered field patterns for different $M\eta_1$ while Fig. 3.12(b) presents the co-polarized component of the scattered field when $M\eta_1 = 0$ (PMC case). From these two plots it is obvious that the co-polarized component for $M\eta_1 \rightarrow \pm\infty$ (PEC case) shows an excellent agreement with the previously published results for the PEC case [25]. While the cross-polarized component is zero in the limiting cases i.e., when $M\eta_1 = \pm\infty$ and $M\eta_1 = 0$.

Fig. 3.13 shows the far-zone scattered field components of a DPS ($\epsilon_r = 9.8$, $\mu_r = 1$) coated PEMC cylinder with $k_0a = 1$, $k_0b = 2$ for both E-polarized and H-polarized cases when $M\eta_1 = \pm 1$. Three incident plane waves with angles of incidence $\phi_1 = 0^0$, $\phi_2 = 180^0$, and $\phi_3 = 135^0$ and amplitudes $E_{01} = E_{02} = E_{03} = 1$ are considered in this case. Fig. 3.13(a) shows the co-polarized component while Fig. 3.13(b) presents the cross-polarized component of the scattered field, for both the E-polarized and H-polarized cases, respectively. Fig. 3.14 presents the behavior of the DNG ($\epsilon_r = -9.8$, $\mu_r = -1$) coated PEMC cylinder in response to the three incident plane waves with $\phi_1 = 0^0$, $\phi_2 = 180^0$, and $\phi_3 = 135^0$ as their angles of incidence with amplitudes $E_{01} = E_{02} = E_{03} = 1$ for both the E-polarized and H-polarized cases with $M\eta_1 = \pm 1$.

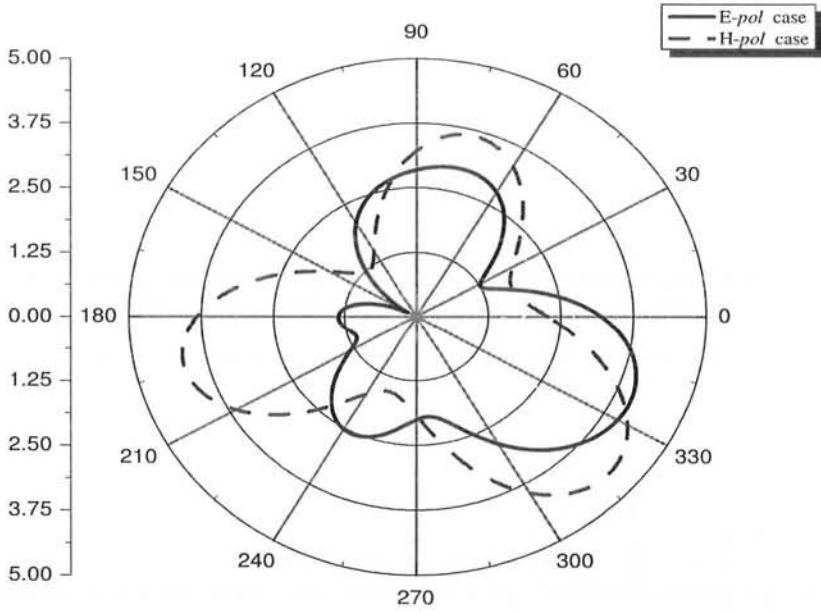


(a)

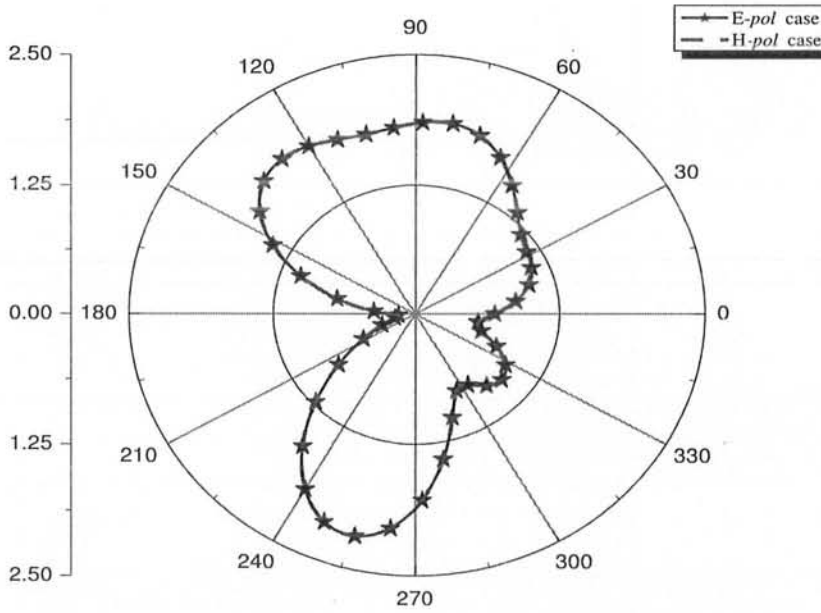


(b)

Figure 3.12. Co- and cross-polarized components of the far-zone scattered field patterns of a DPS coated PEMC cylinder (E-pol case). $\epsilon_r = 5, \mu_r = 1, E_{01} = E_{02} = 1$ and $k_0a = 5, k_0b = 5.1, \phi_1 = -90^\circ, \phi_2 = 0^\circ$. (a) for different $M\eta_1$ (b) $M\eta_1 = 0$

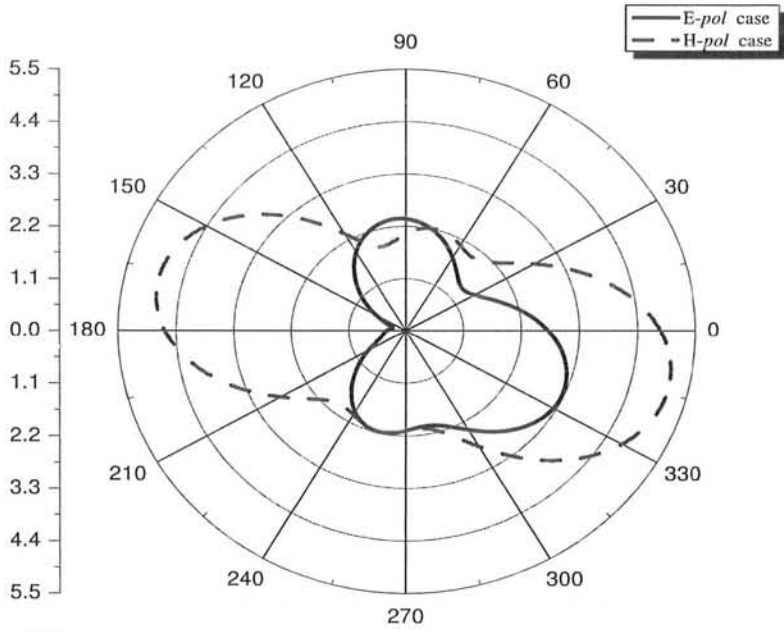


(a)

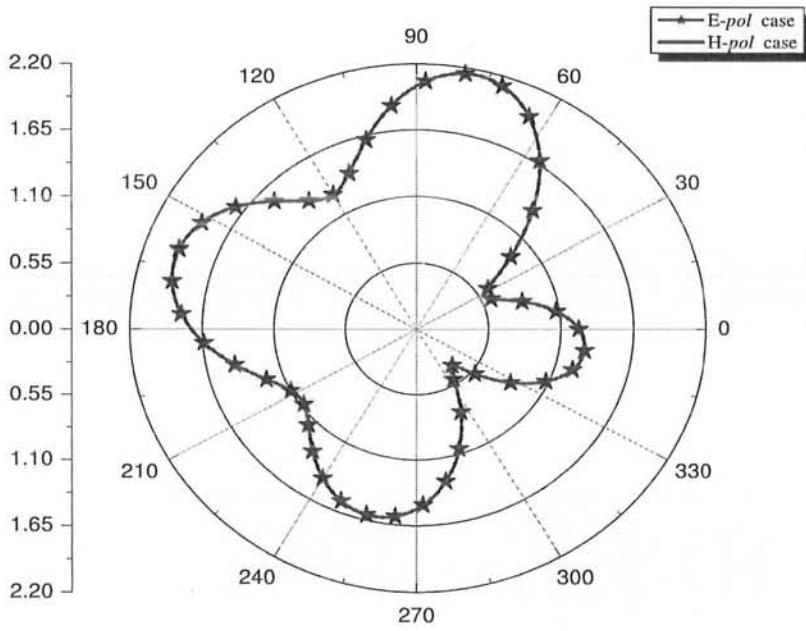


(b)

Figure 3.13. Far-zone scattered field from a dielectric coated PEMC cylinder, $M\eta_1 = \pm 1$, $k_0a = 1$, $k_0b = 2$, $\epsilon_r = 9.8$, $\mu_r = 1$, $\phi_1 = 0^\circ$, $\phi_2 = 180^\circ$, $\phi_3 = 135^\circ$ and $E_{01} = E_{02} = E_{03} = 1$, (a) Co-polarized components. (b) Cross-polarized components.



(a)



(b)

Figure 3.14. Far-zone scattered field from a dielectric coated PEMC cylinder, $M\eta_1 = \pm 1$, $k_0a = 1$, $k_0b = 2$, $\epsilon_r = -9.8$, $\mu_r = -1$, $\phi_1 = 0^\circ$, $\phi_2 = 180^\circ$, $\phi_3 = 135^\circ$ and $E_{01} = E_{02} = E_{03} = 1$, (a) Co-polarized components. (b) Cross-polarized components.

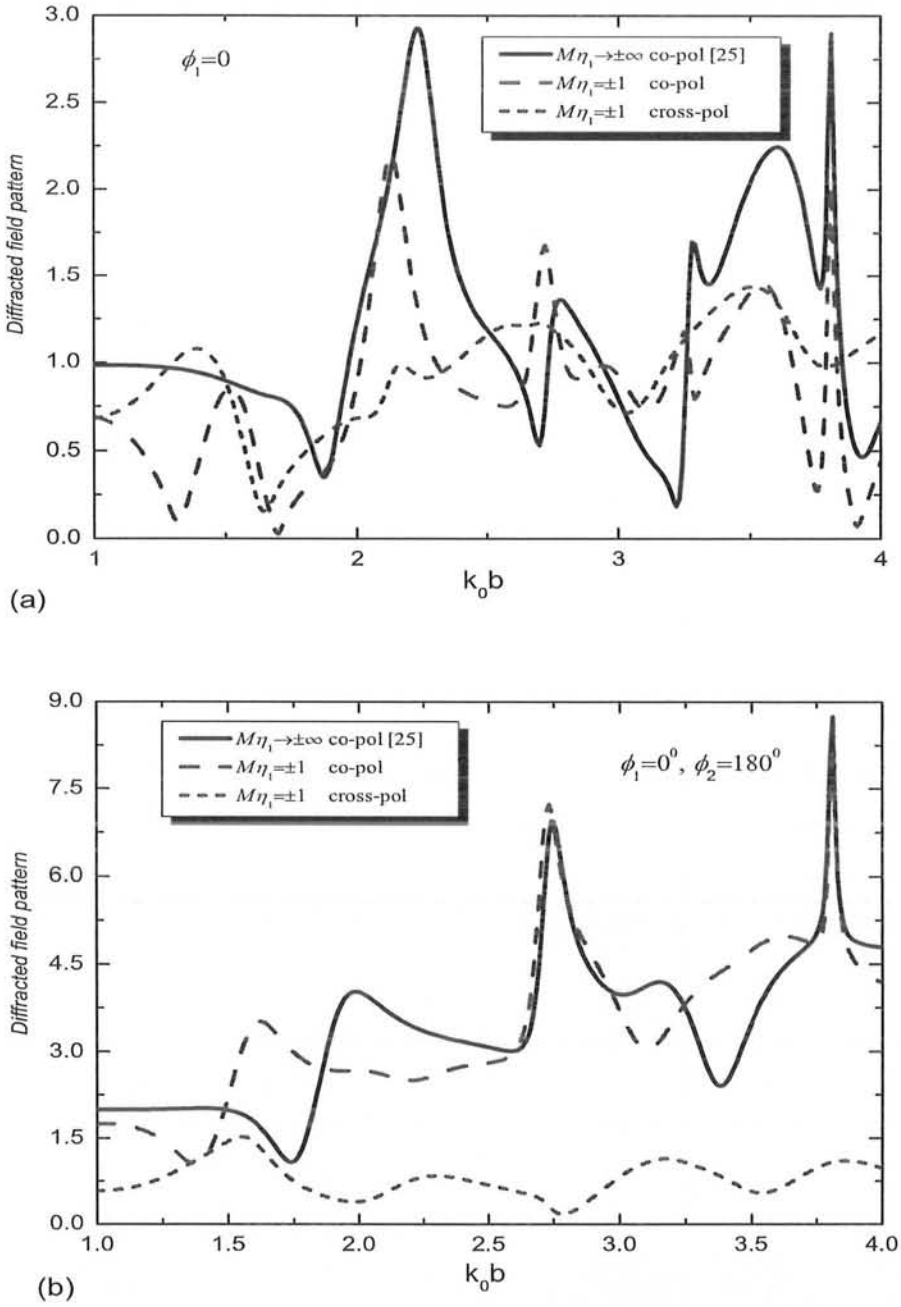


Figure 3.15. Co- and cross-polarized components of the diffracted field patterns (E-pol case), versus $k_0 b$ at $\phi = 0$, for $k_0 a = 1, \epsilon_r = 5, \mu_r = 1$.

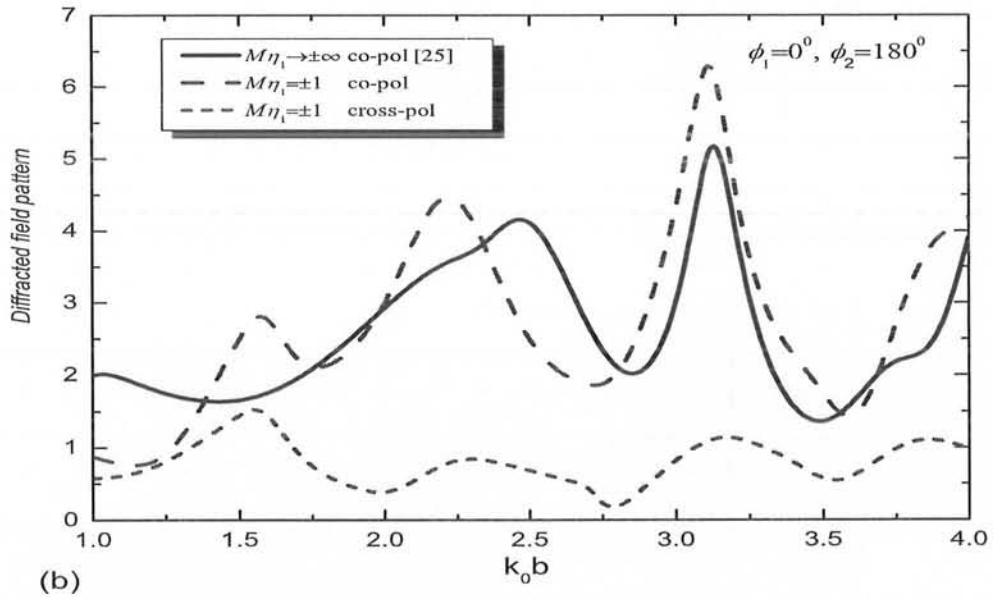
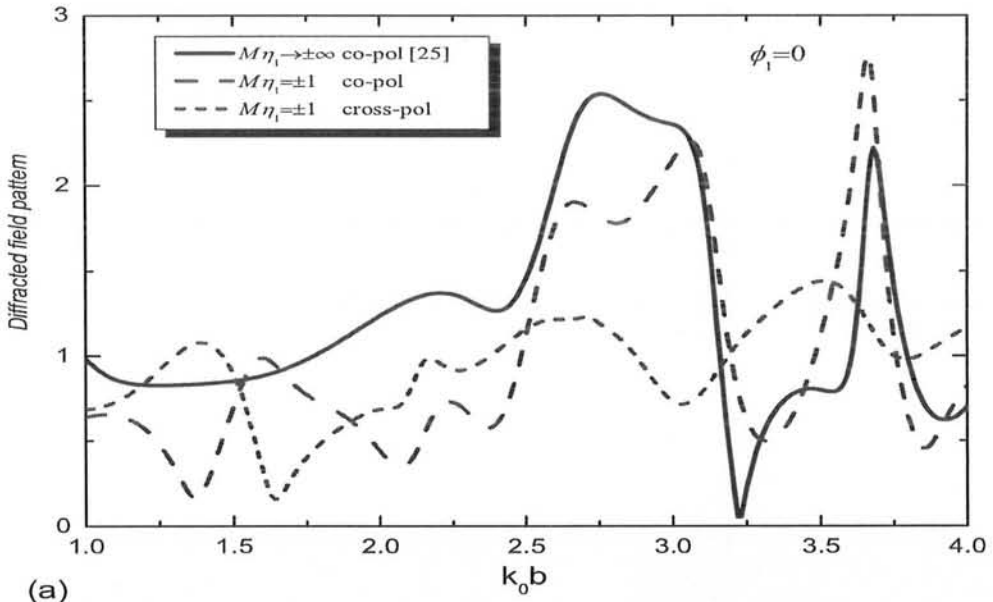


Figure 3.16. Co- and cross-polarized components of the diffracted field patterns (E-pol case), versus $k_0 b$ at $\phi = 0$, for $k_0 a = 1$ and $\epsilon_r = 1, \mu_r = 5$.

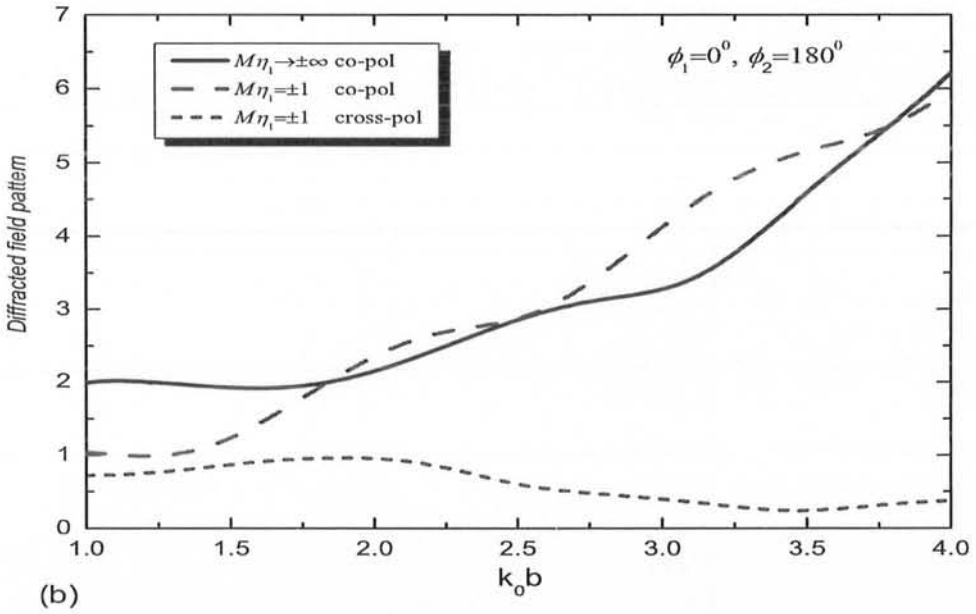
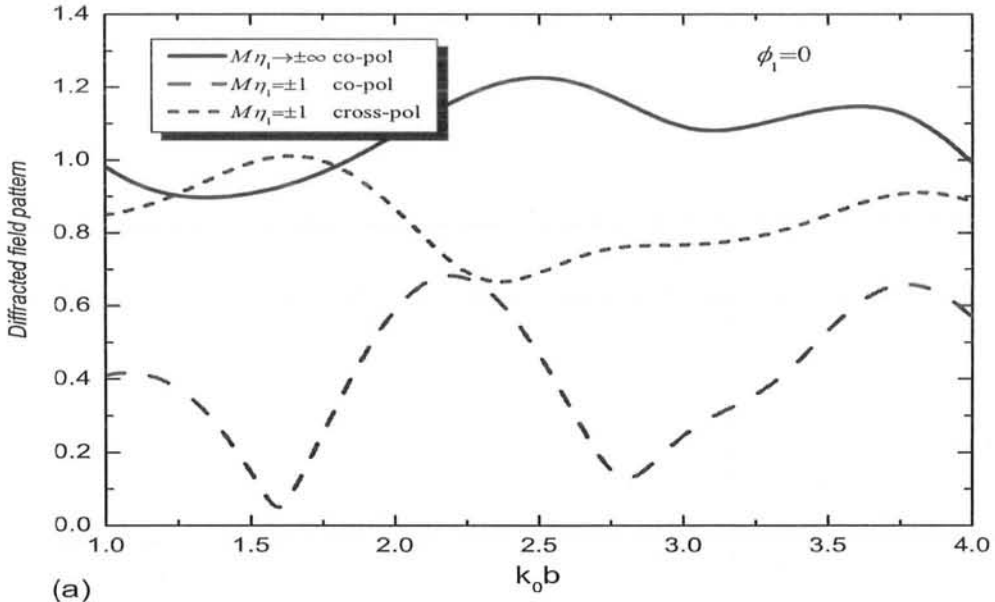


Figure 3.17. Co- and cross-polarized components of the diffracted field patterns (H-pol case) versus $k_0 b$ at $\phi = 0$, for $k_0 a = 1$ and $\epsilon_r = 2.2, \mu_r = 1$.

Fig. 3.14(a) shows the co-polarized scattered field patterns while Fig. 3.14(b) presents the cross-polarized scattered field patterns.

Figs. 3.15 and Fig. 3.16, show the dependence of the co- and cross-polarized components of the diffracted far-field patterns on the thickness of the coating layer. In these two figures the radius of the inner cylinder, is taken as $k_0a = 1$, while the thickness of the coating layer is varied between $k_0b = 1$ and $k_0b = 4$. Fig. 3.15(a), presents the variations in the co- and cross-polarized field components, when a single plane wave with $\phi_1 = 0^0$ excites the geometry versus k_0b , when $\epsilon_r = 5$ and $\mu_r = 1$. Fig 3.15(b) shows the variations of the field components for two incident plane waves, with $\phi_1 = 0^0, \phi_2 = 180^0$. Figs. 3.16(a) and (b), show the co- and cross-polarized components of the diffracted far-field with the variation in the coating thickness for one and two incident plane waves, respectively. Here in Fig. 3.15, coating layer has the parameters as $\epsilon_r = 1$ and $\mu_r = 5$. From Figs. 3.15 and 3.16, it is obvious that the co-polarized components of the coated PEMC cylinder with $M\eta_1 \rightarrow \pm\infty$ shows a good agreement with that of a coated PEC cylinder [25]. And cross-polarized component vanishes in this case.

Figs. 3.17(a) and (b), show the co and cross-polarized components of the diffracted far-field in the H-polarized case, for one and two incident plane waves, respectively. Here in Fig. 3.17, the coating layer with constitutive parameters $\epsilon_r = 2.2$ and $\mu_r = 1$ is chosen while the admittance parameter is taken as $M\eta_1 = \pm 1$ and $M\eta_1 = \pm\infty$.

Fig. 3.18 presents the far-zone scattered field of a PEMC cylinder when coated with a dissipative and dispersive DNG material with $\epsilon_r = -0.40 + j0.26, \mu_r = -1.40 + j0.62, k_0a = 1, k_0b = 2$ for both E-polarized and H-polarized cases when $M\eta_1 = \pm 1$. Three incident plane waves with angles of incidence $\phi_1 = 0^0, \phi_2 = 180^0$, and $\phi_3 = 135^0$ and amplitudes $E_{01} = E_{02} = E_{03} = 1$ are considered in this case. Fig. 3.18(a) shows the co-polarized components while Fig. 3.18(b) presents the cross-polarized components of scattered field for both E-polarized and H-polarized cases.

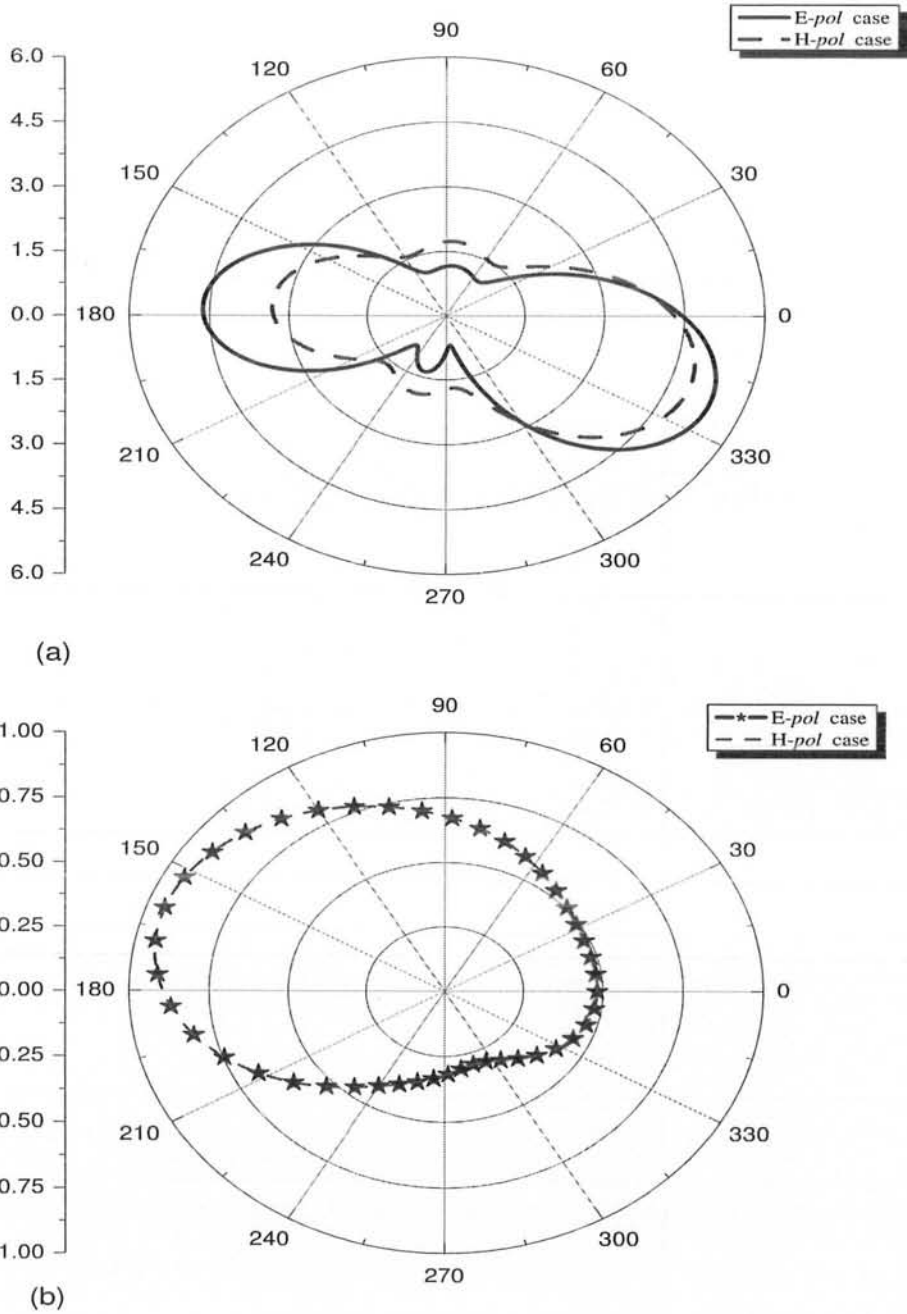


Figure 3.18. Far-zone scattered field of a PEMC cylinder coated with a dissipative and dispersive DNG material with $\epsilon_r = -0.40 + j0.26$, $\mu_r = -1.40 + j0.62$, $M\eta_1 = \pm 1$, $k_0a = 1$, $k_0b = 2$, $\epsilon_r = -9.8$, $\mu_r = -1$, $\phi_1 = 0^\circ$, $\phi_2 = 180^\circ$, $\phi_3 = 135^\circ$ and $E_{01} = E_{02} = E_{03} = 1$, (a) Co-polarized components. (b) Cross-polarized components.

CHAPTER 4

Directive EM scattering from a coated PEMC cylinder

Electromagnetic scattering of a real (actual) line source from a PEMC circular cylinder, coated with DNG is investigated theoretically. The response of DNG coated PEMC circular cylinder is observed and it is noted that how the results obtained for this configuration differ from those of a coated PEC cylinder. The effect of dissipative and dispersive DNG coating layer on the scattered field from the coated PEMC cylinder is also discussed. It is assumed that both the PEMC cylinder and the coating layer are infinite along the cylinder axis. The obtained numerical results are compared with the published literature, and are found to be in good agreement with them.

4.1. DNG coated PEMC cylinder

The geometry of the scattering problem is shown in Fig. 4.1, where the inner cylinder is a PEMC cylinder while the outer cylinder is the DNG coating of uniform thickness. The radius of the PEMC cylinder without coating is a while its radius with coating is b . A line source has been used as the source of excitation for the configuration which is located at (ρ_0, ϕ_0) . The cylinder is supposed to be infinite along the axis and is of circular cross section. Discussion has been divided into two cases. In the first case, the line source is placed outside the coating layer and in the second case the line source is placed inside the coating layer.

4.1.1. Line source outside the coating layer

For the case of the line source outside the coating layer, the geometry has been divided into three regions. The region occupying the space away from the line source, i.e., $\rho \geq \rho_0$ is named as Region I. And the region between the line source and the coating layer, i.e., $b \leq \rho \leq \rho_0$ is named as Region II. Region I and Region II are free

space with (μ_0, ϵ_0) , and wavenumber $k_0 = \omega\sqrt{\mu_0\epsilon_0}$. While DNG layer $a \leq \rho \leq b$, with $k_1 = \omega\sqrt{\mu_1\epsilon_1}$ is taken as Region III. The incident electric field

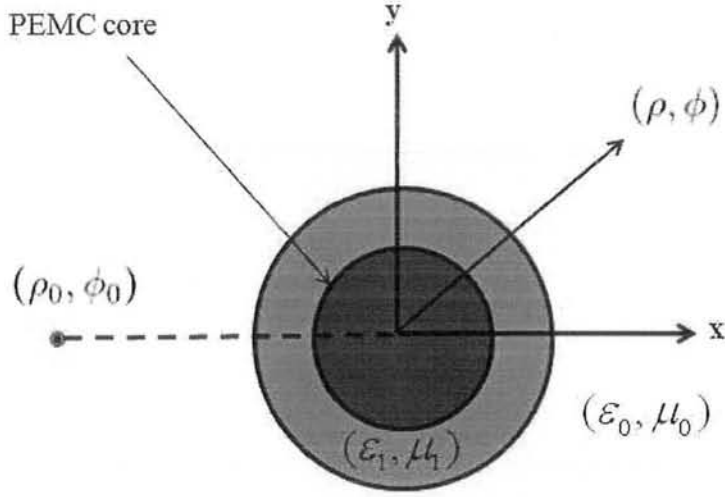


Figure 4.1. DNG coated PEMC circular cylinder.

from the line source is given by

$$E_{0z}^{inc}(\rho, \phi) = -\frac{k_0^2 I}{4\omega\epsilon_0} H_n^{(1)}(k_0|\rho - \rho_0|) \quad (4.1.1)$$

Using addition theorem of Hankel functions, above can be written as

$$E_z^{inc}(\rho, \phi) = \begin{cases} -\frac{k_0^2 I}{4\omega\mu} \sum_{n=-\infty}^{\infty} H_n^{(1)}(k_0\rho_0) J_n(k_0\rho) e^{jn(\phi-\phi_0)} & b \leq \rho \leq \rho_0 \\ -\frac{k_0^2 I}{4\omega\mu} \sum_{n=-\infty}^{\infty} J_n(k_0\rho_0) H_n^{(1)}(k_0\rho) e^{jn(\phi-\phi_0)} & \rho_0 \leq \rho \end{cases} \quad (4.1.2)$$

As the core is a PEMC circular cylinder, the scattered field will contain a cross-polarized field component in addition to the co-polarized field component. The total fields in Region I, in terms of unknown expansion coefficients are given by following expressions

$$E_z^I = -\frac{k_0^2 I}{4\omega\epsilon_0} \sum_{n=-\infty}^{\infty} H_n^{(1)}(k_0\rho) [J_n(k_0\rho_0) + a_n H_n^{(1)}(k_0\rho_0)] e^{jn(\phi-\phi_0)} \quad (4.1.3)$$

$$H_{\phi}^I = \frac{k_0^2 I}{4j\omega\epsilon_0\eta_0} \sum_{n=-\infty}^{\infty} H_n^{(1)'}(k_0\rho)[J_n(k_0\rho_0) + a_n H_n^{(1)}(k_0\rho_0)]e^{jn(\phi-\phi_0)} \quad (4.1.4)$$

$$H_z^I = -\frac{k_0^2 I}{4j\omega\epsilon_0\eta_0} \sum_{n=-\infty}^{\infty} H_n^{(1)}(k_0\rho)[J_n(k_0\rho_0) + b_n H_n^{(1)}(k_0\rho_0)]e^{jn(\phi-\phi_0)} \quad (4.1.5)$$

$$E_{\phi}^I = \frac{k_0^2 I}{4\omega\epsilon_0} \sum_{n=-\infty}^{\infty} H_n^{(1)'}(k_0\rho)[J_n(k_0\rho_0) + b_n H_n^{(1)}(k_0\rho_0)]e^{jn(\phi-\phi_0)} \quad (4.1.6)$$

While the total fields in the Region II may be written as

$$E_z^{\text{II}} = -\frac{k_0^2 I}{4\omega\epsilon_0} \sum_{n=-\infty}^{\infty} H_n^{(1)}(k_0\rho_0)[J_n(k_0\rho) + a_n H_n^{(1)}(k_0\rho)]e^{jn(\phi-\phi_0)} \quad (4.1.7)$$

$$H_{\phi}^{\text{II}} = \frac{k_0^2 I}{4j\omega\epsilon_0\eta_0} \sum_{n=-\infty}^{\infty} H_n^{(1)}(k_0\rho_0)[J_n'(k_0\rho) + a_n H_n^{(1)'}(k_0\rho)]e^{jn(\phi-\phi_0)} \quad (4.1.8)$$

$$H_z^{\text{II}} = -\frac{k_0^2 I}{4j\omega\epsilon_0\eta_0} \sum_{n=-\infty}^{\infty} H_n^{(1)}(k_0\rho_0)[J_n(k_0\rho) + b_n H_n^{(1)}(k_0\rho)]e^{jn(\phi-\phi_0)} \quad (4.1.9)$$

$$E_{\phi}^{\text{II}} = \frac{k_0^2 I}{4\omega\epsilon_0} \sum_{n=-\infty}^{\infty} H_n^{(1)}(k_0\rho_0)[J_n'(k_0\rho) + b_n H_n^{(1)'}(k_0\rho)]e^{jn(\phi-\phi_0)} \quad (4.1.10)$$

The total fields in Region III is

$$E_z^{\text{III}} = -\frac{k_0^2 I}{4\omega\epsilon_0} \sum_{n=-\infty}^{\infty} H_n^{(1)}(k_0\rho_0)[c_n J_n(k_1\rho) + d_n H_n^{(1)}(k_1\rho)]e^{jn(\phi-\phi_0)} \quad (4.1.11)$$

$$H_{\phi}^{\text{III}} = \frac{k_0^2 I}{4j\omega\epsilon_0\eta_1} \sum_{n=-\infty}^{\infty} H_n^{(1)}(k_0\rho_0)[c_n J_n'(k_1\rho) + d_n H_n^{(1)'}(k_1\rho)]e^{jn(\phi-\phi_0)} \quad (4.1.12)$$

$$H_z^{\text{III}} = -\frac{k_0^2 I}{4j\omega\epsilon_0\eta_1} \sum_{n=-\infty}^{\infty} H_n^{(1)}(k_0\rho_0)[e_n J_n(k_1\rho) + f_n H_n^{(1)}(k_1\rho)]e^{jn(\phi-\phi_0)} \quad (4.1.13)$$

$$E_{\phi}^{\text{III}} = \frac{k_0^2 I}{4\omega\epsilon_0} \sum_{n=-\infty}^{\infty} H_n^{(1)}(k_0\rho_0)[e_n J_n'(k_1\rho) + f_n H_n^{(1)'}(k_1\rho)]e^{jn(\phi-\phi_0)} \quad (4.1.14)$$

In the above expressions $a_n, b_n, c_n, d_n, e_n,$ and f_n are the six unknown scattering coefficients which are to be determined. These unknowns can be found by using appropriate boundary conditions at the interfaces, $\rho = a,$ and $\rho = b.$ The boundary conditions at the interface, $\rho = a,$ are

$$H_z^{\text{III}} + ME_z^{\text{III}} = 0, \quad \rho = a, \quad 0 \leq \phi \leq 2\pi \quad (4.1.15)$$

$$H_{\phi}^{\text{III}} + ME_{\phi}^{\text{III}} = 0, \quad \rho = a, \quad 0 \leq \phi \leq 2\pi \quad (4.1.16)$$

And the boundary conditions at the interface, $\rho = b$, are

$$E_z^{\text{II}} = E_z^{\text{III}}, \quad \rho = b, \quad 0 \leq \phi \leq 2\pi \quad (4.1.17)$$

$$H_\phi^{\text{II}} = H_\phi^{\text{III}}, \quad \rho = b, \quad 0 \leq \phi \leq 2\pi \quad (4.1.18)$$

$$H_z^{\text{II}} = H_z^{\text{III}}, \quad \rho = b, \quad 0 \leq \phi \leq 2\pi \quad (4.1.19)$$

$$E_\phi^{\text{II}} = E_\phi^{\text{III}}, \quad \rho = b, \quad 0 \leq \phi \leq 2\pi \quad (4.1.20)$$

Application of these boundary conditions at $\rho = a$ and $\rho = b$, yields a linear matrix equation about the unknown scattering coefficients. Solution of this matrix equation gives us the values of all the unknowns scattering coefficients in the above equations. The scattered co- and cross-polarized fields radiated by the coated PEMC cylinder may be found by using the values of a_n and b_n in equations (4.1.3) and (4.1.6). Far-zone scattered fields are obtained by using the asymptotic form of Hankel functions.

4.1.2. Numerical results and discussion

In this section the numerical results of the far-field radiation due to a coated PEMC circular cylinder, have been presented. In order to verify the analytical formulation and the numerical code, the results obtained are compared with the published literature and are found to be in good agreement with them. In all the plots the radius of the PEMC cylinder is taken as $a = 1.25\lambda_0$ and λ_0 is the wavelength of the free space. Also in all the plots, the full black line shows the scattering behavior for PEC as special case of PEMC i.e., $M\eta_1 \rightarrow \pm\infty$. While dashed and short dashed lines are used for co- and cross-polarized components of PEMC case with $M\eta_1 = \pm 1$, respectively. Fig. 4.2 presents the scattering behavior of the PEMC cylinder coated with either DPS or DNG, when the line source is outside the coating layer. The parameters for the scattering phenomena for this figure are, $b = 2.2, \rho_0 = 2.3$. In Fig. 4.2(a), the far-field radiation patterns of coated PEMC cylinder for $\epsilon_r = 1.5$ and $\mu_r = 1.5$, are shown. It is obvious from this figure, that for DPS coated PEMC cylinder is some what directive

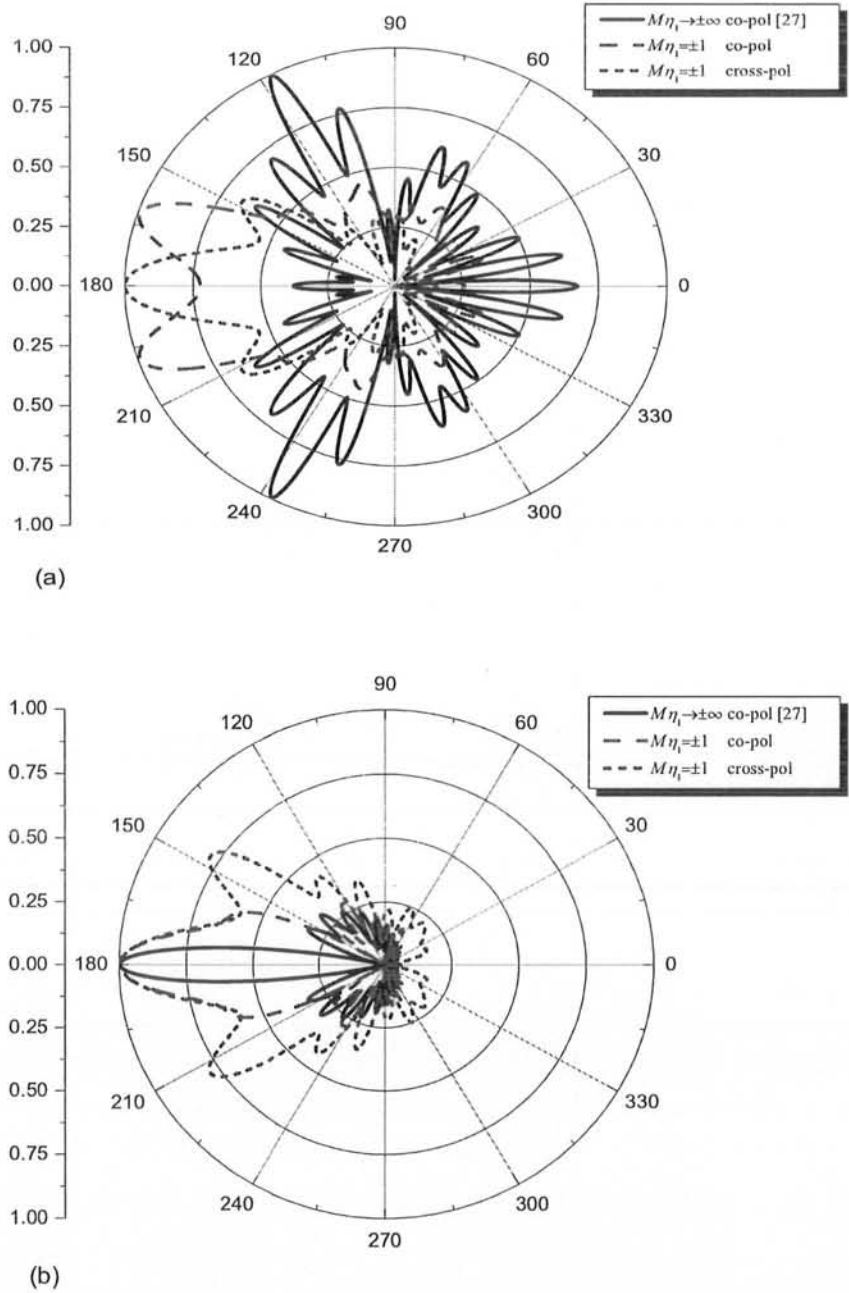


Figure 4.2. Far-field radiation pattern of a PEMC cylinder when line source is outside the coating layer, i.e., $a = 1.25\lambda_0$, $b = 2.2\lambda_0$, and $\rho_0 = 2.3\lambda_0$ (a) DPS coating with $\epsilon_r = 1.5$, $\mu_r = 1.5$, (b) DNG coating $\epsilon_r = -1.5$, $\mu_r = -1.5$.

than a DPS coated PEC cylinder. Fig. 4.2(b), shows the behavior of the co- and cross-polarized components of the far-field radiation patterns of DNG ($\epsilon_r = -1.5$, $\mu_r = -1.5$) coated PEMC cylinder for the same parameters as for Fig. 4.2. This figure shows that the radiation patterns due to a DNG coated PEMC cylinder are less directive than those of a PEC cylinder coated by DNG material.

4.1.3. Line source inside the coating layer

When the electric line source is placed inside the coating layer, Region I ($b \leq \rho$) is free space while Region II ($\rho_0 \leq \rho \leq b$) and Region III ($a \leq \rho \leq \rho_0$), are in the coating layer. The scattered fields in Region I may be expressed as

$$E_z^I = -\frac{k_1^2 I}{4\omega\epsilon_1} \sum_{n=-\infty}^{\infty} a_n H_n^{(1)}(k_1 \rho_0) H_n^{(1)}(k_0 \rho) e^{jn(\phi-\phi_0)} \quad (4.1.21)$$

$$H_\phi^I = \frac{k_1^2 I}{4j\omega\epsilon_1 \eta_0} \sum_{n=-\infty}^{\infty} a_n H_n^{(1)}(k_1 \rho_0) H_n^{(1)'}(k_0 \rho) e^{jn(\phi-\phi_0)} \quad (4.1.22)$$

$$H_z^I = -\frac{k_1^2 I}{4j\omega\epsilon_1 \eta_0} \sum_{n=-\infty}^{\infty} b_n H_n^{(1)}(k_1 \rho_0) H_n^{(1)}(k_0 \rho) e^{jn(\phi-\phi_0)} \quad (4.1.23)$$

$$E_\phi^I = \frac{k_1^2 I}{4\omega\epsilon_1} \sum_{n=-\infty}^{\infty} b_n H_n^{(1)}(k_1 \rho_0) H_n^{(1)'}(k_0 \rho) e^{jn(\phi-\phi_0)} \quad (4.1.24)$$

Total fields in Region II may be written as

$$E_z^{II} = -\frac{k_1^2 I}{4\omega\epsilon_1} \sum_{n=-\infty}^{\infty} H_n^{(1)}(k_1 \rho_0) [c_n J_n(k_1 \rho) + d_n H_n^{(1)}(k_1 \rho)] e^{jn(\phi-\phi_0)} \quad (4.1.25)$$

$$H_\phi^{II} = \frac{k_1^2 I}{4j\omega\epsilon_1 \eta_1} \sum_{n=-\infty}^{\infty} H_n^{(1)}(k_1 \rho_0) [c_n J_n'(k_1 \rho) + d_n H_n^{(1)'}(k_1 \rho)] e^{jn(\phi-\phi_0)} \quad (4.1.26)$$

$$H_z^{II} = -\frac{k_1^2 I}{4j\omega\epsilon_1 \eta_1} \sum_{n=-\infty}^{\infty} H_n^{(1)}(k_1 \rho_0) [e_n J_n(k_1 \rho) + f_n H_n^{(1)}(k_1 \rho)] e^{jn(\phi-\phi_0)} \quad (4.1.27)$$

$$E_\phi^{II} = \frac{k_1^2 I}{4\omega\epsilon_1} \sum_{n=-\infty}^{\infty} H_n^{(1)}(k_1 \rho_0) [e_n J_n'(k_1 \rho) + f_n H_n^{(1)'}(k_1 \rho)] e^{jn(\phi-\phi_0)} \quad (4.1.28)$$

And the total fields in Region III are

$$E_z^{III} = -\frac{k_1^2 I}{4\omega\epsilon_1} \sum_{n=-\infty}^{\infty} H_n^{(1)}(k_1 \rho_0) [g_n J_n(k_1 \rho) + h_n H_n^{(1)}(k_1 \rho)] e^{jn(\phi-\phi_0)} \quad (4.1.29)$$

$$H_{\phi}^{\text{III}} = \frac{k_1^2 I}{4j\omega\epsilon_1\eta_1} \sum_{n=-\infty}^{\infty} H_n^{(1)}(k_1\rho_0)[g_n J_n'(k_1\rho) + h_n H_n^{(1)'}(k_1\rho)]e^{jn(\phi-\phi_0)} \quad (4.1.30)$$

$$H_z^{\text{III}} = -\frac{k_1^2 I}{4j\omega\epsilon_1\eta_1} \sum_{n=-\infty}^{\infty} H_n^{(1)}(k_1\rho_0)[l_n J_n(k_1\rho) + p_n H_n^{(1)}(k_1\rho)]e^{jn(\phi-\phi_0)} \quad (4.1.31)$$

$$E_{\phi}^{\text{III}} = \frac{k_1^2 I}{4\omega\epsilon_1} \sum_{n=-\infty}^{\infty} H_n^{(1)}(k_1\rho_0)[l_n J_n'(k_1\rho) + p_n H_n^{(1)'}(k_1\rho)]e^{jn(\phi-\phi_0)} \quad (4.1.32)$$

Here $a_n, b_n, c_n, d_n, e_n, f_n, g_n, h_n, l_n,$ and p_n are the unknown scattering coefficients which are to be determined, using appropriate boundary conditions at the interfaces $\rho = a, \rho = \rho_0,$ and $\rho = b.$ The boundary conditions at the interface, $\rho = a,$ are

$$H_z^{\text{III}} + ME_z^{\text{III}} = 0, \quad \rho = a, \quad 0 \leq \phi \leq 2\pi \quad (4.1.33)$$

$$H_{\phi}^{\text{III}} + ME_{\phi}^{\text{III}} = 0, \quad \rho = a, \quad 0 \leq \phi \leq 2\pi \quad (4.1.34)$$

While boundary conditions at the interface, $\rho = \rho_0,$ are

$$E_z^{\text{II}} = E_z^{\text{III}}, \quad \rho = \rho_0, \quad 0 \leq \phi \leq 2\pi \quad (4.1.35)$$

$$H_{\phi}^{\text{II}} - H_{\phi}^{\text{III}} = j\omega\mu_1\delta(\phi - \phi_0), \quad \rho = \rho_0, \quad 0 \leq \phi \leq 2\pi \quad (4.1.36)$$

$$H_z^{\text{II}} = H_z^{\text{III}}, \quad \rho = \rho_0, \quad 0 \leq \phi \leq 2\pi \quad (4.1.37)$$

$$E_{\phi}^{\text{II}} = E_{\phi}^{\text{III}}, \quad \rho = \rho_0, \quad 0 \leq \phi \leq 2\pi \quad (4.1.38)$$

And the boundary conditions at the interface, $\rho = b,$ are

$$E_z^{\text{I}} = E_z^{\text{II}}, \quad \rho = b, \quad 0 \leq \phi \leq 2\pi \quad (4.1.39)$$

$$H_{\phi}^{\text{I}} = H_{\phi}^{\text{II}}, \quad \rho = b, \quad 0 \leq \phi \leq 2\pi \quad (4.1.40)$$

$$H_z^{\text{I}} = H_z^{\text{II}}, \quad \rho = b, \quad 0 \leq \phi \leq 2\pi \quad (4.1.41)$$

$$E_{\phi}^{\text{I}} = E_{\phi}^{\text{II}}, \quad \rho = b, \quad 0 \leq \phi \leq 2\pi \quad (4.1.42)$$

Applying these boundary conditions, a linear matrix equation is obtained about the unknown scattering coefficients. Solution of this matrix equation gives us the values of all the unknowns scattering coefficients in the above equations. Using the values of a_n and b_n in equations (4.1.21) and (4.1.24), the scattered co- and cross-polarized fields radiated by the coated PEMC cylinder are obtained.

4.1.4. Numerical results and discussion

Figs. 4.3-4.5, are reserved for the discussion about the scattering patterns of a DNG coated PEMC cylinder when the line source is inside the coating layer. Fig. 4.3 presents the comparison of the radiation power gain of a coated PEMC and a coated PEC cylinders. This figure shows that the co-polarized component of the power gain in the case of coated PEMC cylinder, increases continuously as the source boundary distance is increased, while the cross-polarized component of the power gain reduces at the same time.

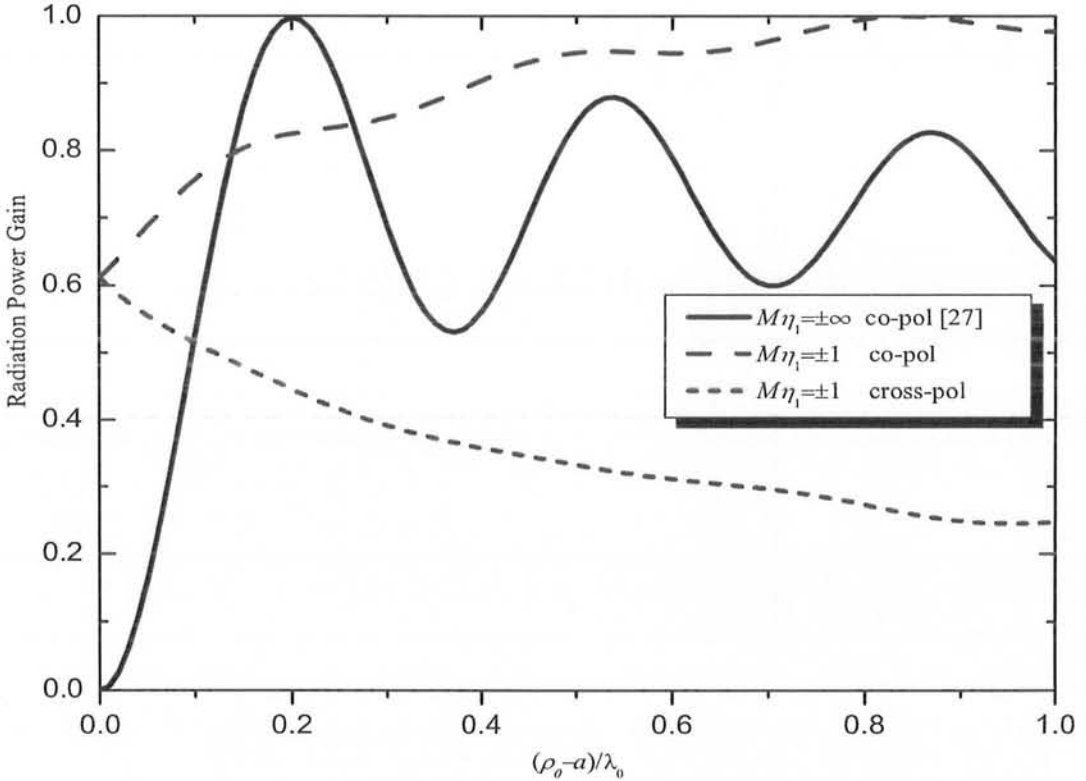
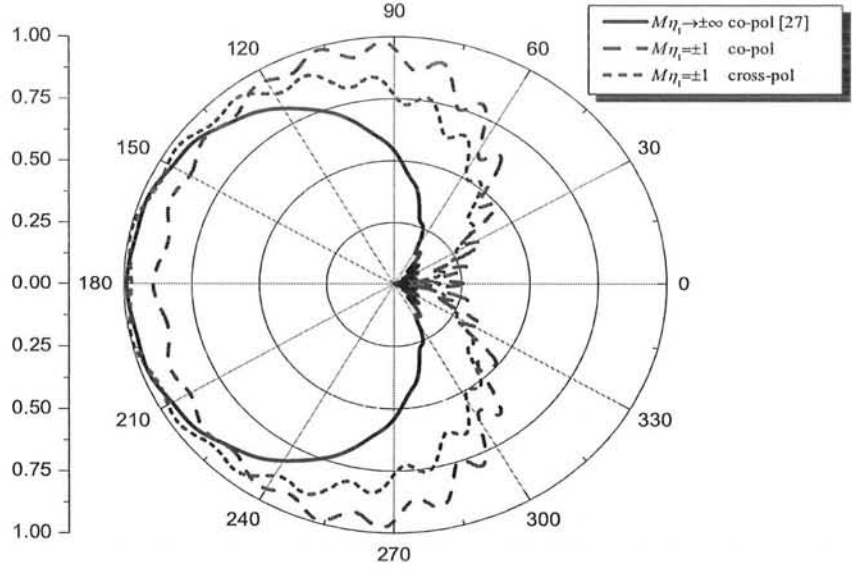
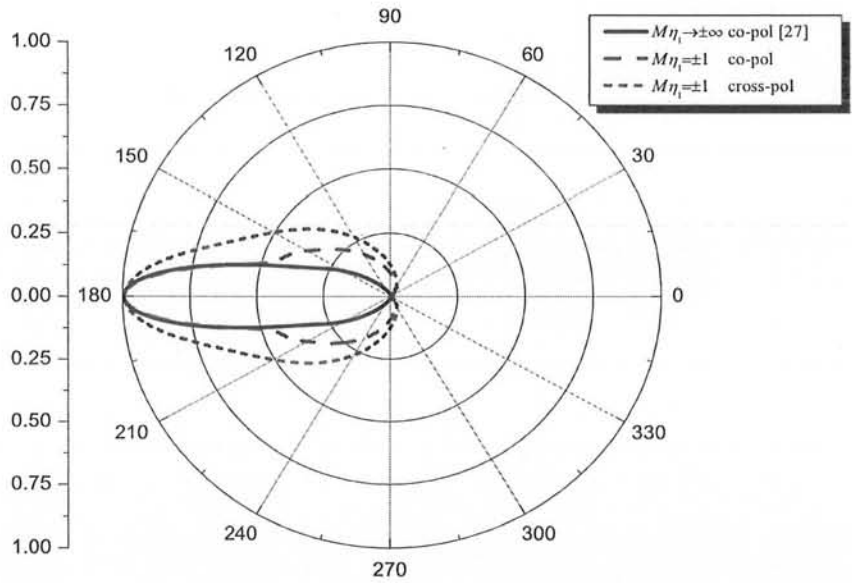


Figure 4.3. Radiation power gain of a PEMC circular cylinder as a function of distance of line source from the cylinder boundary when $a = 1.25\lambda_0$, $b = 3\lambda_0$ and DNG with $\epsilon_r = -1.5$, $\mu_r = -1.5$, coating layer is used.

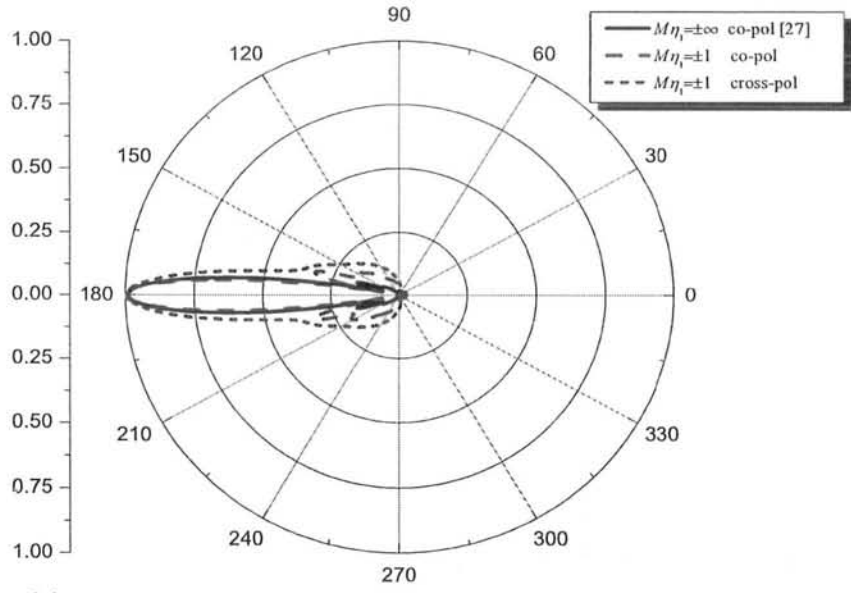


(a)

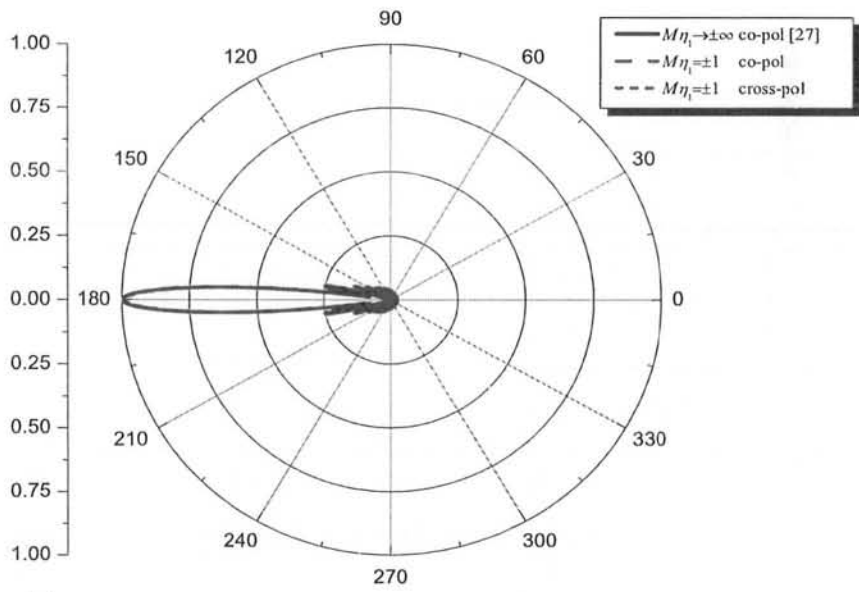


(b)

Figure 4.4. Far-field radiation pattern of a PEMC cylinder when line source is inside the coating layer, i.e., $a = 1.25\lambda_0$, $b = 3\lambda_0$, and $\rho_0 = 1.4\lambda_0$ (a) DPS coating with $\epsilon_r = 1.5$, $\mu_r = 1.5$, (b) DNG coating with $\epsilon_r = -1$, $\mu_r = -1$.



(a)



(b)

Figure 4.5. Far-field radiation pattern of a PEMC cylinder when line source is inside the coating layer, i.e., $a = 1.25\lambda_0$, $b = 3\lambda_0$, and $\rho_0 = 1.4\lambda_0$ (a) DNG coating with $\epsilon_r = -1.5$, $\mu_r = -1.5$, (b) DNG coating with $\epsilon_r = -4.28$, $\mu_r = -2.62$.

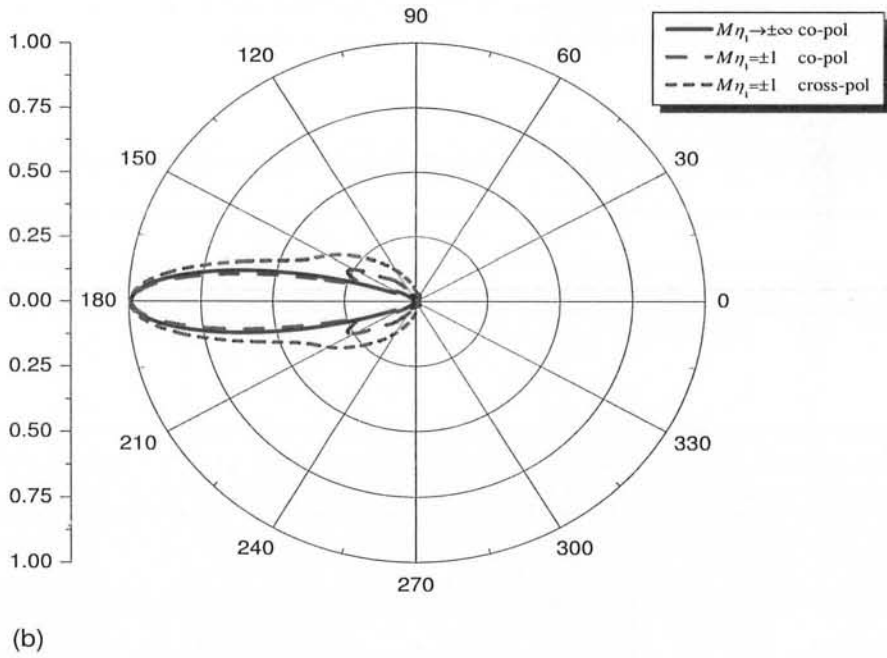
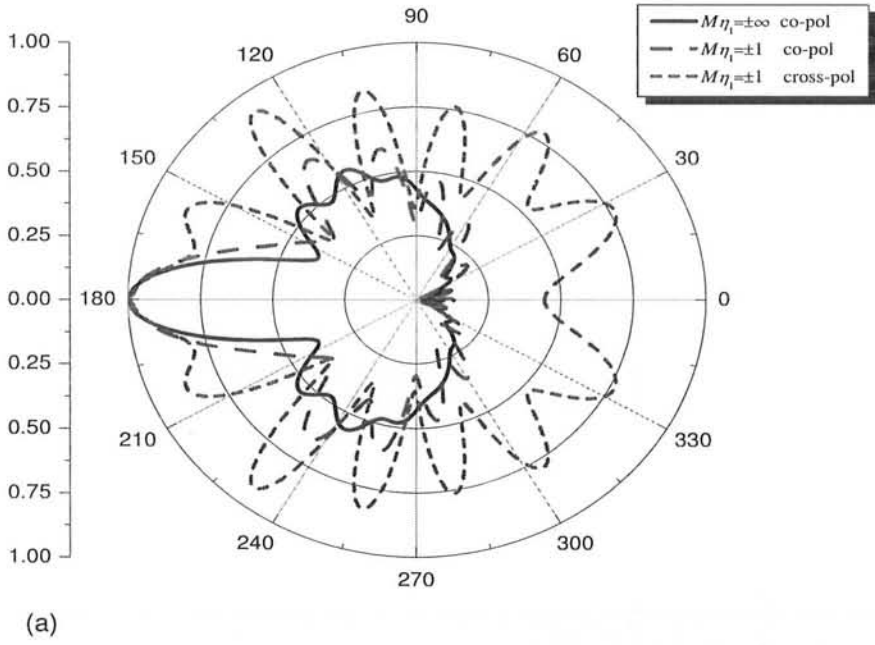


Figure 4.6. Far-field radiation pattern of a PEMC cylinder when Dispersive and dispersive DNG coating layer with $\epsilon_r = -0.63 + j0.034$, $\mu_r = -2.70 + j0.14$, is used (a) $a = 1.25\lambda_0$, $b = 2.2\lambda_0$, and $\rho_0 = 2.3\lambda_0$, (b) $a = 1.25\lambda_0$, $b = 3\lambda_0$, and $\rho_0 = 1.4\lambda_0$.

Fig. 4.4 gives the far-field radiation patterns of the coated PEMC cylinder for two types of the coating layers. In Fig. 4.4(a), the radiation patterns are shown when the coating layer is an DNG with $\epsilon_r = -1$ and $\mu_r = -1$. This plot also predicts the difference between PEC and PEMC materials when they are used as the core of the geometry. Fig. 4.4(b) shows the difference between radiation patterns of a coated PEC and a coated PEMC cylinders when they are coated by an ordinary dielectric material with $\epsilon_r = 1.5$ and $\mu_r = 1.5$. Fig. 4.5(a) exhibits the far-field radiation patterns for the same configuration as in the case of Fig. 4.3, for an DNG coating layer. This figure also shows the comparison between a coated PEC and a coated PEMC cylinder when the coating layer is defined by $\epsilon_r = -1.5$ and $\mu_r = -1.5$. Fig. 4.5(b) shows the far-field radiation patterns of a PEMC cylinder, when it is coated by a DNG material with $\epsilon_r = -4.28$, $\mu_r = -2.62$. It is observed that for this type of the DNG material the proposed geometry is highly directive. Also it is seen from this figure that coated PEMC cylinder behaves just like a coated PEC cylinder for this type of coating layer.

Fig. 4.6 present the far-field radiation patterns when the PEMC cylinder is coated by a dissipative and dispersive DNG material having relative permittivity and permeability as $\epsilon_r = -0.63 + j0.034$ and $\mu_r = -2.70 + j0.14$, respectively. Figs. 4.6(a) and (b) show the radiation patterns when the line source is placed outside ($a = 1.25\lambda_0$, $b = 2.2\lambda_0$, and $\rho_0 = 2.3\lambda_0$) and inside ($a = 1.25\lambda_0$, $b = 3\lambda_0$, and $\rho_0 = 1.4\lambda_0$) the coating layer, respectively.

CHAPTER V

Analysis of Field due to a buried PEMC cylinder

In this chapter an analytical solution for the scattering of an electromagnetic plane wave from a perfect electromagnetic conducting circular cylinder, buried in the dielectric half-space, is presented. The solution is based on the spectral (plane wave) representations of the fields and accounts for all the multiple interactions between the buried circular cylinder and the dielectric interface separating the two half spaces.

5.1. Buried PEMC cylinder

The geometry of the problem used for the analysis here is shown in Figure 5.1.

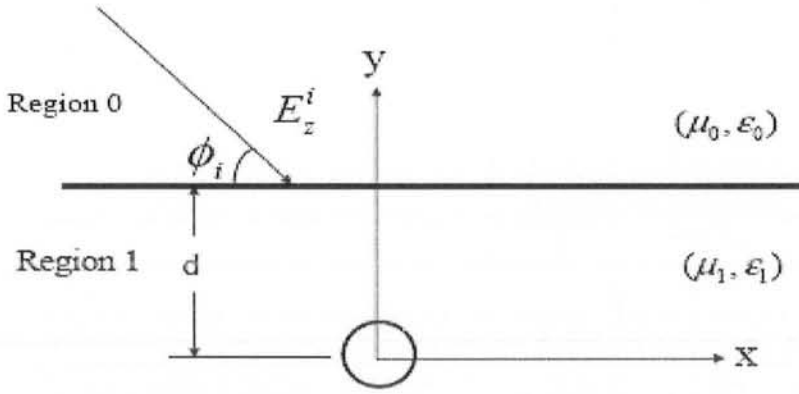


Figure 5.1. Buried PEMC circular cylinder inside a dielectric half space.

Geometry contains a PEMC circular cylinder of infinite extent and buried in a dielectric half space, as shown in Fig. 5.1. For the sake of simplicity, it is assumed that axis of the cylinder is coincident with z -axis of the coordinate system. Radius of the cylinder is a and depth of the cylinder from dielectric interface is d . It is assumed that the dielectric half spaces is has small losses. Region above the dielectric interface has been termed as region 0 and has wavenumber $k_0 = \omega\sqrt{\mu_0\epsilon_0}$, while region between the dielectric interface and cylinder is termed as region 1 and has wavenumber $k_1 = \omega\sqrt{\mu_1\epsilon_1}$. Also

$\mu_1 = \mu_0\mu_r$ and $\epsilon_1 = \epsilon_0\epsilon_r$, is the permeability and permittivity of the dielectric region respectively.

5.1.1. Initial reflected and transmitted fields

Electric field component of an obliquely incident electromagnetic plane wave is given as

$$E_z^i = e^{j(k_x^i x - k_{0y}^i y)} \quad (5.1.1)$$

where $k_0^2 = k_x^2 + k_0y^2$. The reflected and transmitted electric field components from the dielectric interface, as if no cylinder is not present, are given as

$$E_z^r = R_{01}(k_x^i) e^{j(k_x^i x + k_{0y}^i y)} \quad (5.1.2)$$

$$E_z^t = T_{01}(k_x^i) e^{j(k_x^i x - k_{1y}^i y)} \quad (5.1.3)$$

where where $k_0^2 = k_x^2 + k_0y^2$, while $R_{01}(k_x^i)$ and $T_{01}(k_x^i)$ are the unknown coefficients of the reflected and transmitted fields respectively. These coefficients are found by the application of boundary conditions on electric and magnetic field components at the dielectric-air interface and are obtained as

$$R_{01}(k_x^i) = \left[\frac{k_{0y}^i - k_{1y}^i}{k_{0y}^i + k_{1y}^i} \right] e^{j2k_{0y}^i d} \quad (5.1.4)$$

$$T_{01}(k_x^i) = \left[\frac{2k_{0y}^i}{k_{0y}^i + k_{1y}^i} \right] e^{j(k_{0y}^i - k_{1y}^i) d} \quad (5.1.5)$$

Incident field given in (5.1.1), in terms of cylindrical coordinates (ρ, ϕ) , can be written as

$$E_z^i = e^{jk_0\rho \cos(\phi - \phi_i)} \quad (5.1.6)$$

ϕ_i is the angle of incidence with respect to the horizontal axis. The transmitted field into the region 1 is given as

$$E_z^t = T_{01}(k_x^i) e^{jk_{1y}\rho \cos(\phi - \phi_i)} \quad (5.1.7)$$

5.1.2. Scattered fields inside dielectric half space (Region 1)

In the presence of a PEMC circular cylinder in the dielectric half space, the transmitted field into region 1 must be written in terms of cylindrical functions. Using Fourier-Bessel series expansion the transmitted field can be written as

$$E_z^i = \sum_{n=-\infty}^{\infty} j^n J_n(k_1 \rho) e^{jn(\phi - \phi_i)} \quad (5.1.8)$$

Using following Maxwell's equation

$$\mathbf{H} = \frac{1}{j\omega\mu_1} \nabla \times \mathbf{E} \quad (5.1.9)$$

corresponding ϕ component of incident magnetic field may be obtained as

$$H_\phi^i = -\frac{1}{j\eta_1} \sum_{n=-\infty}^{\infty} j^n J_n'(k_1 \rho) e^{jn(\phi - \phi_i)} \quad (5.1.10)$$

where $J_n(\cdot)$ is the Bessel function and prime represents the derivative with respect to the argument. In response to this incident plane wave, the co-polarized component of the scattered field by the PEMC cylinder may be written in terms of unknown coefficient as

$$E_z^s = \sum_{n=-\infty}^{\infty} j^n b_n H_n^{(1)}(k_1 \rho) e^{jn(\phi - \phi_i)} \quad (5.1.11)$$

The ϕ component of magnetic field, using (5.1.9) is written as

$$H_\phi^s = -\frac{1}{j\eta_1} \sum_{n=-\infty}^{\infty} j^n b_n H_n^{(1)'}(k_1 \rho) e^{jn(\phi - \phi_i)} \quad (5.1.12)$$

As is known [66], that unlike PEC or a PMC cylinder, the scattered field from a PEMC cylinder, contains H-polarized fields in addition to the E-polarized fields for E-polarized excitation. And hence the cross-polarized component of the scattered field may be expressed as

$$H_z^s = -\frac{j}{\eta_1} \sum_{n=-\infty}^{\infty} j^n c_n H_n^{(1)}(k_1 \rho) e^{jn(\phi - \phi_i)} \quad (5.1.13)$$

Using Maxwell's equation

$$\mathbf{E} = -\frac{1}{j\omega\epsilon_1}\nabla \times \mathbf{H} \quad (5.1.14)$$

corresponding ϕ component of scattered electric field may be obtained as

$$E_{\phi}^s = -\sum_{n=-\infty}^{\infty} j^n c_n H_n^{(1)'}(k_1\rho) e^{jn(\phi-\phi_i)} \quad (5.1.15)$$

The unknown scattering coefficients b_n and c_n , may be calculated by applying the boundary conditions at the surface of the PEMC cylinder. The boundary conditions for the tangential components and radial components, at the surface of PEMC cylinder are given as [66]

$$H_t^i + ME_t^i + H_t^s + ME_t^s = 0 \quad (5.1.16)$$

$$\epsilon_0 E_{\rho}^i - M\mu_0 H_{\rho}^i + \epsilon_0 E_{\rho}^s - M\mu_0 H_{\rho}^s = 0 \quad (5.1.17)$$

where M is the admittance parameter of the PEMC material. Using the values of the incident and scattered field components from (5.1.8) through (5.1.15) in (5.1.16), and solving the two resultant equations, it is found that

$$b_n = -\frac{H_n^{(1)}(k_1a)J_n'(k_1a) + M^2\eta_0^2 J_n(k_1a)H_n^{(1)'}(k_1a)}{(1 + M^2\eta_0^2)H_n^{(1)}(k_1a)H_n^{(1)'}(k_1a)} \quad (5.1.18)$$

$$c_n = \frac{2M\eta_0}{\pi k_1a(1 + M^2\eta_0^2)H_n^{(1)}(k_1a)H_n^{(1)'}(k_1a)} \quad (5.1.19)$$

Inserting the values of b_n and c_n in (5.1.11) and (5.1.15), the co-polarized and cross-polarized scattered fields from an isolated PEMC cylinder are obtained, in an infinite dielectric medium.

When the dielectric-free space planer interface is taken into consideration, the cylindrical waves scattered from the PEMC cylinder are required to be expressed in the form of plane waves. The scattered fields given in equations (5.1.11) to (5.1.15) may easily be written to account for the spectrum of incident plane waves by integration

over k_x . Integrating the eigenfunction solutions in (5.1.11) and (5.1.15), over k_x and using the appropriate weighting from (5.1.7), the initial scattered co-polarized field, for half space geometry, becomes

$$\begin{aligned} E_z^{s1} &= \int_{-\infty}^{\infty} \sum_{n=-\infty}^{\infty} j^n b_n H_n^{(1)}(k_1 \rho) e^{jn[\phi - \tan^{-1}(-k_{1y}^i/k_x^i)]} [T_{01} \delta(k_x - k_x^i)] dk_x \\ &= \sum_{n=-\infty}^{\infty} j^n b_n C_n^{(1)} H_n^{(1)}(k_1 \rho) e^{jn\phi} \end{aligned} \quad (5.1.20)$$

Similarly the initially scattered cross-polarized field becomes

$$\begin{aligned} E_\phi^{s1} &= \int_{-\infty}^{\infty} \sum_{n=-\infty}^{\infty} j^n c_n H_n^{(1)'}(k_1 \rho) e^{jn[\phi - \tan^{-1}(-k_{1y}^i/k_x^i)]} [T_{01} \delta(k_x - k_x^i)] dk_x \\ &= \sum_{n=-\infty}^{\infty} j^n c_n C_n^{(1)} H_n^{(1)'}(k_1 \rho) e^{jn\phi} \end{aligned} \quad (5.1.21)$$

where

$$C_n^{(1)} = T_{01}(k_x^i) e^{-jn \tan^{-1}(-k_{1y}^i/k_x^i)}$$

Equations (5.1.20) and (5.1.21), are the scattered co- and cross-polarized fields resulting from the first interaction of the incident field with the buried PEMC cylinder.

Subsequent discussion takes into account, the multiple interactions between the cylinder and dielectric interface separating the two half spaces. Using the integral representation of $H_n^{(1)}(k_1 \rho) e^{jn(\phi)}$, equations (5.1.20) and (5.1.21), may be expanded into their spectral representation as

$$E_z^{s1} = \frac{1}{\pi} \int_{-\infty}^{\infty} \frac{1}{k_{1y}} e^{j(k_x x + k_{1y} y)} \sum_{n=-\infty}^{\infty} b_n C_n^{(1)} e^{jn \tan^{-1}(k_{1y}/k_x)} dk_x \quad (5.1.22)$$

$$E_\phi^{s1} = \frac{j}{\pi} \int_{-\infty}^{\infty} \frac{1}{k_{1y}} e^{j(k_x x + k_{1y} y)} \sum_{n=-\infty}^{\infty} c_n C_n^{(1)} e^{jn \tan^{-1}(k_{1y}/k_x)} dk_x \quad (5.1.23)$$

Expressions (5.1.22) and (5.1.23), show the linear combination of co- or cross-polarized plane waves propagating in $+y$ direction, specifically determined by k_x and incident

upon the interface from below. Downward travelling waves which are reflected by the interface can be obtained by incorporating the reflection coefficient and are given as

$$\tilde{E}_z^{s1} = \frac{1}{\pi} \int_{k_x} \frac{1}{k_{1y}} \sum_{n=-\infty}^{\infty} b_n C_n^{(1)} e^{jn \tan^{-1}(k_{1y}/k_x)} [R_{10}(k_x) e^{j(k_x x - k_{1y} y)}] dk_x \quad (5.1.24)$$

$$\tilde{E}_\phi^{s1} = \frac{j}{\pi} \int_{k_x} \frac{1}{k_{1y}} \sum_{n=-\infty}^{\infty} c_n C_n^{(1)} e^{jn \tan^{-1}(k_{1y}/k_x)} [R_{10}(k_x) e^{j(k_x x - k_{1y} y)}] dk_x \quad (5.1.25)$$

where $R_{10}(k_x)$ is the reflection coefficient of the wave reflected back into the dielectric half space, and is given as

$$R_{10}(k_x) = \frac{k_{1y} - k_{0y}}{k_{1y} + k_{0y}} e^{-2jk_{1y}d}$$

where $k_{0y} = \sqrt{k_0^2 - k_x^2}$ and $k_{1y} = \sqrt{k_1^2 - k_x^2}$. The superposition of downward travelling plane waves given in (5.1.24) and (5.1.25), excite the PEMC cylinder for the second order interaction. Once again, the known eigenfunction solutions for a PEMC, cylinder with plane waves incident are employed. When the superposition of downward travelling waves described by (5.1.24), become incident upon the cylinder, it radiates both co- and cross-polarized fields. Thus equations (5.1.11) and (5.1.15) are used for the scattered fields. Again integrating (5.1.11) and (5.1.15), over k_x and using the appropriate weighting from (5.1.24), the second order scattered fields by the cylinder, inside the dielectric half space, may be written as

$$E_z^{s2} = \sum_{n=-\infty}^{\infty} j^n b_n H_n^{(1)}(k_1 \rho) e^{jn(\phi)} \left[\frac{1}{\pi} \sum_{m=-\infty}^{\infty} (b_m C_m^{(1)} + j c_m C_m^{(1)}) I_{(m,n)} \right] \quad (5.1.26)$$

$$E_\phi^{s2} = \sum_{n=-\infty}^{\infty} j^n c_n H_n^{(1)'}(k_1 \rho) e^{jn(\phi)} \left[\frac{1}{\pi} \sum_{m=-\infty}^{\infty} (b_m C_m^{(1)} + j c_m C_m^{(1)}) I_{(m,n)} \right] \quad (5.1.27)$$

where

$$I_{(m,n)} = \int_{k_x} \frac{1}{k_{1y}} R_{10}(k_x) e^{jm \tan^{-1}(k_{1y}/k_x)} e^{-jn \tan^{-1}(-k_{1y}/k_x)} \quad (5.1.28)$$

Equations (5.1.26) and (5.1.27), may be written in the following form

$$E_z^{s2} = \sum_{n=-\infty}^{\infty} j^n b_n H_n^{(1)}(k_1 \rho) e^{jn\phi} [C_n^{(2)} + D_n^{(2)}] \quad (5.1.29)$$

$$E_\phi^{s2} = \sum_{n=-\infty}^{\infty} j^n c_n H_n^{(1)'}(k_1 \rho) e^{jn\phi} [C_n^{(2)} + D_n^{(2)}] \quad (5.1.30)$$

where

$$C_n^{(2)} = \frac{1}{\pi} \sum_{m=-\infty}^{\infty} b_m C_m^{(1)} I_{(m,n)} \quad (5.1.31)$$

$$D_n^{(2)} = \frac{j}{\pi} \sum_{m=-\infty}^{\infty} c_m D_m^{(1)} I_{(m,n)} \quad (5.1.32)$$

and

$$D_m^{(1)} = C_m^{(1)}$$

Equations 5.1.29 and 5.1.30, give the total second order scattered co-polarized and cross-polarized fields.

In general the total qth order scattered co-polarized and cross-polarized fields may be written as

$$E_z^{s(q)} = \sum_{n=-\infty}^{\infty} j^n b_n H_n^{(1)}(k_1 \rho) e^{jn\phi} [C_n^{(q)} + D_n^{(q)}] \quad (5.1.33)$$

$$E_\phi^{s(q)} = \sum_{n=-\infty}^{\infty} j^n c_n H_n^{(1)'}(k_1 \rho) e^{jn\phi} [C_n^{(q)} + D_n^{(q)}] \quad (5.1.34)$$

where

$$C_n^{(q)} = \frac{1}{\pi} \sum_{m=-\infty}^{\infty} b_m C_m^{(q-1)} I_{(m,n)} \quad (5.1.35)$$

$$D_n^{(q)} = \frac{j}{\pi} \sum_{m=-\infty}^{\infty} c_m D_m^{(q-1)} I_{(m,n)} \quad (5.1.36)$$

Expressions (5.1.35) and (5.1.36), show that the qth order scattering coefficients are found in terms of (q-1)th order scattering coefficients, thus indicating the recursive

$M\eta_1 = \pm 1$ and $d = 2\lambda_0$, have been taken. Fig. 5.3, shows the behavior of the co-polarized component of the far-zone scattered field component for $M\eta_1 = 0$ (PMC case). Fig. 5.4 gives the variations of the co- and cross-polarized components of the far-zone scattered field for $M\eta_1 = \pm 1$, when $d = 5\lambda_0$. And finally in Fig. 5.5, the plot of the co-polarized component for $M\eta_1 = 0$ and $d = 5\lambda_0$, are shown. From Figs. 5.2 and 5.4, it is observed that both co- and cross-polarized components are present for the case of PEMC cylinder with $M\eta_1 = \pm 1$. Fig. 5.3 and 5.5, reveal that the cross-polarized component vanishes for the case of PEMC cylinder with $M\eta_1 = 0$. Fig. 5.6 shows the variation of the scattered cross-polarized components for different values of $M\eta_1$. It is obvious from this figure that the cross-polarized component is maximum at $M\eta_1 = 1$ and decreases otherwise. In Figs. 5.7 and 5.8 the co- and cross-polarized components of the far-zone scattered field in free, are shown for $d = 2\lambda_0$ and $d = 5\lambda_0$, respectively. Also in these two figures $M\eta_1 = \pm 1$ has been chosen. Fig. 5.9 shows the behavior of the co-polarized component of the scattered field above the dielectric half space for $M\eta_1 = 0$.

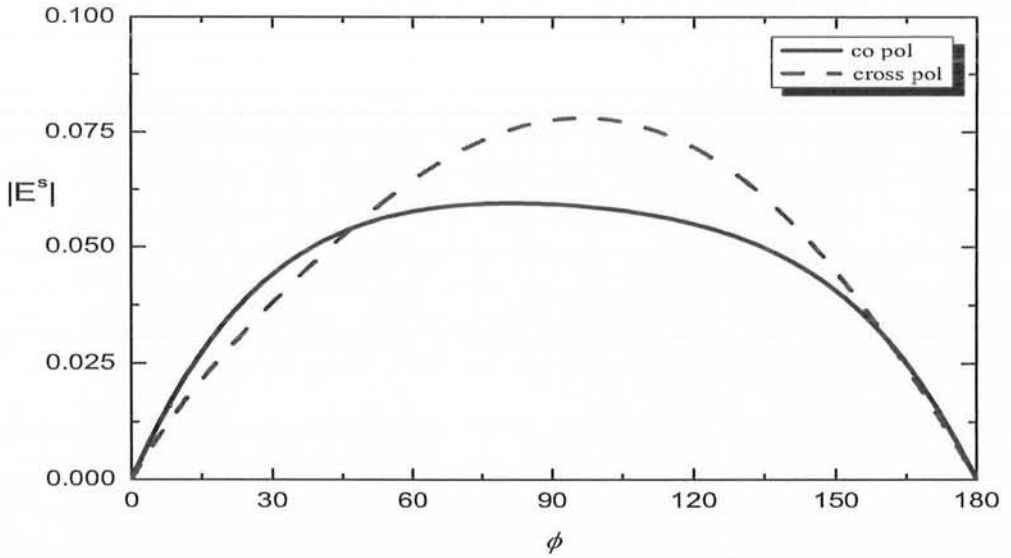


Figure 5.2. Co- and cross-polarized components of far-zone scattered field above the dielectric half space (E-pol case), $a = 0.1\lambda_0$, $d = 2\lambda_0$ and $M\eta_1 = \pm 1$.

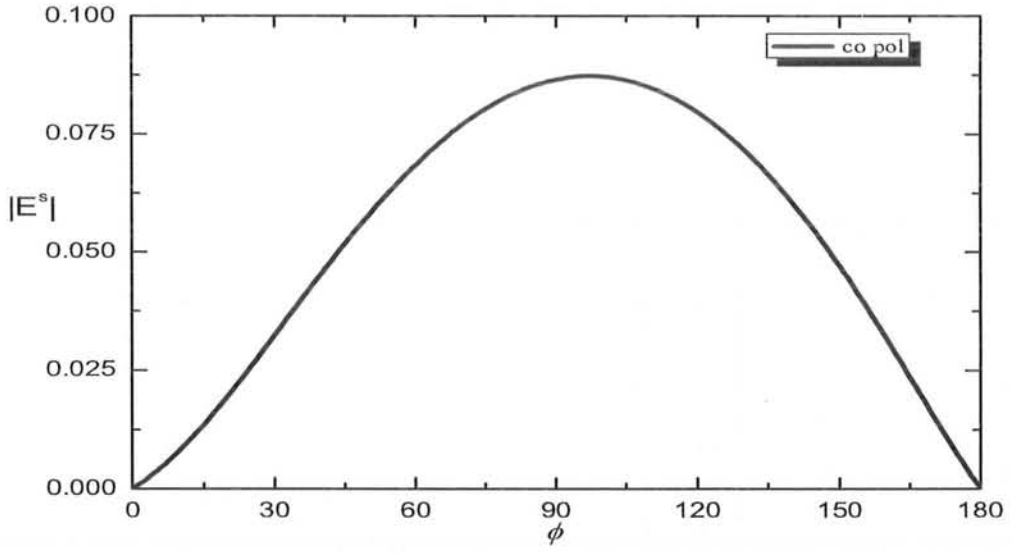


Figure 5.3. Co-polarized component of far-zone scattered field above the dielectric half space (E-pol case), $a = 0.1\lambda_0$, $d = 2\lambda_0$ and $M\eta_1 = 0$.

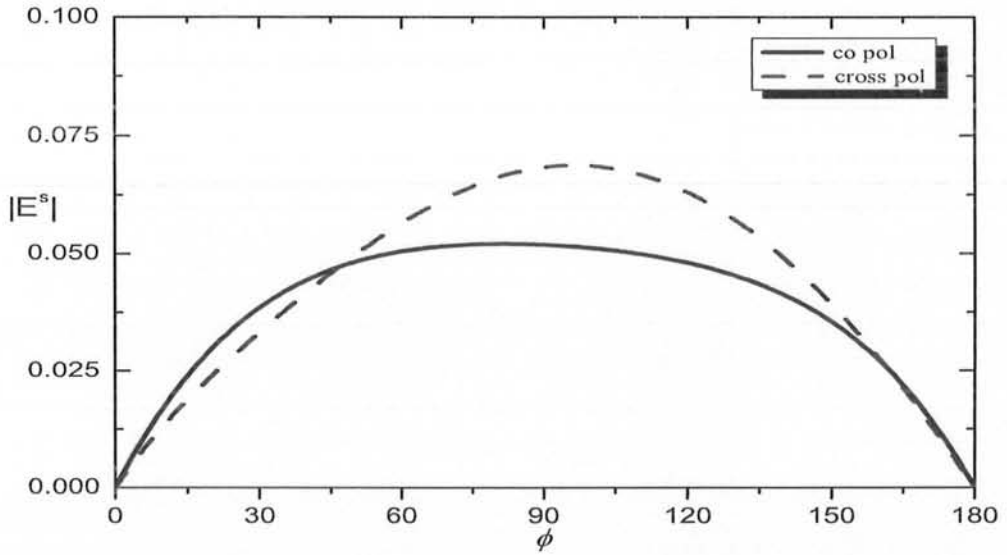


Figure 5.4. Co- and cross-polarized components of far-zone scattered field above the dielectric half space (E-pol case), $a = 0.1\lambda_0$, $d = 5\lambda_0$ and $M\eta_1 = \pm 1$.

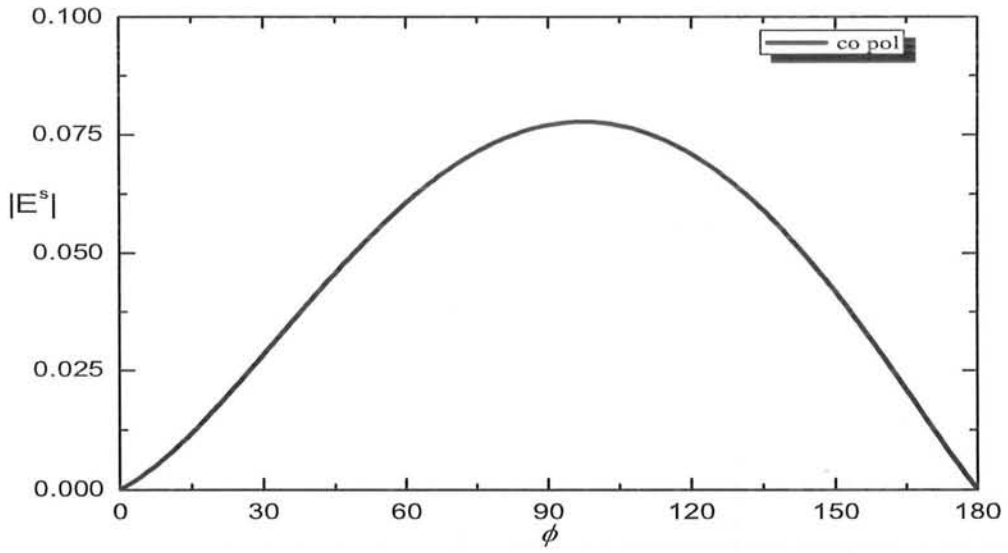


Figure 5.5. Co-polarized component of far-zone scattered field above the dielectric half space (E-pol case), $a = 0.1\lambda_0$, $d = 5\lambda_0$ and $M\eta_1 = 0$.

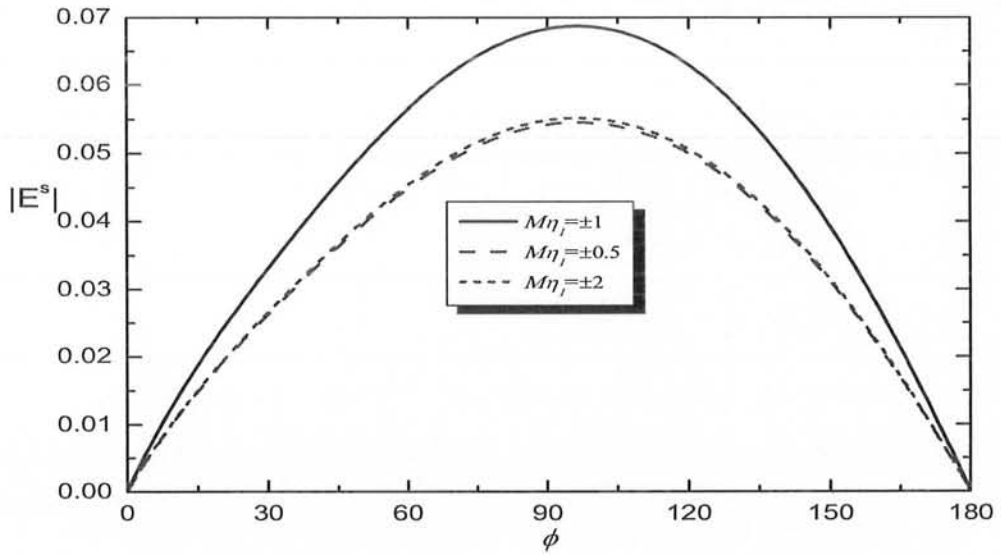


Figure 5.6. Cross-polarized component of far-zone scattered field above the dielectric half space (E-pol case), $a = 0.1\lambda_0$, $d = 5\lambda_0$ for different $M\eta_1$.

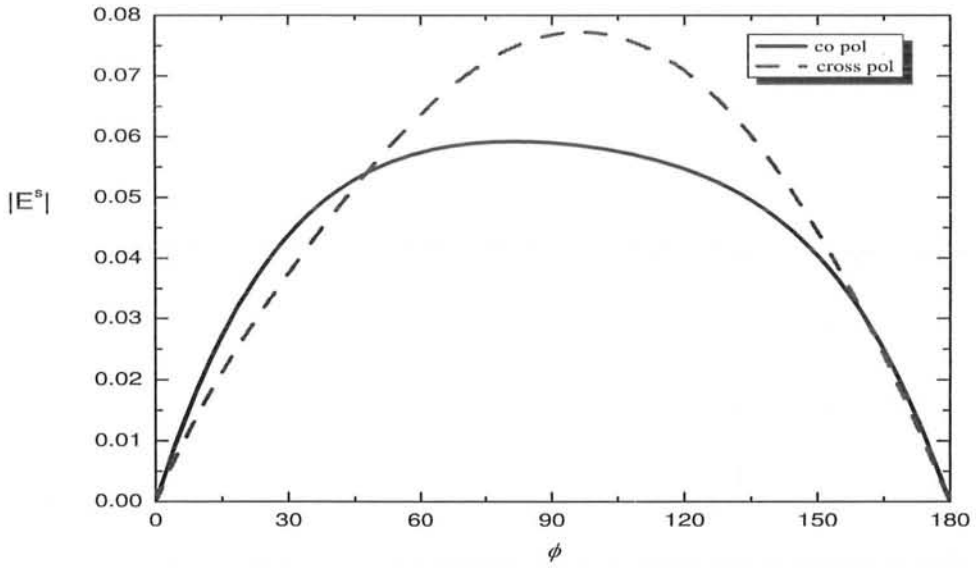


Figure 5.7. Co- and cross-polarized components component of far-zone scattered field above the dielectric half space (H-pol case), $a = 0.1\lambda_0$, $d = 2\lambda_0$ and $M\eta_1 = \pm 1$.

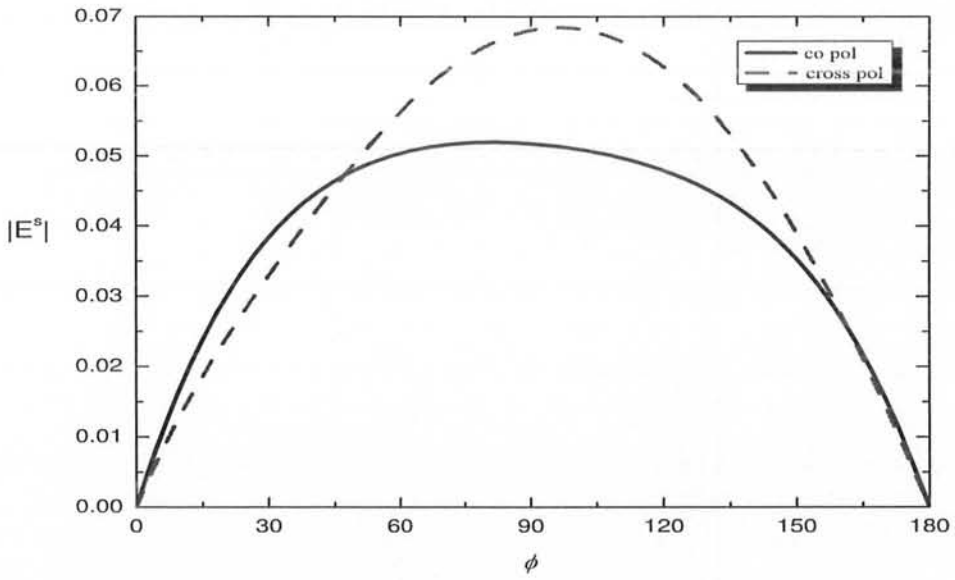


Figure 5.8. Co- and cross-polarized components of far-zone scattered field above the dielectric half space (H-pol case), $a = 0.1\lambda_0$, $d = 5\lambda_0$ and $M\eta_1 = \pm 1$.

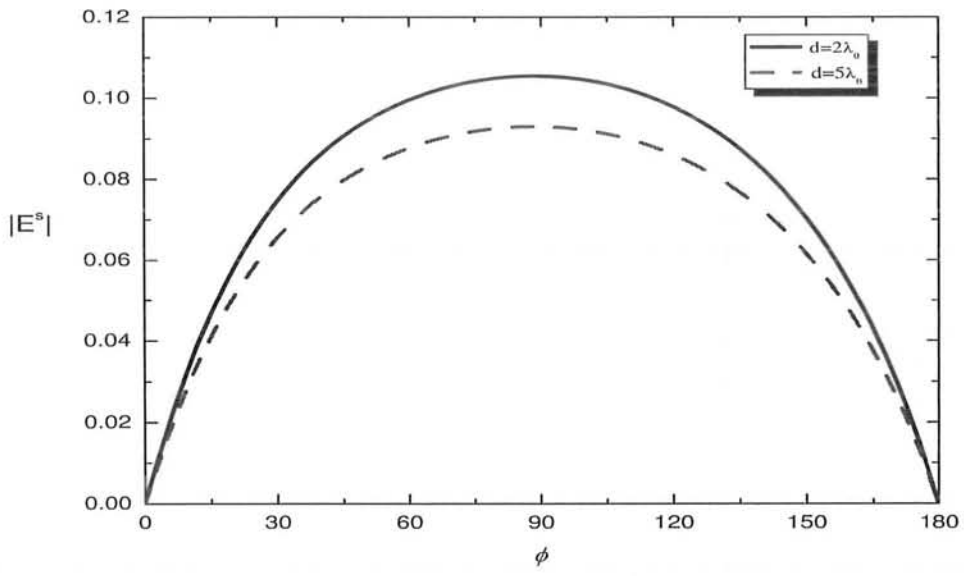


Figure 5.9. Co-polarized component of far-zone scattered field above the dielectric half space (H-pol case), $a = 0.1\lambda_0$ and $M\eta_1 = 0$.

CHAPTER VI

Conclusions

This chapter contains conclusions based on the research work carried out in this thesis which are presented below.

The behavior of the scattered co- and cross-polarized components of the monostatic scattering width from a PEMC circular cylinder placed in free space is the same for both E-polarized and H-polarized cases. With the variation in the admittance parameter $M\eta_0$ it is observed that the cross-polarized component of the normalized monostatic scattering width is maximum at $M\eta_0 = \pm 1$ while the co-polarized component is minimum at this value of $M\eta_0$. And the cross-polarized component reduces to zero while the co-polarized component increases to get a constant value when $M\eta_0$ is increased from ± 1 . It is also observed that the co- and cross-polarized components of the normalized bistatic scattering width for an isolated PEMC cylinder in free space are independent of the type of the polarization of the incident plane wave. However the scattering widths depend on the values of the parameter $M\eta_0$ when it varies from 0 to $\pm\infty$.

In case of multiple PEMC circular cylinders, it is observed that the forward and backward scattered field components are fairly different from those of multiple PEC circular cylinders. And forward and backward scattered field components may be well controlled in the case of PEMC cylinders. The difference in the scattered field components of PEMC strip and PEMC strip grating for different values of $M\eta_0$ is also observed.

The scattering characteristics of a PEMC circular cylinder may be altered or changed according to the requirement by coating it with a suitable material e.g., DPS, ENG, MNG, or DNG. It is observed that when the PEMC cylinder is coated with

a DPS or DNG materials, the co-polarized component of the normalized monostatic scattering width is different for E-polarized and H-polarized cases. While the cross-polarized component of the monostatic scattering width does not depend on the type of the polarization. Also the maximum (minimum) value of the cross-polarized component (co-polarized component) of the monostatic scattering width does not occur at $M\eta_1 = \pm 1$. And it is not necessary for a coated PEMC cylinder that the co-polarized component is minimum where the cross-polarized component is maximum. All these features of a coated PEMC cylinder are different from an un-coated PEMC cylinder located in free space.

Using DPS, ENG, MNG, or DNG materials as the coating layers on the PEMC cylinder transparency and scattering maximization can be achieved for both the E-polarized and H-polarized cases. Which is a different behavior of the PEMC cylinder as a core of the coated geometry as compared to a PEC cylinder for which these two phenomena can occur only for the H-polarization. Also using dissipative and dispersive DNG material as coating on the PEC or PEMC core forward and backward scattered field can tremendously decreased which will help in cloaking and transparency of the objects.

Coated PEMC cylinder may also be used to achieve the directivity in the presence of a nearby line source. It is observed that the coated PEMC cylinder is more directive as compared to a coated PEC cylinder for some special type of the coating layers. While it is less directive for some other types of coatings. Also for a specific DNG coating layer the coated PEMC cylinder becomes equally directive as a coated PEC cylinder.

Possible extensions of the work has been mentioned in the following paragraphs.

Multiple PEMC circular cylinders may be used to make a cylindrical reflector. The characteristics of this type of the reflector may be considered for the operational

efficiency over that obtained from PEMC contour reflector. Also multiple PEMC cylinders coated by different materials may be studied to improve the efficiency and directivity of the antenna. Also using the PEMC circular cylinders many two dimensional geometries may be simulated to find out the behavior of the PEMC material for different shapes.

As the transparency and scattering maximization are the burning issues currently. So achieving transparency and scattering maximization using coated PEMC cylinder is a new problem for future work. And using the concept of the multiple cylinders these characteristics may be observed for different two-dimensional shapes.

A coated cylinder nearby a line source is considered to be better than a parabolic reflector antenna. Therefore increasing the number of the coated cylinders when the source of excitation is a line source, the effect on the directivity of the coated geometry may be observed in future.

Finally in the case of buried geometries the effect on the scattering pattern in the upper half plane due to a coated PEMC cylinder may be checked for the sake of stealing the mines from detection.

References

- [1] Wait, J. R., "Scattering of a plane wave from a circular dielectric cylinder at oblique incidence," *Can. J. Phys.*, Vol. 33, 189-195, 1955.
- [2] Balanis, C. A., *Advanced Engineering Electromagnetics*, Wiley, New York, 1989.
- [3] Mei, K. K., and Van Bladel, J., "Scattering by perfectly conducting rectangular cylinder," *IEEE Trans. Antennas Propagat.*, Vol. 11, 185-192, 1963.
- [4] Richmond, J. H., "Scattering by a dielectric cylinder of arbitrary cross-section shape," *IEEE Trans. Antennas Propagat.*, Vol. 13, 334-341, 1965.
- [5] Richmond, J. H., "TE-wave scattering by a dielectric cylinder of arbitrary cross-section shape," *IEEE Trans. Antennas Propagat.*, Vol. 14, 460-464, 1966.
- [6] Wu, T. K., and Tsai, L. L., "Scattering by arbitrary cross sectioned layered lossy dielectric cylinders," *IEEE Trans. Antennas Propagat.*, Vol. 25, 518-524, 1977.
- [7] Hongo, K., "Multiple scattering by two conducting cylinders," *IEEE Trans. Antennas Propagat.*, Vol. 26, 748-751, 1978.
- [8] Twersky, V., "Multiple scattering of radiation by an arbitrary configuration of parallel cylinders," *J. Acoust. Soc. Am.*, Vol. 24, 42-46, 1952.
- [9] Burke, J., Censor, D., and Twersky, V., "Exact inverse separation series for multiple scattering in two dimensions," *J. Acoust. Soc. Am.*, Vol. 37, 5-13, 1965.
- [10] Ragheb, H. A., and Hamid, M., "Scattering by N parallel conducting circular cylinders," *Znt. J. Electron.*, Vol. 59, 407-421, 1985.
- [11] Ragheb, H. A., and Hamid, M., "Simulation of a cylindrical reflector by conducting circular cylinders," *IEEE Trans. Antennas Propagat.*, Vol. AP-35, 349-353,

1987.

- [12] Elsherbeni, A. Z., and M. Hamid, "Scattering by parallel conducting circular cylinders," *IEEE Trans. Antennas Propagat.*, Vol. 35, 355-358, 1987.
- [13] Elsherbeni, A. Z., and Kishk, A., "Modeling of cylindrical objects by circular cylinders," *IEEE Trans. Antennas Propagat.*, Vol. 40, 96-99, 1992.
- [14] Elsherbeni, A. Z., M. Hamid, and Tian, G., "Iterative scattering of a gaussian beam by an array of circular conducting and dielectric cylinders," *Journal of Electromagnetic Waves and Applications*, Vol. 7, No. 10, 1323-1342, 1993.
- [15] Elsherbeni, A. Z., "A comparative study of two-dimensional multiple scattering techniques," *Radio Sci.*, Vol. 29, No. 4, 1023-1033, 1994.
- [16] Yin, W. Y., and Li, L. W., "Multiple scattering from gyrotropic bianisotropic cylinders of arbitrary cross sections using the modeling technique," *Phys. Rev. E*, Vol. 60, No. 1, 918-925, 1999.
- [17] Yin, W. Y., Li, L. W., and Leong, M. S., "Scattering from multiple bi-anisotropic cylinders and their modeling of cylindrical objects of arbitrary cross-section," *Progress In Electromagnetics Research, PIER* 27, 159-184, 2000.
- [18] Henin, B. H., Elsherbeni, A. Z., and Al Sharkawy, M., "Oblique incidence plane wave scattering from an array of circular dielectric cylinders," *Progress In Electromagnetics Research, PIER* 68, 261-279, 2007.
- [19] Tang, C. C. H., "Back-scattering from dielectrically coated infinite cylindrical obstacles," *Ph.D. Thesis, Harvard University*, 1956.
- [20] Tang, C. C. H., "Backscattering from dielectrically coated infinite cylindrical obstacles," *J. Appl. Phys.*, Vol. 28, 628-633, 1957.

- [21] Wang, N., “Electromagnetic scattering from a dielectric-coated circular cylinder,” *IEEE Trans. Antennas Propagat.*, Vol. 33, 9, 960-963, 1985.
- [22] Chen, H. C., and Cheng, D. K., “Scattering of electromagnetic waves by an anisotropic plasma-coated conducting cylinder,” *IEEE Trans. Antennas Propagat.*, Vol. AP-12, 348-353, 1964.
- [23] Shen, Z. X., “Electromagnetic scattering by an impedance cylinder coated eccentrically with a chiro-plasma cylinder,” *IEE Pro. Microwaves, Antennas and Propagation*, Vol. 141, 279-284, 1994.
- [24] Shen, Z., and Li, C., “Electromagnetic scattering by a conducting cylinder coated with metamaterials,” *Progress In Electromagnetics Research, PIER* 42, 91-105, 2003.
- [25] Mushref, M. A., “Transverse magnetic scattering of two incident plane waves by a dielectric coated cylindrical reflector,” *CEJP*, Vol 3, Issue 2, 229-246, 2005.
- [26] Mushref, M. A., “Closed solution to electromagnetic scattering of a plane wave by an eccentric cylinder coated with metamaterials,” *Opt. Commun.*, Vol. 270, 441-446, 2007.
- [27] Jun Sun, Wei Sun, Tian Jiang, and Yijiun Feng, “Directive electromagnetic radiation of a line source scattered by a conducting cylinder coated with left-handed metamaterial,” *Microwave Opt. Technol. Lett.*, Vol. 47, 274-279, 2005.
- [28] Erdinc Irci, and Vakur B. Ertürk, “Achieving transparency and maximizing scattering with metamaterial-coated conducting cylinders,” *Phys. Rev. E*, 76, 056603, 2007.
- [29] Ahmed, S., and Naqvi, Q. A., “Directive EM radiation of a line source in the presence of a coated nihility cylinder,” *J. of Electromagn. Waves and Appl.*, Vol. 23, 761-771, 2009

- [30] Ahmed, S., and Naqvi, Q. A., "Scattering of electromagnetic waves by a coated nihility cylinder," *Journal of infrared millimeter terahertz waves.*, 30, 1044-1052, DOI 10.1007/ s10762-009-9531-5, 2009.
- [31] D'Yakonov, B. P., "The diffraction of electromagnetic waves by a circular cylinder in a homogeneous half-space," *Bull. Acad. Sci. U.S.S.R., Geophysics, ser. No. 9*, 950-955, 1959.
- [32] Parry, J. R., and Ward, S. H., "Electromagnetic scattering from cylinders of arbitrary cross-section in a conductive half-space," *Geophys.*, Vol. 36, 67100, 1971.
- [33] Howard, A. Q., "The electromagnetic fields of a subterranean cylindrical inhomogeneity excited by a line source," *Geophys.*, Vol. 37, 975-984, 1972.
- [34] Ogunade, S. O., "Electromagnetic response of an embedded cylinder for line current excitation," *Geophys.*, Vol. 46, 45-52, 1981.
- [35] Mahmoud, S. F., Ali, S. M., and Wait, J. R., "Electromagnetic scattering from a buried cylindrical inhomogeneity inside a lossy earth," *Radio Sci.*, Vol. 16, No. 6, 1285-1298, 1981.
- [36] Butler, C. M., Xu, X. B., and Glisson, A. W., "Current induced on a conducting cylinder located near the planar interface between two semi-infinite half-spaces," *IEEE Trans. Antennas Propagat.*, Vol. 33, 616-624, 1985.
- [37] Hongo, K., and Hamamura, A., "Asymptotic solutions for the scattered field of plane wave by a cylindrical obstacle buried in a dielectric half-space," *IEEE Trans. Antennas Propagat.*, Vol. 34, 1306-1312, 1986.
- [38] Moaveni, M. K., Rizvi, A. A., and Kamran, B. A., "Planewave scattering by gratings of conducting cylinders in an inhomogeneous and lossy dielectric," *J. Opt. Soc. Am. A*, Vol. 5, 834-842, 1988.

- [39] Naqvi, Q. A., Rizvi, A. A., and Yaqoob, Z., Corrections to: "Asymptotic solutions for the scattered fields of plane wave by a cylindrical obstacle buried in a dielectric half-space," *IEEE Trans. Antennas Propagat.*, Vol. AP-48, 846-848, 2000.
- [40] Naqvi, Q. A., and Rizvi, A. A., "Low contrast circular cylinder buried in a grounded dielectric layer," *J. Electromagn. Waves Appl.*, Vol. 12, No. 11, 1527-1536 1998.
- [41] Lambert, M., "The scattering by a cylindrical dielectric obstacle buried in a half-space: a H-field-based solution method," *J. Electromagn. Waves Appl.*, Vol. 9, 1129-1262, 1998.
- [42] Naqvi, Q. A, Rizvi, A. A., and Yaqoob, Z., "Scattering of electromagnetic waves from a deeply buried circular cylinder," *Progress In Electromagnetics Research*, PIER 27, 37-59, 2000.
- [43] Lawrence, D. E., and Sarabandi, K., "Electromagnetic scattering from a dielectric cylinder buried beneath a slightly rough surface," *IEEE Trans. Antennas Propagat.*, Vol. 50, No. 10, 1368-1376, 2002.
- [44] Ciambra, F., Frezza, F., Pajewski, L., and Schettini, G., "A spectral domain solution for the scattering problem of a circular cylinder buried in a dielectric half-space," *Progress In Electromagnetics Research*, PIER Vol. 38, Vol. 22, 223-252, 2002.
- [45] Ciambra, F., Frezza, F., Pajewski, L., and Schettini, G., "A spectral domain solution for the scattering problem of a circular cylinder buried in a dielectric half-space," *J. of Electromagn. Waves and Appl.*, Vol. 17, No. 4, 607- 609, 2003.
- [46] Di Vico, M., Frezza, F., Pajewski, L., and Schettini, G., "Scattering by a finite set of perfectly conducting cylinders buried in a dielectric half space: a spectral-domain solution," *IEEE Trans. Antennas Propagat.*, Vol. 53, 719-727, 2005.

- [47] Veselago, V. G., “The electrodynamics of substances with simultaneously negative values of ϵ and μ ,” *Sov. Phys. Usp.*, 10, 509-514, 1968.
- [48] Pendry, J. B., “Negative refraction makes a perfect lens,” *Phys. Rev. Lett.*, 85, 3966-3969, 2000.
- [49] Shelby, R. A., Smith, D. R., and Schultz, S., “Experimental verification of a negative index of refraction,” *Science*, 292, Issue 5514, 77-79, 2001.
- [50] Ziolkowski, R. W., Heyman, E., “Wave propagation in media having negative permittivity and permeability,” *Phys. Rev. E*, 64, 056625, 2001.
- [51] Lakhtakia A., “An electromagnetic trinity from ”negative permittivity” and ”negative permeability,” *Int. J. Infrared Millim. Waves* 22, 1731-4, 2001.
- [52] Lakhtakia A., “An electromagnetic trinity from ”negative permittivity” and ”negative permeability,”” *Int. J. Infrared Millim. Waves* 23, 813-8 2002.
- [53] McCall, M. W., Lakhtakia, A., and Weiglhofer, W. S., “The negative index of refraction demystified,” *Eur. J. Phys.* 23, 353-359, 2002.
- [54] Engheta, N., “An idea for thin sub wavelength cavity resonators using metamaterials with negative permittivity and permeability,” *IEEE Antennas Wireless Propag. Lett.*, 1, 10-13, 2002.
- [55] Depine, R. W., Lakhtakia, A., “A new condition to identify isotropic dielectric-magnetic materials displaying negative phase velocity,” *Microwave Opt. Technol. Lett.*, Vol. 41, No. 4, 2004.
- [56] Ziolkowski, R. W., and Kipple, A., “Application of double negative metamaterials to increase the power radiated by electrically small antennas,” *IEEE Trans. Antennas Propag.*, 51, 2626-2640, 2003.

- [57] Alú, A., and Engheta, N., “Guided modes in a waveguide filled with a pair of single-negative (SNG), double-negative (DNG) and/or double-positive (DPS) layers,” *IEEE Trans. Microwave Theory Tech.*, 52, 199-210, 2004.
- [58] Eleftheriades, G. V., and Balmain, K. G., (Eds.), “Negative- Refraction Metamaterials: Fundamental Principles and Applications,” John Wiley, Hoboken, N. J, 2005.
- [59] Alú, A., and Engheta, N., “Polarizabilities and effective parameters for collections of spherical nano-particles formed by pairs of concentric double-negative (DNG), single-negative (SNG) and/or double-positive (DPS) metamaterial layers,” *J. Appl. Phys.*, 97, 094310, 2005.
- [60] Ziolkowski, R. W., and Kipple, A., “Reciprocity between the effects of resonant scattering and enhanced radiated power by electrically small antennas in the presence of nested metamaterials shells,” *Phys. Rev. E*, 72, 036602, 2005.
- [61] Caloz, C., and Itoh, T., (Eds.), “Electromagnetic metamaterials: Transmission line theory and microwave applications,” John Wiley, Hoboken, N. J, 2006.
- [62] Arslanagic, S., Ziolkowski, R. W., and Breinbjerg, O., “Excitation of an electrically small metamaterial-coated cylinder by an arbitrarily located line source,” *Microwave Opt. Technol. Lett.*, 48, 2598-2605, 2006.
- [63] Stuart, H., and Pidwerbetsky, A., “Electrically small antenna elements using negative permittivity and permeability resonators,” *IEEE Trans. Antennas Propagat.*, 54, 1644-1654, 2006.
- [64] Ziolkowski, R. W., and Erentok, A., “Metamaterial-based efficient electrically small antennas,” *IEEE Trans. Antennas Propagat.*, 54, 2113-2130, 2006.
- [65] Alú, A., Bilotti, F., Engheta, N., and Vegni, L., “Sub wavelength, compact, reso-

- nant patch antennas loaded with metamaterials,” *IEEE Trans. Antennas Propagat.*, 55, 13-25, 2007.
- [66] Lindell, I.V., and Sihvola, A.H., “Perfect electromagnetic conductor,” *J. of Electromagn. Waves and Appl.*, Vol. 19, 861-869, 2004.
- [67] Lindell, I. V., *Differential forms in electromagnetics*, New York: Wiley and IEEE Press, 2004.
- [68] Lindell, I. V., and Sihvola, A. H., “Realization of the PEMC boundary,” *IEEE Trans. Antennas Propagat.*, Vol. 53, No. 9, 3012-3018, 2005.
- [69] Lindell, I. V., and Sihvola, A. H., “Transformation method for problems involving perfect electromagnetic conductor (PEMC) structures,” *IEEE Trans. Antennas Propagat.*, Vol. 53, No. 9, 3005-3011, 2005.
- [70] Ruppin, R., “Scattering of electromagnetic radiation by a perfect electromagnetic conductor cylinder,” *J. of Electromagn. Waves and Appl.*, Vol. 20, No. 13, 1853-1860, 2006.
- [71] Lindell, I. V., and Sihvola, A. H., “Losses in PEMC boundary,” *IEEE Trans. Antennas Propagat.*, Vol. 54, No. 9, 2553-2558, 2006.
- [72] Sihvola, A., and Lindell, I. V., “Possible applications of perfect electromagnetic conductor (pemc) media,” *Proc. EuCAP 2006, Nice, France 610, 2006 (ESA SP-626, 2006)*.
- [73] Lindell, I. V., Sihvola, A., “The PEMC resonator,” *J. of Electromagn. Waves and Appl.*, Vol. 20, No. 7, 849-859, 2006.
- [74] Jancewicz, B., “Plane electromagnetic wave in PEMC,” *J. Electromagn. Waves Appl.*, Vol. 20, No. 5, 647-659, 2006.

- [75] Ahmed, S., and Naqvi, Q. A., “Electromagnetic scattering from a perfect electromagnetic conductor cylinder buried in a dielectric half space,” *Progress In Electromagnetics Research*, PIER 78, 25-38, 2008.
- [76] Ahmed, S., and Naqvi, Q. A., “Electromagnetic scattering form parallel perfect electromagnetic conductor cylinders of circular cross-sections using iterative procedure,” *J. of Electromagn. Waves and Appl.*, Vol. 22, 987-1003, 2008.
- [77] Ahmed, S., and Naqvi, Q. A., “Electromagnetic scattering from a two dimensional perfect electromagnetic conductor (PEMC) strip and PEMC strip grating simulated by circular cylinders,” *Opt. Commun.*, Vol. 281, 4211-4218, 2008.
- [78] Ahmed, S., and Naqvi, Q. A., “Electromagnetic scattering from a perfect electromagnetic conductor cylinder coated with a metamaterial having negative permittivity and/or permeability,” *Opt. Commun.*, Vol. 281, 5664-5670, 2008.
- [79] Ahmed, S., and Naqvi, Q. A., “Electromagnetic scattering of two or more incident plane waves by a perfect electromagnetic conductor cylinder coated with a metamaterial,” Accepted for publication, *Progress In Electromagnetics Research B*, Vol. 10, 75-90, 2008.
- [80] Fiaz, M. A., Ghaffar, A., and Naqvi, Q. A., “High Frequency Expressions for the Field in the Caustic Region of a PEMC Cylindrical Reflector using Maslovs method,” *J. of Electromagn. Waves and Appl.*, 22, 358-397, 2008.
- [81] Fiaz, M. A., Ghaffar, A., and Naqvi, Q. A., “High Frequency Expressions for the Field in the Caustic Region of a PEMC Gregorian system using Maslovs method,” *Progress in Electromagnetics Research*, PIER 81, 135-148, 2008.
- [82] Illahi, A., and Naqvi, Q. A., “Scattering of an arbitrarily oriented dipole field by an infinite and a finite length PEMC circular cylinder,” *CEJP*, in print, 2009.